Understanding the Robustness of Regulatory Motifs in Generating Biological Switches Relevant to Cell-fate Decisions

A Thesis Submitted

For the Degree of

Doctor of Philosophy

By

Anupam Dey



School of Chemistry

University of Hyderabad

(P.O.) Central University, Gachibowli

Hyderabad – 500046

Telangana

India

June, 2021



DECLARATION

I, Anupam Dey, hereby declare that the matter embodied in the thesis entitled "Understanding the Robustness of Regulatory Motifs in Generating Biological Switches Relevant to Cell-fate Decisions" is the result of my investigation carried out in the School of Chemistry, University of Hyderabad, Hyderabad, India, under the supervision of Dr. Debashis Barik.

In keeping with the general practice of reporting scientific observations, due acknowledgements have been made wherever the work described is based on the findings of other investigators. Any omission, which might have occurred by oversight error, is regretted. This research work is free from plagiarism. I hereby agree that my thesis can be deposited in Shodhganga/INFLIBNET. A report on plagiarism statistics from the University library is enclosed.

Anupam Dey

15CHPH34

School of Chemistry
University of Hyderabad
Hyderabad – 500046
Telangana
India



CERTIFICATE

This is to certify that the thesis entitled "Understanding the Robustness of Regulatory Motifs in Generating Biological Switches Relevant to Cell-fate Decisions" submitted by Anupam Dey bearing Reg. No. 15CHPH34 in partial fulfilment of the requirements for the award of Doctor of Philosophy in Chemistry in the School of Chemistry is a bonafide work carried out by him under my supervision and guidance.

This thesis is free from plagiarism and has not been submitted previously in part or in full to this University or any other University or Institution for award of any degree or diploma.

Parts of this thesis have been published in the following publications:

- 1. "Potential Landscapes, Bifurcations, and Robustness of Tristable Networks." Anupam

 Dey and Debashis Barik*, ACS Synth. Biol., 10, 2, 391-401, (2021) (Chapter 2)
- "Dichotomous Nature of Bistability Generated by Negative Cooperativity in Receptor-Ligand Binding." <u>Anupam Dey</u> and Debashis Barik*, *ACS Synth. Biol*, 8, 6, 1294-1302, (2019) (Chapter 5)
- "Parallel Arrangements of Positive Feedback Loops Limit Cell-to-cell Variability in Differentiation." <u>Anupam Dey</u> and Debashis Barik*, *PLoS One*, 12, e0188623, (2017) (Chapter 4)
- Tentative title: "The Origin and Robustness of Atypical Mushroom and Isola Bifurcations" Anupam Dey and Debashis Barik*. (Chapter 3) Manuscript to be communicated

He has also participated in oral/poster presentations in the following conferences:

- 1. CHEMFEST-2021, March 19-20, 2021
 - Oral: "Topology of Network Motifs dictate the Robustness in Cell-fate decisions"
 - School of Chemistry, University of Hyderabad, Hyderabad, India
- 2. CHEMFEST-2019, February 22-23, 2019
 - Poster: "Dichotomous Nature of Bistability Generated by Negative Cooperativity in Receptor-Ligand Binding"
 - School of Chemistry, University of Hyderabad, Hyderabad, India
- 3. 16th Indian Theoretical Chemistry Symposium (TCS), February 13-17, 2019
 - Poster: "Dichotomous Nature of Bistability Generated by Negative Cooperativity in Receptor-Ligand Binding"
 - Birla Institute of Technology and Science (BITS), Pilani, India
- 4. Conference on Electronic Structure, Spectroscopy and Dynamics (CESSD), February 22-25, 2018
 - Poster: "Parallel Arrangement of Positive Feedback Loops Limit Cell-to-Cell Variability in Differentiation"
 - Indian Association for the Cultivation of Science (IASC), Kolkata, India
- 8th International Collaborative and Cooperative Chemistry Symposium (ICCCS-8),
 December 18-19, 2017
 - Poster: "Parallel Arrangement of Positive Feedback Loops Limit Cell-to-Cell Variability in Differentiation"
 - University of Hyderabad, India
- National Meeting of Synthetic and Theoretical Chemists (NMSTC), October 13-14,
 2017
 - Poster: "Robust Bistability from Negative Cooperativity for a Receptor-Ligand Binding"
 - University of Hyderabad, India
- 7. Current Trends in Computational Natural Sciences (CTCNS), March 5, 2017
 - Poster: "Topology of Positive Feedback Loops Regulates Variability in Cellular Differentiation"

• International Institute of Information Technology (IIIT), Hyderabad, India

8. CHEMFEST-2017, March 3-4, 2017

- Poster: "Topology of Positive Feedback Loops Regulates Variability in Cellular Differentiation"
- School of Chemistry, University of Hyderabad, Hyderabad, India

9. 15th Indian Theoretical Chemistry Symposium (TCS), December 14-16, 2016

- Poster: "Architecture of Positive Feedback Loops Dictates the Variability in Cellular Differentiation"
- School of Chemistry, University of Hyderabad, Hyderabad, India

Further, the student has passed the following courses towards fulfilment of coursework requirement for Ph.D.:

Title of the Course	Credits	Result	
Research Proposal	3	Pass	
Instrumental Methods-A	3	Pass	
Instrumental Methods-B	3	Pass	
Mathematics for Chemists	3	Pass	
	Research Proposal Instrumental Methods-A Instrumental Methods-B	Research Proposal 3 Instrumental Methods-A 3 Instrumental Methods-B 3	

(Supervisor)

Dr. Debashis Barik

Associate Professor School of Chemistry University of Hyderabad Hyderabad-500 046, India. Dean
School of Chemistry

Dean SCHOOL OF CHEMISTRY University of Hyderabad Hyderabad-500 046

Acknowledgements

Acknowledgement is the most difficult section in the thesis, at least for me. For thesis, we record our investigations and results so we know what to write. But for acknowledgement, there might be hundreds of people who might have helped us in some or the other way in things related to our research work and to deal with life in general. Out of those hundreds, some names we remember, some names we forget, so it becomes difficult in acknowledging everyone. I am sorry if I miss out any one in acknowledging them for their kind help. Nevertheless, in general, I would like to sincerely thank all those who have helped me in being the person I am today and to all those who have helped and encouraged me in my research work.

On top of the list is my supervisor Dr. Debashis Barik, who stood by me both in my professional and personal life. I would like to extend my heartfelt gratitude to Dr. Debashis for his continuous support and encouragement throughout my thesis work. He has always been approachable and has been patient in listening to my doubts, queries and discussing and clarifying them. I have learnt a lot from him. Few things of him that I would like to inculcate in me are discipline, sincere, the quest for learning and the habit of reading research articles. Thank you sir for understanding me and my problems and helping me in many different ways in my thesis work and in life.

I extend my sincere regards to Prof. K.C. Kumaraswamy, Dean, School of Chemistry for the facilities to carry out my research work. I would also like to thank the former Deans of the School for cooperation on many aspects. I am also thankful to Prof. M. Durga Prasad and Prof. Lalitha Guruprasad for their guidance as doctoral committee members. I would like to extend my gratitude to all the faculty members for assisting me in many different ways. Acknowledgements are due to all the non-teaching and house-keeping staffs for keeping the research environment clean and green.

A big thank you to all my wonderful lab mates, Soutrick, Hafijur, Archana for all the scientific, non-scientific and non-sense discussions. I had lovely time with you all. Thank you for creating a friendly environment in the lab and for all the 'tour plans' that we made but succeeded in having few. Thank you Soutrick for the many scientific discussions and for the laughing out loud at 'non-sense salman khan movie' discussions in the tea breaks. Many thanks to Hafijur and his family for the many *daawats* in many different occasions. A special thanks to Archana for teaching me Malayalam and for the many discussions in lab. In addition, I would also like to thank Suchana, Rabiul, Samyuktha, Theinmozhi, Meghana, Bijit, Amruta, Rakesh, Moinak for being my colleagues in the lab. On a special note, I would like to thank Suchana for being a supportive and understanding friend.

I would also like to extend my gratitude to Dr. Durba Roy in helping me be a better person. Thank you ma'am for making me feel at home and for all those tasty homely foods. I would also like to thank Trinabh (pupu) for all the wonderful times and all the 'high-tech' conversations that I had with you in the lab. *Thank you for not complaining to the principal to give me T.C. a thousand times*.

I would like to show deep sense of gratitude to my parents Shri. Abhay Kumar Dey, Smt. Kakoli Dey and Late Smt. Rupali Dey for teaching me values and bringing me up to be a better person and for their immense support in doing whatever I want or wanted to do . I would also like to thank my sisters Ashima and Arpita for all the playful non-sense sibling things and teaching me some good things.

At this juncture, I would like to extend my thanks to all my teachers from Jawahar Navodaya Vidyalaya, Gachibowli for their persistent encouragement and support towards finding a goal and for inculcating ethical values in me. Special thanks to Aruna ma'am for believing in me and for encouraging me to take up research and also for helping my family. I still remember the gel pen she gifted me when I scored 100% in science in VI standard.

I am very fortunate to have friends like Dibyendu Dutta and Madhuri Dey. Dibyendu is my goto person for any problem I face in life. He is very patience, rational and logical and is always there for me no matter what. I sincerely thank him for helping me throughout in many different ways. I thank Madhuri also for helping me understand quantum mechanics and clear

exams. I thank her for listening to my problems and helping me solve them. I am also fortunate to have Kishore, Manoj, Venu, Ravinder who are my friends from school. I owe it to Kishore for all the travels that we made in Tamil Nadu by hopping into random buses and traveling throughout the state of Tamil Nadu during my initial days of Ph.D.

I am lucky to have a senior like Sugata da, who is always ready to help. I would like to thank him for the many conversations that we had during the unlocking phase of the pandemic. Through him, I got to know many things related to Bengali culture and literature. I remember we used to have after dinner and late night discussion on Rabindranath Tagore, Satyajit Ray and his films, about the *zaminder bari* durga puja celebrations and rituals and many more. I would also like to extend my thanks to Pradeep Chakravarthy, Periketi Naveen, Koneti Naveen, Deekshith Reddy, Abhishek, Bandagi Teja, Krishnakanth, Ganesh Maurya, Y Rakesh, Praveendra, Tanmaya, Arun, Ajay Rawat, Ajay Yerram, Alamgir, Dorodi, Jayakrushna, Bandita, Prachi, Rameswari, Subrata da, Lalita di, Shyam, Satyam, Nilam and many others for helping me in many different ways. I would also like to thank my *Malayali* friends Jasna, Nimitha, Anil, Vipula, Neetu, Jawhar, Ashwant, Sandeep, Shajil and others for teaching me so many things about Kerala and its culture and the food and for the *mund*.

Being a hosteller, no amount of research can be done without having proper edible food at hostel mess. I would like to thank all the mess workers at NRS hostel for providing somewhat edible food. I would also like to extend my thanks to all the house-keeping staffs for keeping the hostels neat and clean.

I acknowledge DST-INSPIRE, Govt. of India for the fellowship.

I would like to extend my heartfelt gratitude to all the doctors, nurses, researchers, frontline workers and all those who are involved in Covid-19 related works and helping us get back to the good old normal days in the future.

Anupam Dey

TABLE OF CONTENTS

			Page Nos.
1. 🤇	Chapter 1: Intr	<u>roduction</u>	
1.1.	Cell-fate decisions and regulatory motifs		
	1.1.1. Feedforward loops		
	1.1.2. Feedback loops		
	1.1.2.1.	Positive feedback loops	5
	1.1.2.2.	Interlinked positive feedback loops	6
	1.1.2.3.	Negative feedback loops	7
	1.1.2.4.	Interlinked positive and negative feedback loops	 7
1.2.	Mathemat	ical modelling of regulatory motifs	8
	1.2.1. Math	ematical modelling of a simple gene regulation	8
	1.2.2. Mathe	ematical modelling of a simple positive feedback loop	9
1.3.	Stochastic	ity and cell-fate decisions	15
	1.3.1. The o	rigin of stochasticity	15
	1.3.1.1.	Intrinsic noise	15
	1.3.1.2.	Extrinsic noise	16
	1.3.1.3.	Transcriptional bursting	17
	1.3.1.4.	Translational bursting	17
	1.3.2. Mathe	ematical modelling of a stochastic system	18
	1.3.2.1.	The general form of the chemical master equation	18
	1.3.2.2.	Gillespie algorithm	19
	1.3.3. Effect	of stochasticity on cell-fate decisions	21
	1.3.3.1.	Stochasticity and population heterogeneity	21
	1.3.3.2.	Stochasticity as a nuisance	21
1.4.	Previous w	vorks	23
1.5.	Aim and la	yout of the thesis	24
2.	Chapter 2: Ro	bustness of Tristable Networks with Fused Positive Feedl	oack Loops
2.1.	Introduction	on	27

2.2.	Mo	delling and methodology
	2.2.1.	Model networks and dynamical equations
	2.2.2.	Potential landscapes and bifurcation diagrams
2.3.	Res	ults and discussions
	2.3.1.	Robustness of tristable networks
	2.3.2.	Robustness of SATS
	2.3.3.	The origin of robustness
	2.3.4.	Sensitivity of model parameters
2.4.	Sun	nmary and conclusions
		r 3: Robustness of Networks with Positive Feedback Loops fused to
3.1.	Intr	oduction
3.2.	Мо	delling and methodology
	3.2.1.	The model networks
3.3.	Res	ults and discussions
	3.3.1.	Bifurcation analysis using the potential energy landscapes
	3.3.2.	Robustness of networks with AND gate configuration
	3.3.3.	The origin of the isola and mushroom bifurcations
	3.3.4.	Robustness of networks with OR gate configuration
	3.3.5.	Robustness of networks with MIXED gate configuration
	3.3.6.	Addition of a second PFL to the model networks
3.4.	Sun	nmary and conclusions
4.	<u>Chapte</u>	r 4: Arrangements of Multiple Positive Feedback Loops and the
,	<u>Robust</u>	ness of Bistable Switches
4.1.		oduction
4.2.		delling of the networks
4.3.	Res	ults and discussions
	4.3.1.	Modelling using AND-gate input signal configuration

	4.3.1.1.	Control of population heterogeneity in presence of extrinsic
		noise
	4.3.1.2.	Control of population heterogeneity in presence of intrinsic
		noise
	4.3.1.3.	Sensitivity of SN bifurcation points in presence of extrinsic
		noise
	4.3.1.4.	Sensitivity of steady states in presence of intrinsic noise
	4.3.2. Mo	delling using OR-gate input signal
	4.3.3. Mod	delling using Hill functions
.4.	Methodol	ogies and calculations
	4.4.1. Calc	ulation of differentiation-dedifferentiation percentages
	4.4.2. Calc	ulation of sensitivity of bifurcation points
	4.4.3. Calc	ulation of mean residence time (MRT)
l.5.	Summary	and conclusions
.1.	Introducti	on
.1.	Introducti Modelling	onand methodology
.1.	Introducti Modelling	onand methodology
.1.	Introduction Modelling 5.2.1. Med 5.2.1.1.	and methodology chanism of the binding dynamics Module 1: Positive feedback in ligand upregulation Module 2: Positive feedback in both ligand and receptor
.1.	Introduction Modelling 5.2.1. Med 5.2.1.1. 5.2.1.2.	on and methodology thanism of the binding dynamics Module 1: Positive feedback in ligand upregulation Module 2: Positive feedback in both ligand and receptor upregulation
.1.	Introduction Modelling 5.2.1. Med 5.2.1.1. 5.2.1.2. Results an	and methodology chanism of the binding dynamics Module 1: Positive feedback in ligand upregulation Module 2: Positive feedback in both ligand and receptor upregulation d discussions
.1.	Introduction Modelling 5.2.1. Med 5.2.1.1. 5.2.1.2. Results ar 5.3.1. Pos	and methodology chanism of the binding dynamics Module 1: Positive feedback in ligand upregulation Module 2: Positive feedback in both ligand and receptor upregulation d discussions
.1.	Introduction Modelling 5.2.1. Med 5.2.1.1. 5.2.1.2. Results ar 5.3.1. Pos	and methodology chanism of the binding dynamics Module 1: Positive feedback in ligand upregulation Module 2: Positive feedback in both ligand and receptor upregulation d discussions tive feedback in ligand upregulation: Single PFL tive feedback in both ligand and receptor upregulation: Fused
.1.	Introduction Modelling 5.2.1. Med 5.2.1.1. 5.2.1.2. Results ar 5.3.1. Pos 5.3.2. Pos PFLs	and methodology
3.	Introduction Modelling 5.2.1. Med 5.2.1.1. 5.2.1.2. Results are 5.3.1. Position 5.3.2. Position PFL: Summary	Module 2: Positive feedback in both ligand and receptor upregulation d discussions tive feedback in ligand upregulation: Single PFL tive feedback in both ligand and receptor upregulation: Fused and conclusions
.1. .2.	Introduction Modelling 5.2.1. Med 5.2.1.1. 5.2.1.2. Results ard 5.3.1. Pos 5.3.2. Pos PFL: Summary	and methodology chanism of the binding dynamics Module 1: Positive feedback in ligand upregulation Module 2: Positive feedback in both ligand and receptor upregulation d discussions tive feedback in ligand upregulation: Single PFL tive feedback in both ligand and receptor upregulation: Fused

List of Abbreviations

TF : Transcription factor

FFL : Feedforward loop

PFL : Positive feedback loop

NFL : Negative feedback loop

DNFL : Double negative feedback loop

EMT : Epithelial to mesenchymal transition

SS : Steady state

SN : Saddle-node

MA : Mutual activation

MI : Mutual inhibition

SA : Self-activation

MIMI : Mutual inhibition mutual inhibition

MIMA : Mutual inhibition mutual activation

MAMA : Mutual activation mutual activation

MISA : Mutual inhibition self-activation

MASA : Mutual activation self-activation

SATS : Self-activating toggle switch

BS : Bistability

TS: Tristability

NI : Normal isola

NM : Normal mushroom

II : Inverted isola

IM : Inverted mushroom

Chapter 1

Introduction

1.1. Cell-fate decisions and regulatory motifs

The cell that forms the fundamental unit of life is a miniature biochemical machine that plays many crucial and complex roles in supporting life. There are receptors present on the cell surface that receive signals from the environment. There are receptors inside the cell as well that check for cytoplasmic pH, damaged proteins or DNAs, availability of energy and various internal requirements. A cell is continuously processing these information, making decisions and exhibiting appropriate responses that include gene expression, metabolic activities, growth, movements, cell-division, cell lineage determination and apoptosis. The process of a cell to make decisions according to the stimuli is known as cell-fate decision making processes^{1–4}. Cell-fate decisions are cellular processes where a cell decides upon its future cell-types and functions. The differentiation of pluripotent stem cells into different cell types that forms the organs during embryo development^{5–8}, the decision a cell makes at each phase of the cell-cycle whether to continue or withdraw from the cycle^{9–11}, the differentiation of

multipotent hematopoietic stem cells into different blood cell types^{12–14} are a few examples of cell-fate decisions. Cell-fate decisions are crucial for cell's growth, survival, proliferation, adaptation, differentiation, lineage commitment, and apoptosis.

The cell-fate decision network host interactions of large number of genes and proteins forming complex network pathways through which the cell process information¹⁵. Proteins are one of the most important biomolecules that play important roles as regulatory entities in these complex networks. Proteins function as receptors and transducers of signals, as output generating moieties, as transcription factors regulating the gene expression and many such crucial functions. The decision making is mainly done by proteins, genes, and RNA molecules that regulate each other's synthesis, degradation, localization and a variety of activities through biochemical reactions that are connected via feedback and feed forward loops with high complexity. The complex biological networks are analogous to the electrical circuits. In electrical circuits, resistors, capacitors, inductors are connected by means of current carrying wires whereas in biological networks, proteins, genes, mRNAs are connected through biochemical interactions.

A cell receives varieties of signals from the environment and responds to these signals by producing appropriate proteins through the process of gene expression regulated by special proteins called transcription factors (TFs) that carry out the burden of regulating gene expression. The TFs bind to the DNA at specific promoter sites and regulate the rate of transcription. Following the binding of the TFs, the mRNAs are transcribed which are then translated into proteins. These proteins can then act on the signals it receives from the environment. Since the cell-fate decision systems have complex networking pathways, it is quite difficult to study them at the systems level. Previous studies suggest that the complex biological network system contains several 'smaller sub-network' patterns that occur frequently and forms the simple building blocks of the larger complex network. These smaller building blocks are termed as network 'motifs'^{16–18}. Network motifs often form the core regulatory networks that regulate the cell-fate decisions. Therefore, study of these network motifs are of paramount importance and helps in understanding the larger complex network pathways of the biological system and its functions.

A network motif usually consist of nodes and edges where the nodes represent the biomolecules such as proteins, genes, TFs, DNAs, mRNAs, etc. and the edges are the biochemical interactions between the nodes. It was in *Escherichia coli* that the network motifs were first defined and studied in a systematic manner¹⁷. The transcription network in *Escherichia coli* were found to have repeated patterns of smaller network motifs. Regulatory motifs are often found in signalling networks and play important roles^{19,20} in signal processing and transduction such as in maintaining homeostasis in the internal functioning of the cell, generating sustained oscillations²¹, in crucial cellular decision making processes such as cell fate and lineage^{22,23} and cellular development²³. Regulatory motifs can be of various types based on the type of interactions between the nodes. The interactions between the nodes can be unidirectional or bidirectional and the regulations can be positive or negative. Positive regulations correspond to activation and negative regulation correspond to inhibition or repression. Based on the type of interactions, the regulatory motifs are named as 1) feedforward loops 2) feedback loops. In the next section, we shall discuss about different regulatory motifs and their functions.

1.1.1. Feedforward loops

A feedforward loop (FFL) is a signalling network motif where a target gene Z is regulated by an input TF, X, either directly (direct arm) or indirectly (indirect arm) through an intermediate TF, Y (Figure 1.1). The FFLs are categorized into two types based on the nature of the regulations between the input and the output node²⁴. A positive regulation (arrow-head bars) represent an activation and a negative regulation (T-head bars) represent an inhibition. If the regulatory signs of the direct and indirect arms are same (either positive or negative), then the FFL is known as a coherent FFL and if they are of opposite signs then the FFL is known as an incoherent FFL. Based on different combinations of positive and negative regulations, the FFLs are of eight types, four of them are coherent and four of them are incoherent types. Incoherent FFLs are sign-sensitive accelerators²⁴- they speed up the response of the output node. On the other hand, coherent FFLs delay responses. Incoherent FFLs can also act as

pulsers 24 . FFLs form the most important regulatory motifs in *Escherichia coli* and also in yeast 16,17 .

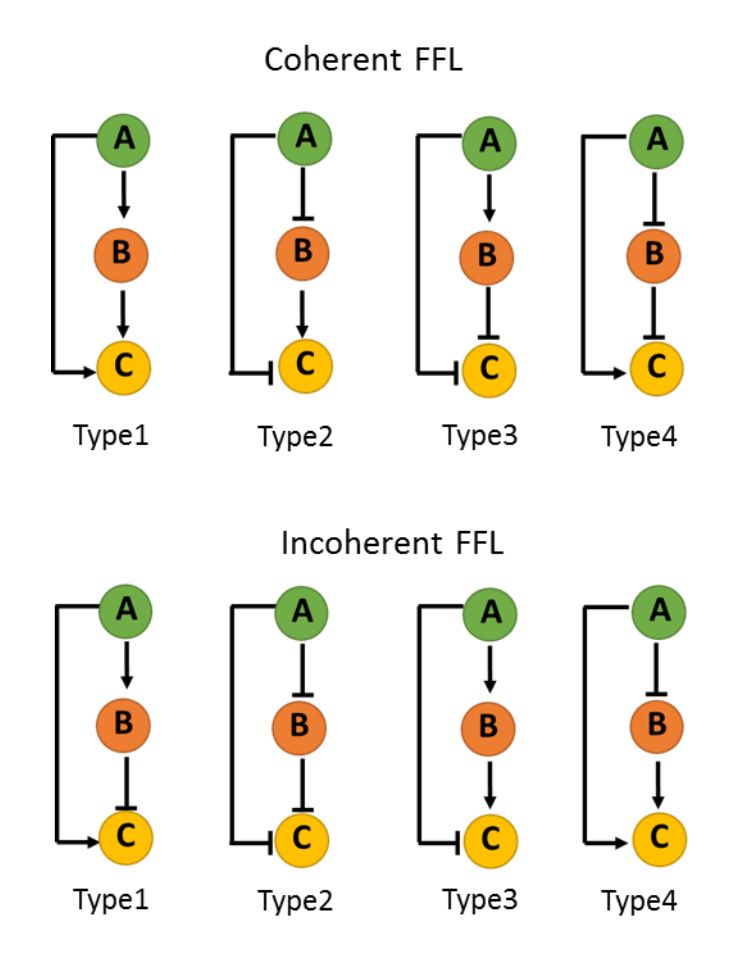


Figure 1.1: Network diagrams of Feedforward Loops (FFL): The two different categories of FFL, coherent (upper panel) and incoherent (lower panel). Each of them has four subtypes shown as Type1, Type2, Type3 and Type4. The arrows represent activation and the T-head bars represent inhibition.

1.1.2. Feedback loops

Feedback loops are networks where the output of a node is fed as input to the same node. Feedback loops are of two types: 1) Positive feedback loop (PFL) and 2) Negative feedback loop (NFL) (Figure 1.2). A PFL is one where the input and the output nodes mutually help each other (Figure 1.2, left panel). The nodes can have regulations with either of them being positive (mutual activation) (Figure 1.2b, left panel) or either of them being negative (mutual

inhibition) (Figure 1.2c, left panel). A mutual inhibitory loop is also known as a double negative feedback loop (DNFL) which is effectively a PFL. A NFL is one where the output and input nodes have opposite functions or regulations (Figure 1.2, right panel). A feedback loop can consist of a single node known as 'self-regulation' or it can have several nodes. In self-regulation, the node self-activates or self-inhibits its own activity (Figure 1.2a, both panels). In a feedback loop with several nodes, the overall sign of the network decides if it is a positive or negative feedback loop. In a circular network, if there are only positive regulations or even number of negative regulations then it is a PFL (Figure 1.2d-f, left panel) overall. Similarly, if there are odd number of negative regulations in a circular network then it is a NFL overall (Figure 1.2c-d, right panel).

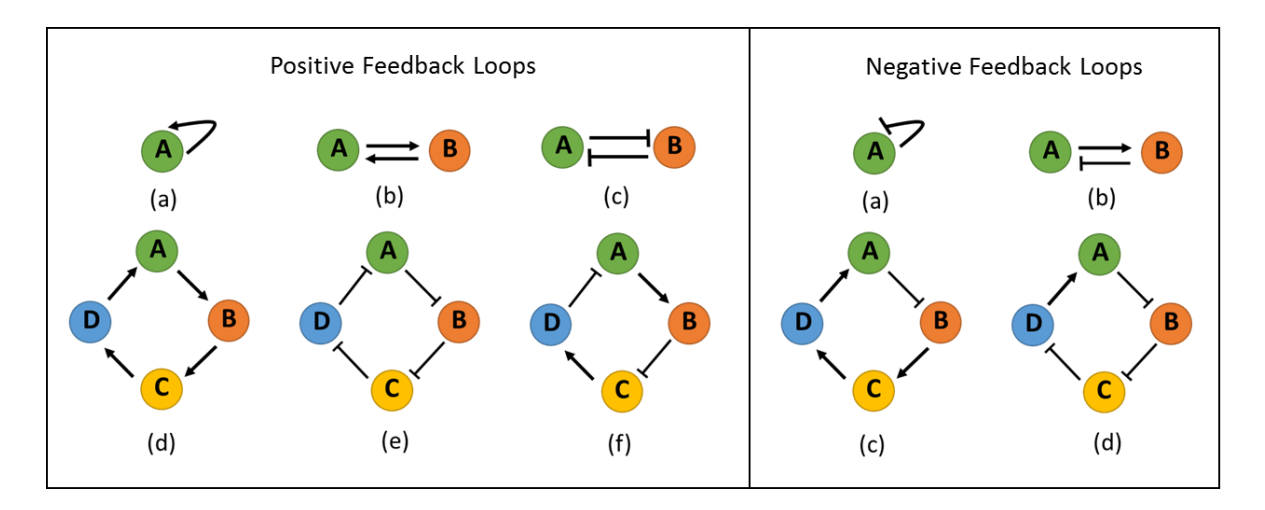


Figure 1.2: Network diagrams for Positive and Negative feedback loops: Left panel: Different types of PFL; self-activatory (a), a mutual activatory PFL (b), a mutual inhibitory or double negative feedback loop (DNFL) (c), circular signalling cascades (d-f). Right panel: Different types of NFLs; self-inhibitory (a), a classic NFL (b), circular cascades (c-d).

1.1.2.1. Positive feedback loops

One of the most important roles of a PFL is that it can amplify signals^{25,26}, where, for a small change in input the change in output is abrupt or large. The other important role is that under proper circumstances PFLs can generate bistable and multistable switches^{27–30}. PFLs are known to regulate many cell-fate decision making systems. The lysis-lysogene decision

making circuit in *Bacteriophage lambda* consist of a PFL³¹. The metabolic gene expression of lactose utilization in *Escherichia coli* and galactose utilization in *Saccharomyces cerevisiae* exhibit bistability that is complimented by the presence of PFLs^{32–34}. One of the firsts synthetically engineered PFL is the construction of a genetic toggle switch in *Escherichia coli* to establish conditions necessary to exhibit bistability³⁵. A PFL with sufficient ultrasensitivity or non-linearity in the feedback system is enough to produce bistability^{27–30}. Bistability is a phenomena that the cell utilizes during crucial decision making processes such as in cellular differentiation^{36–38}, memory^{39,40}, *Xenopus* oocyte maturation^{41,42}, cell-cycle^{43–45}. A bistable system has the capacity to convert a graded signal into a digital switch-like "all-or-none" response^{28,46}. In the context of cellular differentiation, bistable switches regulate epithelial to mesenchymal transitions (EMT)³⁷, adipocyte differentiation³⁶ and osteogenic-myogenic differentiation⁴⁷.

1.1.2.2. Interlinked positive feedback loops

A single PFL can have a single node with self-activation or can have two nodes with mutual inhibition or mutual activation between the nodes. In addition to this, often times the PFLs are coupled to each other forming interlinked PFLs. In fact, it is quite intriguing that a large number of physiological or cellular systems such as cell cycle, polarisation of budding yeast, maturation of *Xenopus* oocytes, calcium signalling, adipocyte differentiation, p53 regulation, eukaryotic chemotaxis, B cell fate decision making, EGF receptor signalling, Bcl2 apoptotic switch have interlinked PFLs as their core regulatory motifs. There are many benefits of interlinked PFLs over a single unit of PFL. One of them is that it produces bistable region over a large parameter space (cellular conditions) that is otherwise not achieved using a single PFL²⁶. This was demonstrated experimentally by constructing a synthetic gene circuit in *Escherichia coli*³⁹.

1.1.2.3. Negative feedback loops

NFLs consist of antagonistic regulations between the participating nodes. The most important role of a NFL is maintenance of homeostasis in cellular systems²⁶. NFLs can also generate oscillatory responses^{48–50}. Few examples of systems with negative feedbacks are circadian rhythms and NF-κB oscillations^{21,51}. A NFL in general, attenuates noisy signals in a system by supressing signal amplitudes^{25,26}. A NFL can respond more rapidly compared to a PFL thus making quick and prompt decisions at crucial times. Interlinked NFLs generate sustained oscillations as seen in many circadian networks and chemotactic signalling network in amoeba. Coupled NFLs can generate sustained oscillations from a damped oscillation generated by a single NFL.

1.1.2.4. Interlinked positive and negative feedback loops

NFL forms the core regulatory network motif in many biological systems like circadian systems^{21,52,53}, cAMP signalling⁵⁴, glycolysis⁵⁵, somitogenesis^{56,57}, DNA damage response (p53)²³, NF-κB signaling systems. However this core negative feedback motif is often accompanied by a positive feedback motif in these systems thus forming an interlinked positive-negative feedback loop. A coupled PFL and a NFL has properties of both individual positive and negative feedback loops. A PFL has a delayed response time and a NFL has a smaller response time whereas a coupled PFL-NFL has an intermediate response time. If the NFL is stronger than the PFL, generating a bistability is quite difficult and oscillations are induced instead. A coupled PFL-NFL can filter out noisy signals with optimum response time. While a PFL can produce bistable response, a NFL helps in efficient switching rates between different phenotypic states^{58,59}.

Often times, owing to the complexity of the regulatory networks, experimental analysis of the underlying biological system becomes difficult at the systems level. Mathematical modelling of regulatory motifs is an important tool to achieve a better understanding of the system and its dynamics. Mathematical modelling can also validate experimental data and predict future

outcomes. In the next section, we shall discuss about the mathematical modelling and modelling methodologies of gene regulations.

1.2. Mathematical modelling of regulatory motifs

1.2.1. Mathematical modelling of a simple gene regulation

Consider a TF, A, that positively regulates its target gene B according to the network motif $A \rightarrow B$. The positive regulation of A on B means that as the concentration or the activity of A increases, the concentration or the activity of B increases. Thus, the rate of change of expression or activity of B is a function of concentration of A and is represented as

$$\frac{dB}{dt} = \beta_0 + f(A) - \gamma_B.B \tag{1.1}$$

where, X represents either the number of molecules or concentration of the species X. The right-hand side of the equation has three terms. The first term β_0 is the basal synthesis rate of B which is a non-zero minimal expression rate. The second term, f(A), is the regulated synthesis rate of B and the third term, γ_B . B, is the degradation rate of B where γ_B is the degradation constant of B. The function f(A) is usually a monotonic sigmoidal shaped function that increases with A. The function f(A) can be represented as a Hill function some some some some some signoidal shaped is commonly used to represent gene regulation. In this regulatory network where A activates B, the Hill function represent the equilibrium binding of the TF, A, to the promoter sites of the gene B thus activating its expression. The function f(A) in Eq. 1.1 is given as

$$f(A) = \frac{\beta \cdot A^n}{K^n + A^n} \tag{1.2}$$

There are three parameters here, K, β and n that determine the behaviour of the function f(A) with A. β is the maximal expression rate of gene B. The maximal expression rate is reached when $A\gg K$. At high concentrations of A, the probability of A binding to the promoter in B is high which causes the gene B to produce more number of proteins per unit time. K is the activation coefficient which is defined as the amount of A needed to activate gene B. At K=A, the expression rate of the gene B is half-maximal $\left(\frac{\beta}{2}\right)$. The parameter n

represents the Hill coefficient that controls the steepness (ultrasensitivity) of the Hill function. The steepness of the Hill function increases with increase in n. The Hill coefficient also describes the cooperativity of the binding dynamics.

- Positive cooperativity (n > 1): Binding of the TF A to the promoter region of gene B
 increases the affinity of binding of subsequent TFs to the same promoter.
- Negative cooperativity (n < 1): Binding of the TF A to the promoter region of gene B
 decreases the affinity of binding of subsequent ligands to the same promoter.
- Noncooperativity (n = 1): Binding of the TF A to the promoter region of gene B does
 not alter the affinity of binding of subsequent ligands to the same promoter.

For A inhibiting B, $A \dashv B$, the Hill function will be a decreasing sigmoidal shaped curve and is represented by the equation

$$f(A) = \frac{\beta}{K^n + A^n} \tag{1.3}$$

Here, *K* is the repression coefficient and the meaning of all other parameters remain same as in the Eq. 1.2. The Hill function approaches a saturating value at large concentration of A. The approach to the saturation is due to the fact that the probability of A binding to the promoter of gene B cannot exceed 1. Having constructed a mathematical modelling methodology for a simple gene regulation, in the next section, we extend the methodology to a simple PFL.

1.2.2. Mathematical modelling of a simple positive feedback loop

Mathematical modelling of a PFL can be an useful tool in understanding bistable phenomena observed in many biological systems. Consider a simple two component PFL between A and B where A and B either mutually activate or inhibit each other (**Figure 1.3**). If A and B mutually activate each other, higher concentrations of A will produce higher concentrations of B and vice-versa. If A and B mutually inhibit each other higher concentration of A will produce lower concentrations of B and vice-versa. Let S be an input signal activating A.

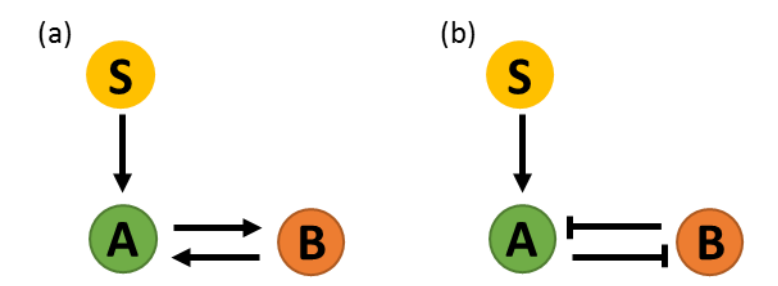


Figure 1.3: The network diagrams for a single positive feedback loop. (a) PFL with mutual activation between A and B. (b) PFL with mutual inhibition between A and B. S is an input signal.

Using the Hill function, the dynamical equations corresponding to A and B in the PFL network motif (**Figure 1.3a**) can be represented as

$$\frac{dA}{dt} = k_A + k_1 \cdot S + k_2 \cdot B - \gamma_A \cdot A \tag{1.4}$$

$$\frac{dB}{dt} = k_B + \frac{\beta \cdot A^n}{K^n + A^n} - \gamma_B \cdot B \tag{1.5}$$

Similarly, the dynamical equations corresponding to A and B in the DNFL network motif (Figure 1.3b) can be represented as

$$\frac{dA}{dt} = k_A + k_1 \cdot S - k_2 \cdot A \cdot B - \gamma_A \cdot A \tag{1.6}$$

$$\frac{dB}{dt} = k_B + \frac{\beta}{K^n + A^n} - \gamma_B.B \tag{1.7}$$

These dynamical equations are deterministic in nature whose exact solutions can be tracked over time. The steady state (SS) equation of A is obtained by setting dA/dt=0 and the SS equation of B is obtained by setting dB/dt=0. The SS equation of A and B are known as nullclines and are plotted as phase-plane diagrams. In the top panel of **Figure 1.4**, the phase-plane (a) and bifurcation diagrams (b,c) for the PFL network are plotted and in the bottom panel of **Figure 1.4**, the phase-plane (d) and bifurcation diagrams (e,f) for the DNFL network

are plotted. The non-linear curves (red, black) in the phase-plane diagrams are the B-nullclines whereas the straight lines (various colors) are the A-nullclines. The A-nullcline move up and down with varying parameter value of S. The point of intersection of the two nullclines represent a SS of the system. For a single intersection, the SS value is always stable and for three intersections, the SSs at the extreme points are stable with unstable SS in between. In the figure, the black filled circles represent the stable and the red filled circles represent the unstable SSs. The loci of the stable and unstable SSs with respect to a parameter is known as a bifurcation diagram and the parameter is known as the bifurcation parameter.

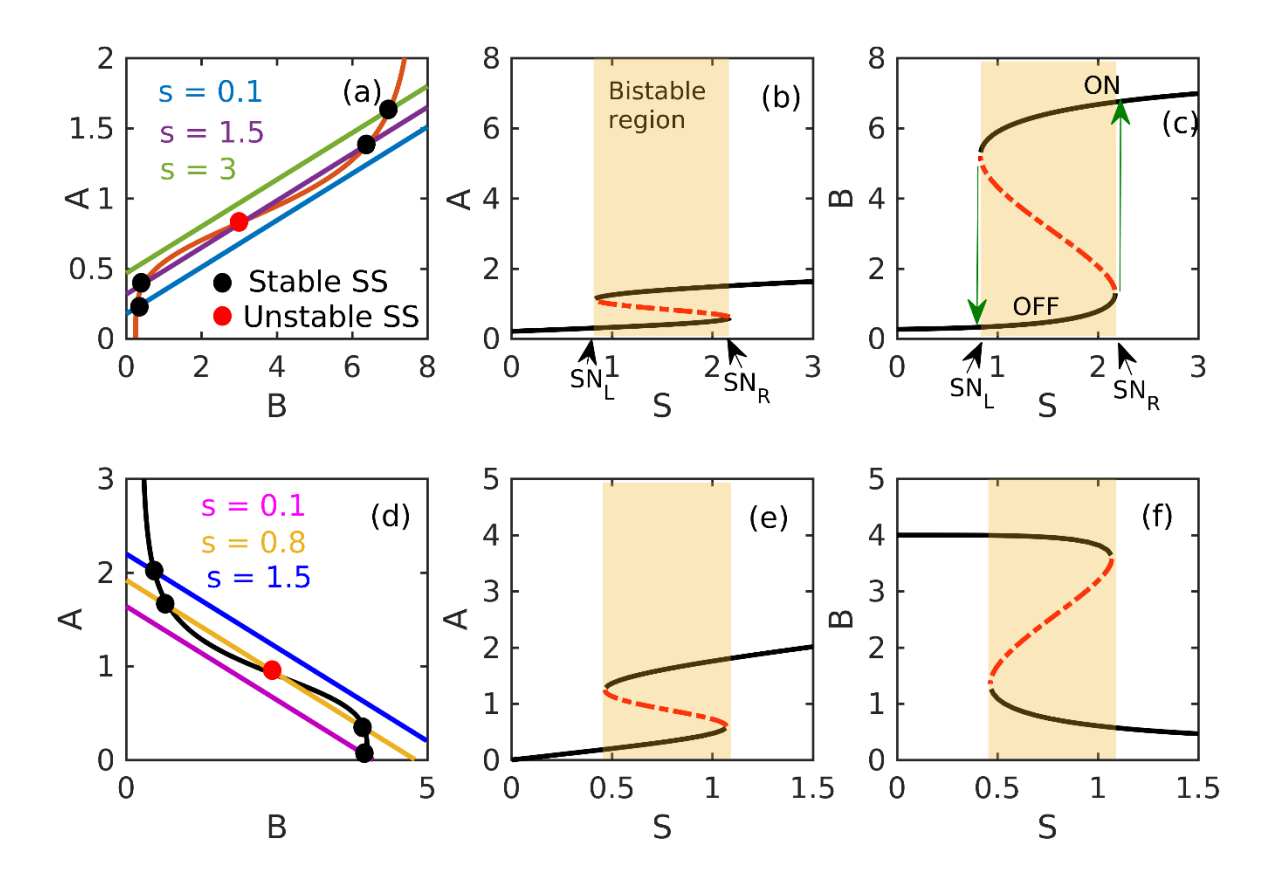


Figure 1.4: Phase-plane and bifurcation diagrams: Top panel (a,b,c): The phase-plane (a) and 1-parameter bifurcation diagrams (b,c) for the classic PFL (mutual activation) network. Bottom panel (d,e,f): The phase-plane (d) and the 1-parameter bifurcation diagrams (e,f) for the DNFL (mutual inhibition) network. The nonlinear line and the straight lines in the phase-plane diagrams represent B nullcline (red and black) and A nullclines (various colors), respectively. The red and black filled circles represent the stable and unstable SSs, respectively. In the bistable bifurcation diagrams, the black solid and the red broken lines

represent the stable and unstable SSs, respectively. The two saddle-node (SN) bifurcation points are shown by arrows as SN_L (saddle-node left) and SN_R (saddle-node right) (b). The green arrows show the transition from OFF to ON state and vice versa (c).

In **Figure 1.4**, (b) and (e) represent the bifurcation for A and (c) and (f) represent the bifurcation for B. Since, there are two stable SSs (black solid lines) separated by an unstable SS (red broken line), this type of bifurcation is known as a bistable bifurcation diagram. The signal value where the stable and unstable SSs coalesce and destroy each other are known as saddle-node (SN) points (**Figure 1.4b**). In case of a reversible bistable diagram, there are two SN points, one at lower S value (SN_L) and one at higher S value (SN_R). The region between two SN points in the bifurcation diagram (yellow region) represent the bistable region where the two stable SSs co-exists simultaneously for a certain range of S values. For A and B mutually activating network (PFL), at low S, the SS values of both A and B are low and at high S, the SS values of both A and B are high (**Figure 1.4b-c**). For A and B mutually inhibiting network (DNFL), at low S, the SS value of A is low whereas the SS value of B is high and at high S it is the opposite (**Figure 1.4e-f**). In a bistable system, the transition from one stable SS to another stable SS occurs at the SN points. The SN points are also known as the threshold points where SN_R is associated with ON threshold and SN_L is associated with OFF threshold (**Figure 1.4c**).

In the context of cell physiology, each of these different stable SSs (lower and upper) represent a distinct phenotypic state of the cell. In a bistable system, depending on the initial concentrations of the molecular species (variables), the system can converge into one of the two stable SSs. For example, adipocyte cellular differentiation is governed by a bistable switch and PPARG is a protein that regulates the differentiation process. Based on the expression level of PPARG, lower stable SS (OFF-state) represent the undifferentiated state of the adipocyte cells whereas the upper stable SS (ON-state) represent the differentiated state 61 . In the lactose utilization system of the *Escherichia coli*, mediated by *lac* operon, the activity of the β -galactosidase can converge into one of the two stable SSs depending upon the initial concentrations of the molecular species involved 62 . Similarly, in cell cycle system, interphase and mitosis are the two stable states corresponding to low and high activity of the kinase Cdc2, respectively 41,63,64 . In the eukaryotic cell cycle, a PFL is formed by Cdc25 and Wee1 on Cyclin B-Cdk. With changing cyclin concentration, the Cdk activity exhibit bistability with one

stable SS representing the interphase state and the other stable SS representing the mitotic state of the cell cycle^{41,42,63,65}. Bistability is also known to regulate many of these cell fate determination systems^{40,66–70}. The bistable system is associated with hysteresis^{28,70} meaning the system's ability to shift between the alternate stable SS at a range of signal values^{28,71}. A bistable system can be reversible or irreversible. In case of a reversible bistable system, there are two SN points and the system can transition to an alternate stable SS with decrease or increase in signal values. While in case of an irreversible bistable system there is only a single SN point and after the transition to an alternate stable SS, the system is unable to transition back to the initial stable SS of the system^{71,72} when the signal is removed.

While a single PFL generates bistability, interlinked PFLs can generate tristability (Figure 1.5) and multistability. The bistable, tristable and multistable switches are known as biological switches and play crucial roles in regulating cell-fate decisions. The interlinked PFL can be through a self-activation on one of the nodes (Figure 1.5a-b) or can be through a third-component via mutual activation or mutual inhibition (Figure 1.5c-e). A tristable switch has three stable SSs separated by two unstable SSs and has four different SN bifurcation points (Figure 1.5f).

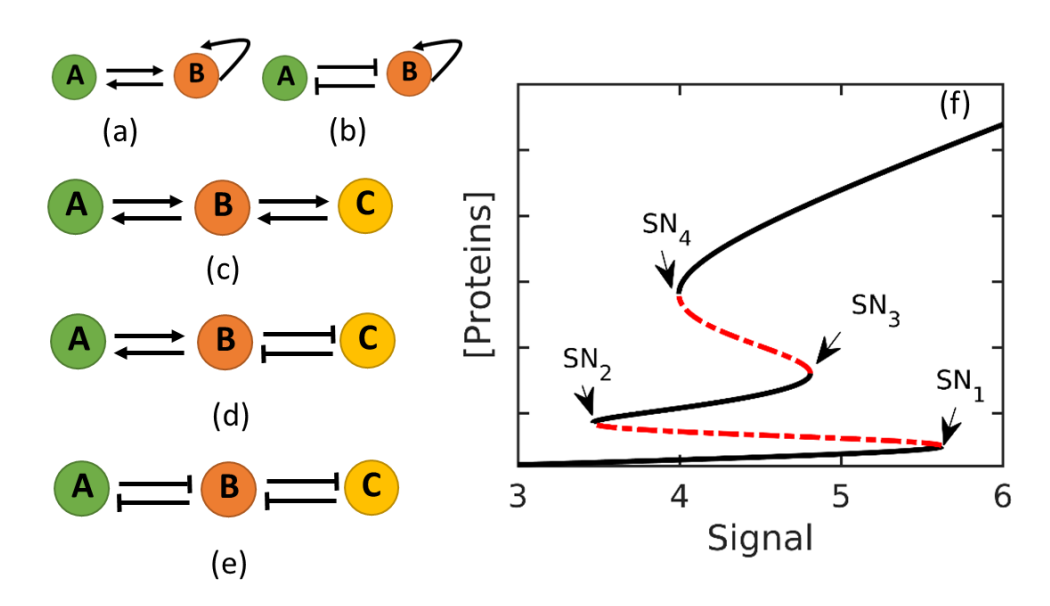


Figure 1.5: Interlinked positive feedback loops: Different types of 2 and 3-component interlinked PFLs. A mutual-activation-self-activation (MASA) motif (a), a mutual-inhibition-self-activation (MISA) motif (b), a mutual-activation-mutual-activation (MAMA) motif (c), a

mutual-inhibition-mutual-activation (MIMA) motif (d), a mutual-inhibition-mutual-inhibition (MIMI) motif (e). A tristable bifurcation diagram of the interlinked PFLs (f). The black solid and red broken lines are stable and unstable SSs respectively. The SN points are indicated accordingly.

In general, in a biological switch, there are 'm' number of stable SSs separated by 'm-1' number of unstable SSs, where m is a positive integer. The tristable switch has an intermediate stable SS that enhances the phenotypic plasticity of the system. A phenotypic plasticity is the organism's ability to adapt to different phenotypic states in response to variation in environmental conditions in order to grow and survive and is considered as an evolutionary strategy. The more the number of phenotypic states the better the chances of the cell's growth and survival under fluctuating environment. In a tristable system, when the three different phenotypic states coexist for some values of control parameter, it is observed both experimentally and theoretically that the most probable state is the intermediate stable SS⁷³. There are many biological systems that exhibit tristability, for example, differentiation of naïve CD4+ T cells^{74,75}, Th1/Th2 differentiation⁷⁶⁻⁷⁸, macrophage-neutrophil differentiation^{68,79}, epithelial-to-mesenchymal transition (EMT)^{37,80}.

When two PFLs were interlinked it resulted in a bigger region of bistability over a broader range of inducer concentrations. When one of the PFLs was removed, the bistable region decreased. It has been observed that an additional PFL to a bistable network shifts the right and left SN points towards right and left respectively thus widening the bistable region⁸¹. Another benefit of coupled PFLs in many biological systems is that if the different PFLs function at different time scales (fast and slow) they make the system more robust and stable. For example, in experimental studies of budding yeast polarisation, the interlinked fast and slow PFLs generated a bistable switch. The slow PFL regulated the polarised ON state and the fast PFL regulated the speed of switching between the unpolarised OFF state and the polarised ON state⁸².

Regulatory motifs serve as the core functional motifs in many cell-fate decision making systems. A biological cell is constantly under the influence of chemical noise or stochasticity which can cause detrimental effect on the smooth and accurate functioning of the cell.

Therefore, it is important to understand the various sources of stochasticity and its effects on the cell-fate decisions.

1.3. Stochasticity and cell-fate decisions

1.3.1. The origin of stochasticity

The process of gene expression, inherently, is random and therefore produces noisy outcomes. In two genetically identical cells, over time, a gene will not produce the same number of mRNAs and proteins even if the cells are kept in identical environmental conditions^{83–89}. This is due to the fact that the copy number of biological molecules like genes, mRNAs, proteins, TFs are low in numbers because of which the chemical reactions are discrete and random. For example, in a single bacterial cell, the mean copy number of genes are 1-2, mRNAs are 1-30 and proteins are 10^2 - 10^6 . These low copy number of biomolecules react with each other to form products. The reaction events are random and discrete in nature which gives rise to stochastic fluctuations in the protein or mRNA abundance over time. Experimental evidences suggest that the number of proteins and mRNAs show remarkable cell-to-cell variability in an isogenic population of cells ^{83,84,87,90–92}. Experimental evidences of cellular variations dates back to 1957 where Novak and Weiner showed that the expression level of the gene producing the enzyme beta-galactosidase in individual Escherichia coli cells was not equal and was highly variable and random ³². The origin of cell-to-cell variability can be tracked down to two sources: the extrinsic noise source and the intrinsic noise source. Together these sums up the total cellular noise 84,88.

1.3.1.1. Intrinsic noise

In an isogenic population of cells, even if all the extrinsic sources of noise are identical, the end products of gene expression will be inherently noisy and each cell will have different amounts of mRNAs and proteins thus giving rise to cell-to-cell variability. This is due to the presence of finite copy number of the reacting species because of which the events in the gene expression are random and hence generate noisy outputs. This is inherent to the chemical reaction and is known as intrinsic noise which arises from the discrete nature of the chemical reactions in gene expression. Intrinsic noise also gives rise to extrinsic noise.

1.3.1.2. Extrinsic noise

In a population of genetically identical cells, each cell is different from the other in terms of its shape, size, density of the cytoplasm, pH, cellular pressure, stage in the cell cycle and number of the participating molecules. These sources of perturbations or noise that differ between isogenic cells is known as extrinsic noise.

Elowitz et al. experimentally demonstrated the consequences of presence of both sources of noise 84. They built copies of Escherichia coli by incorporating the cyan and yellow alleles of green fluorescence proteins as the reporter genes. The two reporter genes were controlled by identical promoters in each copy. In presence of extrinsic noise only, they observed that in a clonal population of Escherichia coli, both the proteins were produced in same quantity in each cell but were different from cell to cell. They also observed that in presence of intrinsic noise only, the amount of proteins produced by the two genes were different in each cell as well as in different cells. Thus, in a population, due to presence of intrinsic noise, a fraction of cells expresses higher level of one of the fluorescent proteins than the other thus giving rise to a population heterogeneity. The presence of stochasticity in gene expression can be quantitatively visualized by experimentally measuring the relative amount of proteins produced by genetically identical living cells using fluorescent proteins ^{83,84,87,91}. However, the measurement of protein abundance using reporter genes is actually the combined result of transcription and translation since the amount of mRNAs are not accounted for. It was much needed to analyse single-mRNA resolution in a single cell to better understand how mRNA expression effects the variability in gene expression. Much later, through the advancement of experimental tools such as single molecule RNA fluorescence in-situ hybridization (sm-FISH) and MS2 tagging, it was revealed that the genes are expressed in a pulse like manner or as bursts 88,92-94.

1.3.1.3. Transcriptional bursting

The pulse-like or the burst phenomena in mRNA production can be theoretically better understood by the two-state random telegraph model ^{83,84,87,90,91,95}, which explains that the gene has two states, namely, the active or the ON state and the inactive or the OFF state ^{92,95–98}. It is only in the active (ON) state that the gene can be transcribed and there is no transcription in the inactive (OFF) state. The transition between these two states is random and mRNAs are produced in short bursts when the gene is in active state. Transcriptional bursting can give rise to cell-to-cell variability in the amount of mRNAs produced in genetically identical cells. Because of the transcriptional bursts, the amount of mRNAs produced will follow a population distribution rather than a single deterministic value. The possible mechanisms reported in recent studies show that the ON and OFF states of the gene is caused by the supercoiling of the DNA during transcriptional elongation ^{99,100} and promoter architecture ¹⁰¹ that ultimately results in transcriptional bursting. After the mRNAs are produced in bursts, the mRNAs also undergoes degradation after a short lifetime.

1.3.1.4. Translational bursting

The mRNAs are translated into proteins until they degrade. Therefore, just like the mRNAs, the proteins are also produced in bursts by these short-lived mRNAs and the protein bursts seize to exist when the mRNAs degrade. This phenomena is known as the translational bursting¹⁰² and has been identified in single molecule experiments¹⁰³.

Just like the production of mRNAs follows a population distribution because of the transcriptional bursting phenomena, protein production over time also follows a similar population distribution because of the translational bursting. The bursting phenomena is inherent to the system and can be advantageous as well as disadvantageous to the functioning of the cell depending upon the circumstances. Several biological circuits regulating gene expression has to carry out the process in presence of this inherent stochasticity. While in many cellular processes, it is necessary to filter out the noise in order to function efficiently and robustly¹⁰⁴, this noise can also be utilized by the cells to adapt to

different useful situations and switch between phenotypes under stressful environmental conditions ¹⁰⁵. To better understand how the dynamics of the regulatory motifs are altered by the chemical noise, it is important to incorporate stochasticity into the mathematical modelling of the regulatory motifs. In the next section, we shall discuss about the mathematical modelling of chemical noise.

1.3.2. Mathematical modelling of a stochastic system

Mathematically, in presence of stochasticity, a system of chemical reactions can be modelled using the well-known Chemical Master Equation (CME)^{106,107}. The CME is a system of dynamical equations that measures the probability of a system to be in a particular state at a given time. The CME can be considered as a jump type Markov process where the current state of a system is achieved by two jump processes, arriving to the current state from the preceding state and leaving the current state.

1.3.2.1. The general form of chemical master equation

For a well stirred system with constant temperature and fixed volume, let there be $S_1, S_2, ..., S_N$ number of chemical species reacting. Let the number of chemical reactions occurring be $R_1, R_2, ..., R_M$. Let $\boldsymbol{X}(t) = (n_1, n_2, ..., n_N)$ be the state of the system at a given time t, where n_i is the number of molecules of the i-th chemical species. Each reaction R_j is associated with a propensity function a_j and state-change vector element v_{ji} where the propensity function a_j is the probability that only one reaction R_j will occur accordingly in the time between t and t+dt. The state-change vector element v_{ji} counts the change in the number of molecules of S_i chemical species after a reaction R_j occurs between t and t+dt.

The General form of the CME is given as

$$\frac{dP(X,t)}{dt} = \sum_{i=1}^{M} [a_i(X - v_i)P(X - v_i) - a_i(X)P(X)]$$
(1.8)

Eq. 1.8 is the general form of the chemical master equation (CME), which is a state-discrete equation in a continuous time. The left-hand side of the equation is the rate of change of probability of the system to be in state X at time t. The right-hand side of the equation has two terms. The first term is the rate of probability of arriving at state X at time t and the second term represents the rate of probability of leaving state X at time t.

Solving for P(X,t) in the equation reveals information about the state X(t) of the system. Finding the exact solution of the CME is a difficult task because of the high dimensionality of the system which arises due to the many number of possible states of the system under consideration. An alternate method known as the Gillespie algorithm is discussed in the next section which exactly captures the dynamics of the CME.

1.3.2.2. Gillespie algorithm

Computationally, the solutions of the CME can be obtained by iterating an ensemble of stochastic trajectories over time and finding the mean of the ensemble. Such ensemble of stochastic trajectories can be generated using the Stochastic Simulation Algorithm (SSA) formulated by D.T. Gillespie ¹⁰⁸. Popularly known as the Gillespie Algorithm and also known as 'next reaction' method, this method makes an assumption that all the reactions are Markovian and the time for the next reaction is calculated based on the current state of the system. Consider the same system as explained above with N number of chemical species and M number of reactions with propensities $a_i(X)$ and X(t) as the state of the system. The time to the next reaction 'dt' is randomly selected from the exponential distribution with mean $\frac{1}{a_0}$ where $a_0 = \sum_{j=1}^M a_j(X)$ the sum of all the propensities of all the reactions. The next step is to find which reaction takes place out of the M possible reactions. The possibility of occurrence of a reaction is decided by the probability of $\frac{a_j(X)}{a_0}$. The time t is advanced to t+dt and the number of molecules of the chemical species are updated depending on the reaction that has occurred in the time interval dt. Using this method many time dependent stochastic solution trajectories of the functions are generated. The mean of ensemble of the stochastic trajectories for a system having dynamical equations expressed as mass-action

kinetics is equal to the deterministic mean. Thus this method is useful in finding the exact solution of a stochastic system.

The noise is measured in terms of coefficient of variation (CV) which is defined as the ratio of standard deviation to the mean and typically scales as $CV \propto 1/\sqrt{N}$, where N is the population number of random variable. This means that if the population number is low, the noise is large and the noise reduces with increase in the population number. To show the effect of population number on the measure of CV, stochastic trajectories for low and high (Figure 1.6) number of mRNAs and proteins are generated using the Gillespie's SSA for the gene expression model where the mRNAs and proteins are produced with constant synthesis rate and are exponentially degraded. From the figures, it is clear that the CV for the population distribution of mRNAs and proteins are relatively high (noisier) when less number of proteins and mRNAs (Figure 1.6, left panel) are present compared to their high abundance (Figure 1.6, right panel).

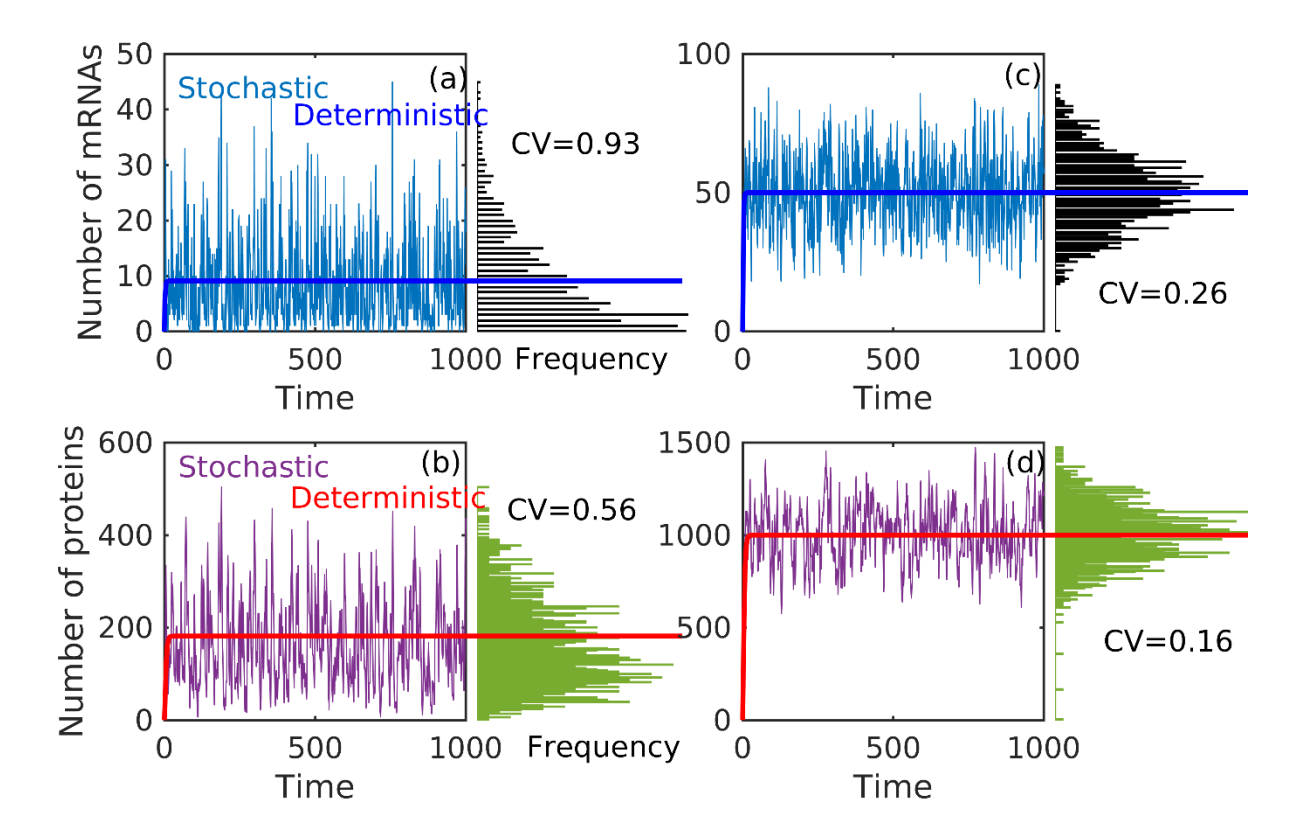


Figure 1.6: The number effect on noise: The time evolution of stochastic and the deterministic trajectories for low number of mRNAs (a) and proteins (b) and high number of

mRNAs (c) and proteins (d). The corresponding population distribution (black for mRNAs and green for proteins) are plotted with the coefficient of variations (CV) values.

Stochasticity in chemical reactions can alter the dynamics of the cell-fate decisions. Stochasticity can have both positive and negative effects on the functioning of a cell. Cells can utilise the noise to survive under stressful conditions or noise can have detrimental effects on the cells. In the next section, we discuss about few effects of stochasticity on cell-fate decisions.

1.3.3. Effect of stochasticity on cell-fate decisions

1.3.3.1. Stochasticity and population heterogeneity

Bistability and multistability is a mechanism utilised by cells to effectively carry out phenotypic state transitions represented by the stable SSs. The expression levels of a master regulator protein determines the phenotypes of the cells. For a clonal population of cells, in a purely deterministic system with bistability, all the cells will switch from one stable SS to another at the SN bifurcation parameter (Figure 1.4c) thus representing an 'all-or-none' mechanism at the population level. Whereas in a stochastic system with bistability, a clonal population of cells will give rise to a population heterogeneity 109,110. In a noisy system, bistability can give rise to a bimodal distribution, whereas tristability and multistability can give rise to a trimodal and multimodal distributions, respectively.

1.3.3.2. Stochasticity as a nuisance

The chemical noise can be advantageous or can act as a nuisance to the system. For example, in the human prostate cancer cells, the cells can switch between two alternate states in presence of noise thus giving rise to a population heterogeneity. A subpopulation of the cells are sensitive to antibiotic treatment and the other subpopulation is tolerant to antibiotic treatment thus making the tumor cells to conveniently escape drug treatment 1111. In preadipocyte to adipocyte differentiation, the noise helps the system to transition from undifferentiated state to the differentiated state. But, the same noise causes the cells to lose the differentiated state and revert back to the undifferentiated state thus resulting in low rate of preadipocyte differentiation⁶¹. p53 is a tumor suppressor gene that plays a master role in cell-fate decision making in cell cycle^{112–115}. Cellular stress such as DNA damage activates p53 gene which in turn promotes cell cycle arrest, DNA damage repair or direct the cell towards apoptosis. Chemical noise can change the expression dynamics of p53 thus making the cells vulnerable to escape from the cell cycle arrest with the DNA damage^{112,116–118}.

Environmental cues affect the functioning of a cell. The receiving of the environmental cues (signals), processing it and exhibiting appropriate response is maintained by the complex signalling pathways in cell-fate decisions. The cell-fate decision making systems must be able to work with high degree of accuracy and produce robust output in presence of chemical noise. Often times, the complex signalling system must also direct the cell to different cell types and lineages and hence the signalling system must be versatile to function in different cell types and in presence of fluctuating input signals. Therefore, the three important properties that a signalling system in cell-fate decisions should require are- precision, robustness and versatility¹¹⁹. Regulatory motifs are found to have all these three requisites and are often found to play important roles in cell-fate decision making systems.

Feedback loops function as the core regulatory network motif in many cell-fate decision making systems such as cell cycle^{120–123}, p53 regulation²³, the lysis-lysogeny decision in phage lambda³¹, cellular differentiation^{36,37,61,68,124,125}, the *lac* operon in *Escherichia coli*⁶². Feedback loops can consist of either as PFLs, or as NFLs or as fused positive and negative feedback loops. The design principles of the feedback regulatory motifs, their dynamical and functional properties in regulating the cell-fate decisions are being explored using both experimental as well as computational approaches. In the next section, we present some findings from previous works highlighting the role of feedback loops as the core regulatory motifs in many cell-fate decision systems.

1.4. Previous works

Cell-fate decisions are carried out by the gene regulatory networks where an input signal triggers gene expression resulting in a desirable decision making as the outcome. Often times, feedback loops form the core regulatory motif of the gene regulatory networks. In Escherichia coli, a majority of the gene regulatory networks have auto-repression (NFL with a single node) as the regulatory motif^{17,126}. Early findings by Becskei et al. showed that NFLs in Escherichia *coli* exhibited stability in the regulatory network¹²⁷. They experimentally demonstrated that negative auto-regulation reduces the cell-to-cell variabilities by resulting in a narrower protein distribution levels. Although NFLs are known to attenuate noise but the noise reduction is traded off with the signal sensitivity 128,129. Many gene regulatory networks also consist of interlinked positive and negative feedback loops as the core regulatory motif. Computational models showed that interlinked positive and negative feedback loops resulted in oscillations with tunable frequency and constant amplitude¹³⁰. Furthermore, it was also shown that tuning the feedback strength can exhibit diverse dynamic behaviour such as monostability, bistability, excitability and oscillations thus rendering a robust desirable outcome¹³¹. The multiple antibiotic resistance activator (MarA) network in *Escherichia coli* consist of a coupled positive and negative feedback loop as the core regulatory network motif. The uninduced MarA under environmental noise generates population heterogeneity for bet hedging and upon induction, it generates uniform deterministic response¹³². The galactose uptake control system of Saccharomyces cerevisiae also consist of interlinked positive and negative feedback loops as the regulatory motif. Experimentation on this system showed that the PFL generated different phenotypic states, the NFL ensured efficient switching between the different phenotypic states⁵⁹.

PFLs are often found to regulate many cell-fate decision making systems such as the maturation of *Xenopus laevis oocytes*^{63,66}, adipogenesis^{36,61}, differentiation of hematopoietic stem cells^{133,134}, differentiation of naïve CD4+ T cells^{74,75}, and EMTs^{135–137}. PFLs have the potential to generate biological switches that are known to convert a graded response into 'all-or-none' response. Brandman *et. al.*, through mathematical modelling, showed that two interlinked PFLs each working at disparate time scales can attenuate noisy stimulus⁸². PFLs are able to reduce the effect of gene expression noise while maintaining signalling sensitivity

even when the input signal fluctuates¹²⁸. Previous experimental and theoretical works predict that PFLs provide an excellent mechanism in limiting cellular variability or chemical noise. Stochastic modelling of the yeast cell cycle revealed that the PFLs present at the G1/S transition point play crucial role in limiting cell cycle variability¹²³. The differentiation of preadipocyte to adipocyte cells consist of fused PFLs which help in controlling the low rate of adipogenesis^{36,61}. Although all the networks having PFLs can generate biological switches, however, not all PFLs are found to act as the regulatory motifs in many cell-fate decisions. Cell-fate decisions are crucial for the cells in terms of their survival, adaptation, lineage choices and proliferation among many others. Therefore, a cell has to carry out the decision making with high degree of accuracy and robustness in presence of stochasticity. How the cells maintain a robust mechanism of the cell-fate decisions? Do the topology of the regulatory networks play any role in generating robust responses to chemical noise? In this thesis, we aim to understand the role of topology of the regulatory networks in generating robust biological switches relevant to cell-fate decisions.

1.5. Aim and layout of the thesis

The main aim of this thesis is to understand how topology of the regulatory network motifs is associated with robustness of the cell-fate decision making systems. Cell-fate decisions such as differentiation are often regulated by PFLs. PFLs are known to generate multistable biological switches which are associated with different phenotypic state of the cells undergoing decision making process. The PFLs can consist of different topologies such as mutual activation (MA), mutual inhibition (MI), self-activation (SA) and coupled PFLs formed by the fusion of same or different regulations. Stochasticity or chemical noise is inherent to the chemical reactions and can interfere and alter the outcome of the cell-fate decisions. It is therefore essential for the cell to function with high degree of accuracy and robustness to produce desirable outcome in the face of stochasticity. What contributes to the robustness in the functioning of the cell in presence of noise? Do the topology of the PFLs play any crucial role in generating robust and tunable regulatory motifs? In this thesis, using mathematical modelling, we seek answers to these questions by investigating the robustness of regulatory

motifs in generating biological switches relevant to cell-fate decisions. This thesis also aims to seek answer to why are certain regulatory motifs recurrently represented in many cell-fate decision systems?

A brief introduction to each chapter in this thesis is discussed below.

In Chapter 2, we discussed about the role of tristable switches in justifying the presence of hybrid or mixed phenotype in many cell-fate decisions. We investigated minimal 2 and 3-component tristable networks that have the potential to generate tristable switches. Our aim was to find the robustness score of each tristable network in generating tristable responses in presence of noise. To do this, we introduced a new automated method of bifurcation analysis using the concept of potential energy landscape of the non-linear system. This energy based method allowed us to generate millions of bifurcation diagrams in an automated manner while the parameters were randomly sampled from independent distributions. Using systematic analysis of the tristable responses generated by each network, we showed that the networks having mutual inhibition self-activation (MISA) motif are the most robust compared to the networks having mutual activation self-activation (MASA) motif. Furthermore, we showed that in EMT, introduction of a new MI loop to the core regulatory motif made the hybrid phenotypic state more accessible as compared to introduction of a new MA loop. We also discussed about the origin and robustness of the tristable networks.

In Chapter 3, we investigated robustness of networks having a PFL fused with a FFL in generating isola and mushroom bifurcations which are known to regulate the differentiation of neural stem cells and the dynamics of heat shock proteins. In particular, our aim was to understand the design principles of the networks in generating mushroom bifurcations and bifurcations with broken branches such as isola. We showed that our energy based method of bifurcation analysis is able to identify bifurcations with broken branches of the SSs in addition to the typical continuous bifurcations. We termed the isola and mushroom bifurcations as the atypical bifurcations. Using systematic analysis, we showed that the incoherent networks have the potential to generate both typical and atypical bifurcations whereas the coherent networks produced only typical bifurcations. Furthermore, by perturbing the incoherent networks, we showed that the atypical bifurcations are formed by

the congregation of two qualitatively different bistable bifurcations. We also explored the dependency of different modelling methodologies in generating normal and inverted atypical bifurcations.

In Chapter 4, we discussed about the different arrangements of multiple PFLs and robustness of bistable switches created by such arrangements. We investigated two different arrangements of multiple PFLs in regulating cellular variability in differentiation. We incorporated both extrinsic and intrinsic noises into our network models and showed that PFLs in parallel arrangement are more efficient in reducing both the noises as compared to PFLs in serial arrangement. Furthermore, we showed that the SN points in the serial PFLs are more susceptible to extrinsic noise as compared to parallel PFLs. Using mean residence time analysis, we showed that the stable SSs in the serial PFLs are more sensitive to intrinsic noise as compared to parallel PFLs.

In Chapter 5, we discussed about the role of different cooperativities in generating bistable switches in receptor-ligand binding system. By incorporating a PFL in the receptor-ligand binding model, we showed that the conditions where a negative cooperativity generated robust bistability, positive cooperativity exhibited poor bistability and vice-versa thus giving rise to a dichotomous nature of the bistable switch. We showed that the control parameters, the bifurcation parameters, and the stability of the receptor-ligand complex regulate the dichotomous nature of the bistability.

In Chapter 6, we summarised the overview and the results of the investigations carried out during the course of this thesis work. The scope of further studies based on the current findings and the application of the energy based bifurcation analysis method is also discussed.

Chapter 2

Robustness of Tristable Networks with Fused Positive Feedback Loops

2.1. Introduction

In many decision making systems, bistability (BS) was able to explain the presence of two mutually exclusive phenotypic states of the cells generated by the mutual inhibition of two genes. However, BS was unable to justify the presence of mixed or hybrid phenotypic state in addition to the two mutually exclusive states. Many *in vivo* and *in vitro* experiments have suggested the presence of mixed phenotypes. For example, subpopulation of interleukin-17 secreting hybrid CD4+Roryt+Foxp3+ cells was observed during the activation of antigen challenged naïve CD4+ T cell^{74,75}. During the primary immune response in murine model, a mixed phenotype of cells having expression levels of both Tbet and GATA3 was observed ^{138–140}. Mixed population has also been observed in differentiation of macrophage/neutrophil system^{68,79}. In epithelial-to-mesenchymal transitions (EMT), partial EMT state (pEMT) was identified which has properties of both the epithelial and mesenchymal cells^{37,80,141}. The hybrid pEMT state is attributed to play important role in metastatic state of cancer¹⁴². Dynamical modelling of the gene regulatory networks suggested that the mixed or hybrid

phenotypic state can be justified by tristability (TS)^{143–148}. A tristable switch consists of three stable SSs each separated by an unstable SS and the intermediate stable SS is associated with the mixed phenotype.

A single PFL with sufficient non-linearity is able to produce BS. To produce TS, an additional PFL is required in the bistable network. Therefore, a fusion of two PFLs can produce tristable signal responses. The fused PFLs can be formed either by coupling two mutual inhibitory loops or by coupling two mutual activatory loops or by coupling a mutual inhibitory loop to a mutual activatory loop. Although all of these fused PFLs are able to generate tristable responses but all may not have the same potential to do so. As robust network motifs are important for decision making, here we investigated the robustness of minimal 2- and 3-component networks with fused PFLs in generating 1-parameter tristable signal response curves. In particular, we aim to find the robustness of the tristable networks under fluctuating parameter space which can be due to extrinsic noise. Genetic mutations which bring variations in the binding constants or other rate parameters can also be incorporated as fluctuating parameter space.

In this chapter, the robustness of the tristable networks is measured in terms of their capacity to produce tristable bifurcation diagrams under random variation in parameter space. To do this in an algorithmic way, we calculated the effective potential landscape of the non-linear system. By monitoring the birth and death of the valleys and hills in the potential landscape, we constructed 1-parameter tristable bifurcation diagrams. By counting the total number of tristable bifurcations generated by each network under fluctuating parameter space, we estimated the robustness of these networks. The tristable responses can be categorized into four different types based on the relative location of the SN points. We also estimated the robustness of the four types of tristable bifurcations for every network. We report that a self-activation to a mutual inhibition loop either directly or indirectly via a third component is the most robust tristable network. Whereas, a self-activation to a mutual activation loop is least robust in producing tristable bifurcations. In addition, by perturbing the network regulations in producing bistable and tristable responses allowed us to determine the origin of the robustness of the mutual inhibition networks. Using the potential energy landscape method, we also investigated the robustness of self-activating toggle switches (SATS) with input signals

on both the components. We report that addition of a mutual inhibition loop to the core regulatory motif of EMT increases its robustness and also stabilizes the pEMT state.

2.2. Modelling and methodology

2.2.1. Model networks and dynamical equations

A 2-component (2-C) motif having mutual activation or mutual inhibition, also known as double negative feedback loop (DNFL) can produce bistability with sufficient non-linearity in the system. To generate tristability, an additional PFL is required such that a new pair of stable-unstable SSs are produced^{145,149,150}. The additional self-activatory PFL can be fused to either a PFL or a DNFL, thus, giving rise to four new 2-C network motifs (Figure 2.1).

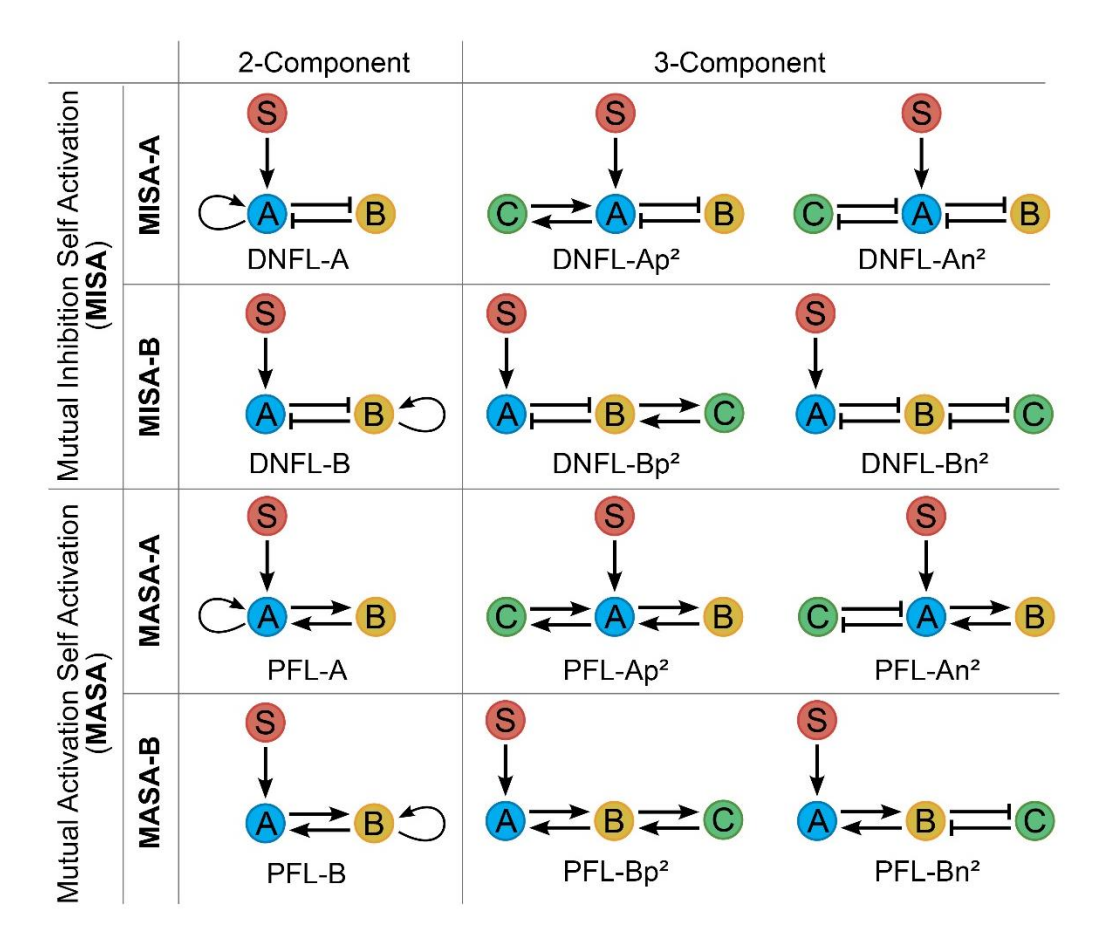


Figure 2.1: Network diagrams and classifications: The two main categories are MISA and MASA. MISA and MASA are further categorised into MISA-A, MISA-B, MASA-A and MASA-B.

In the 3-component networks, the self-activation is replaced by a third component C. The name of the network is mentioned at the bottom of the network. The –A and –B indicate the node that consists the self-activation. The 'p²' and 'n²' indicate the self-activation is through mutual activation and mutual inhibition, respectively. The T-arrows and the arrow-headed lines represent inhibition and activation, respectively.

Based on the regulations and fusions, the four motifs are classified into two groups of motifs, MISA (mutual inhibition self-activation) and MASA (mutual activation self-activation) motifs. In MISA motifs, the additional PFL was fused as a self-activation into a DNFL circuit and in MASA motifs, the self-activation was fused to a PFL (MA) circuit. We further classified MISA into two subcategories (MISA-A and MISA-B) based on the node where the self-activation was fused to. We used similar classification for MASA motifs as well (MASA-A and MASA-B). The self-activation can happen indirectly through a third TF either by a mutual activation or mutual inhibition. Therefore, every 2-C network will have two equivalent 3-C networks. Thus, there are eight 3-C network motifs in total (Figure 2.1).

We modelled these gene regulatory networks by following the modelling methodology proposed by Lu *et al.*¹⁵¹ In this, the dynamical equation of each TF consist of two terms- the gain term, representing the production of the TF and the loss term, representing the dilution due to cell growth or degradation. For the 2-C motifs with self-activation on B (MISA-B and MASA-B), the dynamical equations are written as

$$\frac{dA}{dt} = G_A(S, B) - k_A.A \tag{2.1}$$

$$\frac{dB}{dt} = G_B(A, B) - k_B . B \tag{2.2}$$

where, $G_A(S,B)$ and $G_B(A,B)$ are the regulated transcription rates of A and B, respectively. The dilution or degradation rate constants of A and B are given by k_A and k_B , respectively. Following Lu et al. and assuming non-competitive binding of S and B to the promoter region of the target gene A, the regulated transcription rate of A is given by

$$G_{A}(S,B) = g_{A,S_B_}H^{-}(S).H^{-}(B) + g_{A,S_+B_}H^{+}(S).H^{-}(B) + g_{A,S_B_}H^{-}(S).H^{+}(B) + g_{A,S_+B_}H^{+}(S).H^{+}(B)$$
(2.3)

The functions $H^-(B)$ and $H^+(B)$ are the inhibition and activation rates of A by B, respectively, and are given by Hill function as $H^-(B) = 1/\left(1+(B/B_{A,0})^{n_{B,A}}\right)$ and $H^+(B) = 1-H^-(B)$, where, $B_{A,0}$ and $n_{B,A}$ are the threshold amount of B required to change the activation state of A and the Hill coefficient, respectively. The relative magnitudes of the rate parameters $g_{A,S-B-}, g_{A,S+B-}, g_{A,S-B+}$ and $g_{A,S+B+}$ determine the nature of regulation between the TF and the target gene. In the 2-C MISA-B network, based on the regulations on the target gene A by the TFs S and B, the following inequalities holds $g_{A,S-B+} < g_{A,S-B-} = g_{A,S+B+} < g_{A,S+B-}$. Similar methodology was used to express $G_B(A,B)$, the regulated transcription rate of B.

The dynamical equations for the 2-C motifs having self-activation on A (MISA-A and MASA-A) are given as

$$\frac{dA}{dt} = G_A(S, A, B) - k_A. A \tag{2.4}$$

$$\frac{dB}{dt} = G_B(A) - k_B.B \tag{2.5}$$

Here, the gene A is regulated by three TFs and the transcription rate of A is expressed as

$$G_{A}(S,A,B) = g_{A,S_A_B_}H^{-}(S).H^{-}(A).H^{-}(B)$$

$$+ g_{A,S_A_B_}H^{+}(S).H^{-}(A).H^{-}(B)$$

$$+ g_{A,S_A_B_}H^{-}(S).H^{+}(A).H^{-}(B)$$

$$+ g_{A,S_A_B_}H^{-}(S).H^{-}(A).H^{+}(B)$$

$$+ g_{A,S_A_B_}H^{+}(S).H^{+}(A).H^{-}(B)$$

$$+ g_{A,S_A_B_}H^{+}(S).H^{-}(A).H^{+}(B)$$

$$+ g_{A,S_A_B_}H^{+}(S).H^{-}(A).H^{+}(B)$$

$$+ g_{A,S_A_B_}H^{+}(S).H^{+}(A).H^{+}(B)$$

$$+ g_{A,S_A_B_}H^{+}(S).H^{+}(A).H^{+}(B)$$

$$+ g_{A,S_A_B_}H^{+}(S).H^{+}(A).H^{+}(B)$$

$$(2.6)$$

Since gene B is regulated by a single TF, the transcription rate of gene B can be represented by the usual Hill function. The transcription rates for inhibition and the activation are given by $G_B(A) = g_{B,0} - g_{B,A_-}H^-(A)$ and $G_B(A) = g_{B,0} - g_{B,A_+}H^+(A)$, respectively with $g_{B,0} < g_{B,A}$. In all these models, S is an external signal and acts as a parameter.

Similar to 2-C networks, we used this methodology to express the transcription rates for 3-C network motifs. For the 3-C MISA-B and MASA-B networks, the general dynamical equations are given as

$$\frac{dA}{dt} = G_A(S, B) - k_A.A \tag{2.7}$$

$$\frac{dB}{dt} = G_B(A, C) - k_B.B \tag{2.8}$$

$$\frac{dC}{dt} = G_C(B) - k_C.C \tag{2.9}$$

For the 3-C MISA-A and MASA-A motifs, the dynamical equations are given as

$$\frac{dA}{dt} = G_A(S, B, C) - k_A.A \tag{2.10}$$

$$\frac{dB}{dt} = G_B(A) - k_B.B \tag{2.11}$$

$$\frac{dC}{dt} = G_C(A) - k_C.C \tag{2.12}$$

2.2.2. Potential landscapes and bifurcation diagrams

At the bifurcation points, the stability of the SS undergoes a qualitative change which is assessed by the eigenvalues of the Jacobian matrix in the linear stability analysis of the non-linear dynamical systems¹⁵². Therefore, to generate the bifurcation diagram, the eigenvalues of the SSs are monitored while the bifurcation parameter is varied¹⁵³. In order to estimate the robustness of the network motifs in producing 1-parameter tristable bifurcation diagrams, we needed to generate a large number of bifurcations with random variation in the parameter space. The existing tools for bifurcation analysis such as XPPAUT and Oscil8 are based on numerical continuation method with initial value approach. In these tools, to see the effect of parameter perturbations on the bifurcation dynamics, the parameters must be manually changed to generate a new bifurcation diagrams. Therefore, for a large set of random parameters, the bifurcation analysis becomes quite challenging and time consuming. In this regard, we used potential energy landscape to generate 1-parameter bifurcation diagrams in

a high-throughput manner that does not require manual interventions during analysis. The potential landscape carries the signatures of the qualitative nature of the SSs where the local minima and maxima in the potential landscapes corresponds to the stable and unstable SSs, respectively. The theory of potential energy landscape in cell-fate decisions was originally proposed by Waddington¹⁵⁴ and has become an alternate approach to study the cell-fate determination¹⁵⁵. At the SN bifurcation point, a pair of stable-unstable SSs are either "born" or "die". Analogous to this, in the potential energy landscape, the SN point can be reflected as the creation or annihilation of a pair of local minima-maxima such that a qualitative change occurs in the landscape beyond the bifurcation point. Therefore, close monitoring of the local minima and maxima for different values of bifurcation parameter allowed us to construct 1-parameter bifurcation diagrams.

The main problem in the calculation of potential energy landscape is the non-Newtonian nature of the dynamical equations of the biochemical system. Therefore, the definitions of the potential energy for the multi-dimensional systems poses a great challenge. To deal with this problem, we used the method of composite function to define the effective potential of multi-dimensional systems. Using the composite function method, we were able to express a multivariate system into a univariate system. From Eq. 2.1, for the 2-C MISA-B and MASA-B networks, the SS expression of A can be written as $A = G_A(S,B)/k_A = G_A^1(S,B)$. On substitution of this expression in Eq. 2.2, we get the expression for effective force of the system as

$$F(B,S) = G_B(G_A^1(S,B),B) - k_B.B$$
(2.13)

With the expression of effective force, the effective potential function of the system can be defined as

$$V(B,S) = -\int_0^B [G_B(G_A^1(S,x),x) - k_B.x] dx$$
 (2.14)

The effective potential in Eq. 2.14 is a function of only B and it parametrically depends on the external input signal S. Similarly, for the 2-C MISA-A and MASA-A motifs, from Eq. 2.5, the SS expression of B is written as $B = G_B(A)/k_B = G_B^1(A)$ and the effective potential is written as

$$V(A,S) = -\int_0^A [G_A(S,x,G_B^1(x)) - k_A.x] dx$$
 (2.15)

For the 3-C network motifs of MISA-B and MASA-B, using the method of composite function, the effective potential is given as

$$V(B,S) = -\int_0^B [G_B(G_A^1(S,x), G_C^1(x)) - k_B.x] dx$$
 (2.16)

where, $G_A^1(S, B) = G_A(S, B)/k_A$ and $G_C^1(S, B) = G_C(B)/k_C$.

Similarly for the 3-C MISA-A and MASA-A motifs, the effective potential is given as

$$V(A,S) = -\int_0^A [G_A(S, G_B^1(x), G_C^1(x)) - k_A \cdot x] dx$$
 (16)

Where, $G_B^1(A) = G_B(A)/k_B$ and $G_C^1(A) = G_C(A)/k_C$. The systematic analysis of the effective potential allowed us to calculate the potential landscape of the variables A or B while we varied the signal S.

2.3. Results and discussions

Using the effective potential function, we calculated the potential landscape as a function of the dynamical variable and the bifurcation parameter S. At each value of S, we calculated the number and nature of the local minima and maxima to determine the qualitative and quantitative nature of the SSs. In the potential landscape, we carefully monitored the creation and annihilation of the local minima-maxima with gradual change in S to determine the bifurcation points (Figure 2.2). The S value at which a pair of local minima-maxima appears or disappears in the potential landscape was identified as the SN bifurcation point.

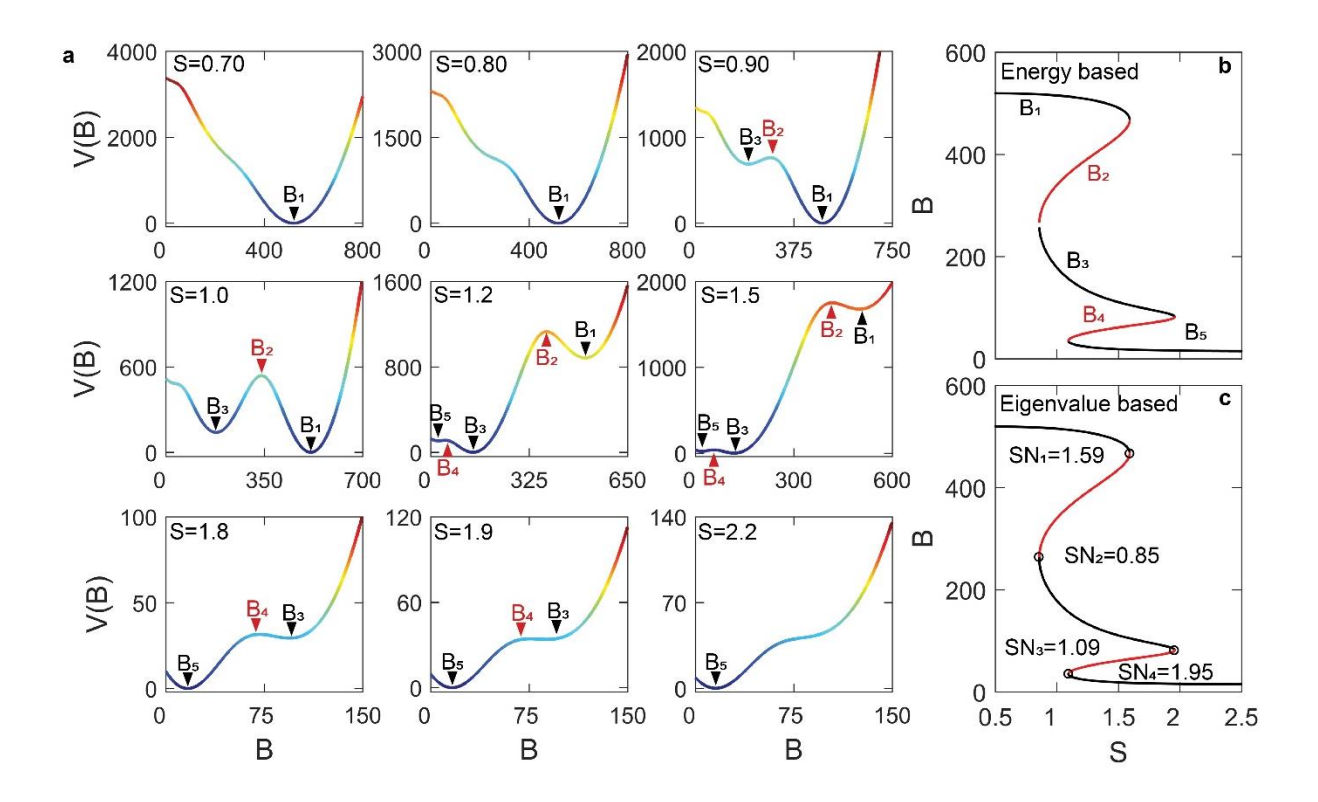


Figure 2.2: The potential energy based method of bifurcation analysis for the DNFL-B network: (a) Plots of the potential energy V(B) (Eq. 2.2) landscape at different values of the input signal S. The local minima are indicated by B_1 , B_3 and B_5 . The local maxima are indicated by B_2 and B_3 . (b) The 1-parameter bifurcation diagram generated from the potential energy landscape. The local minima and maxima of the potential energy represent the stable and unstable SSs respectively in the bifurcation diagram. (c) The 1-parameter bifurcation diagram generated using XPPAUT. Starting from the upper branch and flowing the SSs, the SN bifurcation points are labelled. The input signal S is scaled as S/100 in this and all other figures in this chapter. The parameter values are mentioned in Table 2.1 under Type I.

In **Figure 2.2**, we present the potential energy landscape for the 2-C DNFL-B network at different values of S. At S = 0.7, and S= 0.8, there is only one local minima (B_1) representing one stable SS (monostability) with a value of B. With gradual increase in S and monitoring the local extrema allowed us to locate the SN bifurcation point at S = 0.85. As a result of this, a new pair of local minima-maxima appeared (B_2 and B_3) at the intermediate value of B at S = 0.9. Thus, at S > 0.85, the system is bistable. Following similar method of gradual increase in S and subsequent monitoring of the local extrema, we located another SN point at S = 1.09.

Consequently, at S = 1.2, a new pair of local minima-maxima appeared (B_4 and B_5) with low levels of B. Therefore, for S > 1.09, the system becomes tristable. As we increased the value of S, a pair of local minima-maxima disappeared (B_1 and B_2) at S = 1.59, indicating another SN point. Similar disappearance of local extrema (B_3 and B_4) occurred at S = 1.95. From these potential landscapes at different values of S, we recorded the coordinates and nature of the local extrema to construct the 1-parameter bifurcation diagram for the system (Figure 2.2b). This bifurcation diagram is identical to the bifurcation produced using XPPAUT¹⁵⁶ which is a conventional tool for bifurcation analysis based on numerical continuation method (Figure 2.2c). Based on the relative locations of the four SN bifurcation points, the reversible tristable bifurcation diagrams can be categorised into four different types¹⁵⁷ (Figure 2.3). The number of SN and SN bifurcation diagrams over their potential energy landscapes to highlight the correlation between the effective potential of the multi-dimensional system and the bifurcation diagrams.

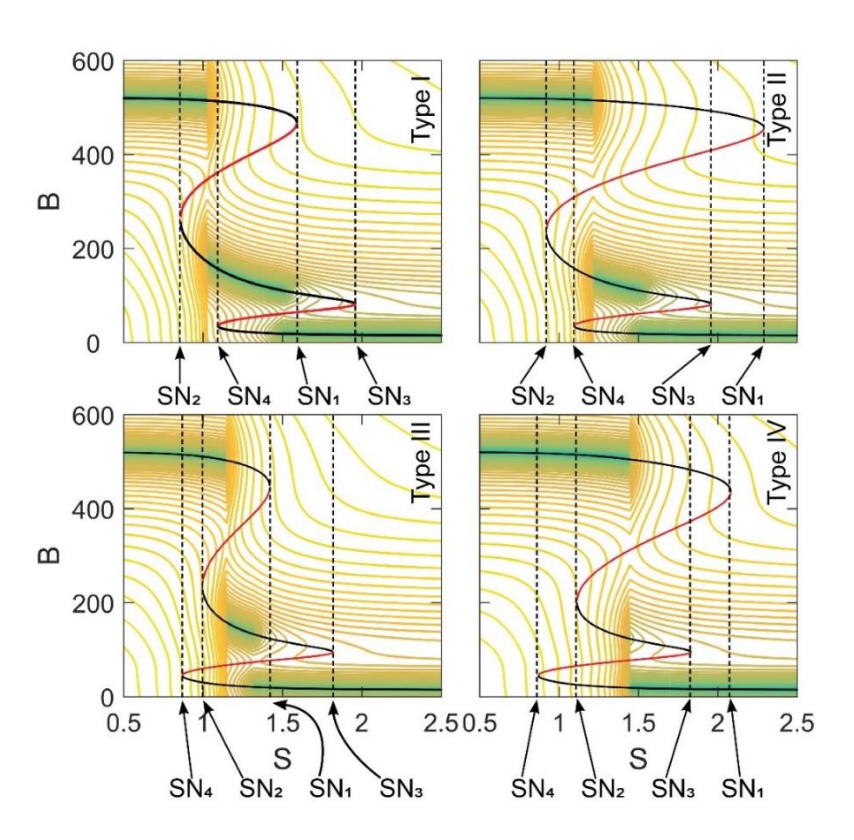


Figure 2.3: Categorisation of the tristable responses: 1-parameter tristable bifurcation diagrams generated using the potential energy based method are projected over the contours

of ln(V(S,B)) for the DNFL-B network. Based on the relative location of the SN bifurcation points, the tristable bifurcations are categorised into four different types: Type-I: $SN_3 >$ $SN_1 > SN_4 > SN_2$, Type-II: $SN_1 > SN_3 > SN_4 > SN_2$, Type-III: $SN_3 > SN_1 > SN_2 > SN_4$, Type-IV: $SN_1 > SN_2 > SN_4$. The color gradient in the contours represent the depth of the potential landscape with green being deepest. The parameter values for each bifurcation type are mentioned in **Table 2.1**.

Table 2.1: The parameter values corresponding to the four types of tristable bifurcations for the DNFL-B network.

	Values					Values			
Parameters	Туре	Туре	Туре	Туре	Parameters	Туре	Туре	Туре	Туре
	I	II	Ш	IV		ı	II	Ш	IV
$g_{A,S_B_}$	4.0	4.0	4.0	4.0	$B_{A,0}$	370.0	335.0	350.0	300.0
g_{A,S_+B}	18.0	18.0	18.0	18.0	$A_{B,0}$	130.0	130.0	130.0	130.0
$g_{A,S_{-}B_{+}}$	0.7	0.7	0.7	0.7	$B_{B,0}$	67.0	67.0	75.0	75.0
g_{A,S_+B_+}	4.0	4.0	4.0	4.0	$n_{S,A}$	2.0	2.0	2.0	2.0
$g_{B,B_A_}$	7.5	7.5	7.5	7.5	$n_{B,A}$	6.0	6.0	4.0	4.0
g_{B,B_+A}	39.0	39.0	39.0	39.0	$n_{A,B}$	5.0	5.0	5.0	5.0
g_{B,B_A_+}	1.0	1.0	1.0	1.0	$n_{B,B}$	4.0	4.0	6.0	6.0
g_{B,B_+A_+}	7.5	7.5	7.5	7.5	k_A	0.05	0.05	0.05	0.05
$S_{A,0}$	140.0	140.0	140.0	140.0	k_B	0.075	0.075	0.075	0.075

2.3.1. Robustness of tristable networks

We applied the high throughput method of generating bifurcations using potential landscapes to determine the robustness of the network motifs (Figure 2.1). We initially created triplicates of 500,000 random parameter sets and in each set the parameters were randomly chosen from independent uniform distributions. For the threshold parameters, we used the halffunctional rule given by Huang et al. 158 to determine the parameter range. The half-functional rule ensured that a regulation has equal probability of being functional or non-functional. For an isolated gene having only synthesis and degradation, the SS distribution was estimated by randomly sampling the synthesis and the degradation rate constants from independent distributions. The SS values in this case are the threshold values for the isolated genes. For a non-isolated gene with incoming regulations only, the threshold values were calculated from the SS equation with the parameters chosen randomly from independent distributions. In order to remove the extreme values, the log₂ of the SS distribution was truncated at 0.02 and 1.98 of the median value. The threshold values in our method were randomly picked from the truncated distribution of the relevant genes.

For every random parameter set, we ran 1-parameter bifurcation analysis with S as the bifurcation parameter using the potential energy landscape method. From the ensemble runs, we calculated the robustness score by counting the total number of tristable bifurcation diagrams each network generated. Further, using the energy based method, we were able to categorise the tristable bifurcations into four different types according to the relative ordering of the SN bifurcation points (Figure 2.3). The automated energy based method generated thousands of tristable bifurcations without any manual interventions. The representative potential landscapes and the corresponding tristable bifurcations are shown in **Figure 2.4.**

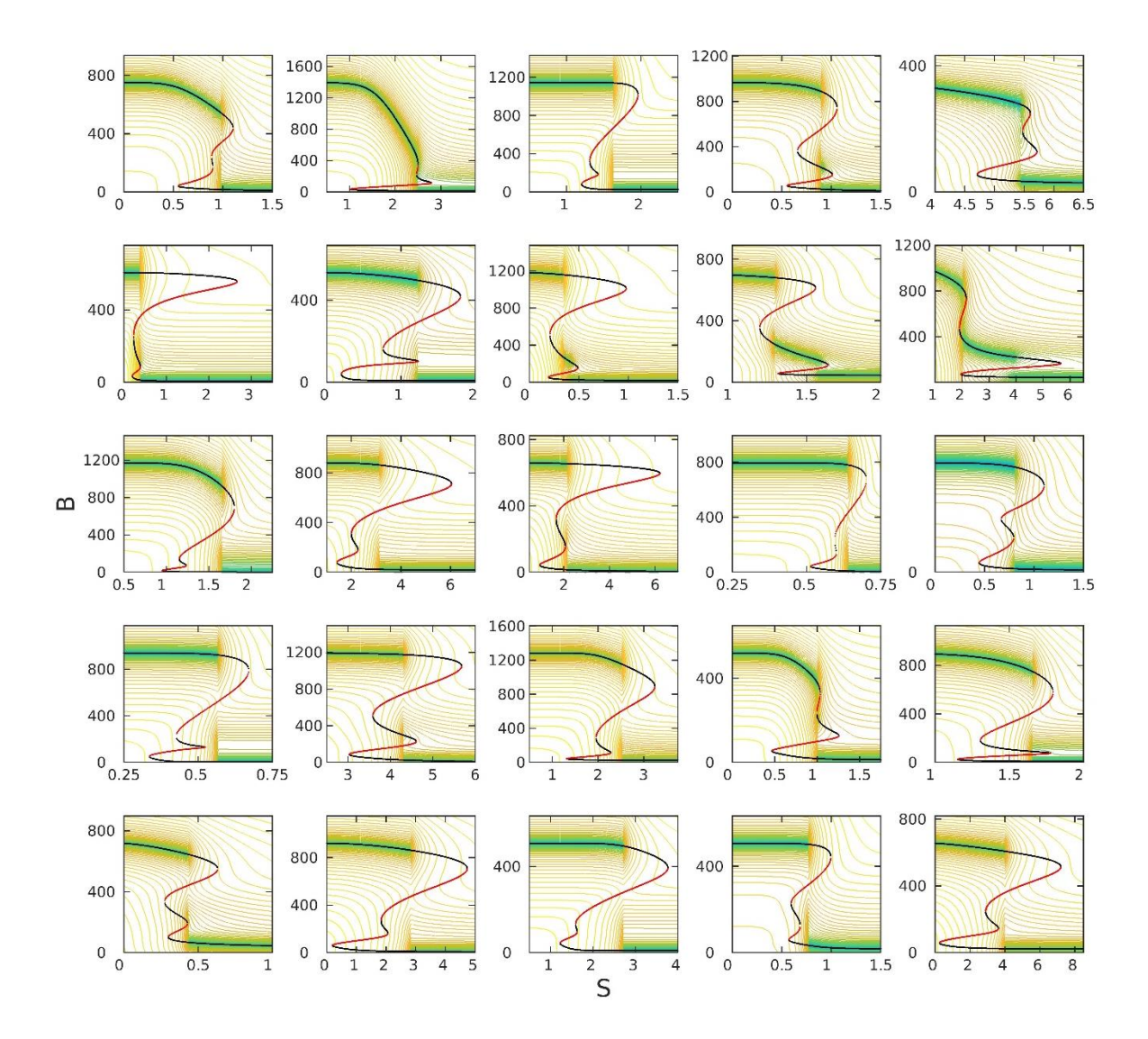


Figure 2.4: Bifurcations on the energy contours: The 1-parameter tristable bifurcations for the network DNFL-B are overlaid on top of the contours of the potential energy. The red and black lines represent the stable and the unstable SSs, respectively.

From the robustness score of each network, we found that MISA networks generated the most number of tristable responses as compared to MASA networks (Figure 2.5a). The average percentage (over triplicate) of tristable responses for MISA was much more than MASA. Among the different subcategories in the MISA and MASA, we found the order of robustness to be MISA-B > MISA-A > MASA-A > MASA-B for the 2-C and 3-C networks together (Figure 2.5b). For the individual 2-C and 3-C networks, the plot of robustness score (Figure 2.5c) reveals consistent nature of the robustness among the different subcategories. These results suggest that MISA motifs having mutual inhibition are significantly more robust in

generating tristable responses as compared to the MASA motifs having mutual activation. Further, MISA-B is robust than MISA-A, suggesting that if the self-activation and the input signal S are on different nodes, the motif is more robust compared to motifs where the self-activation and S are on the same node. Based on the nature of interactions between the nodes, the 3-C networks can further be classified into 3 subtypes- mutual activation mutual activation (MAMA), mutual inhibition mutual activation (MIMA) and mutual inhibition mutual inhibition (MIMI). The network motifs under the MAMA are PFL-Ap², and PFL-Bp². The networks under the MIMA are DNFL-Ap², DNFL-Bp², PFL-An², and PFL-Bn². The networks under the MIMI are DNFL-An², and DNFL-Bn². The robustness score among these categories again point out the importance of mutual inhibition in generating robust tristable responses (Figure 2.5d).

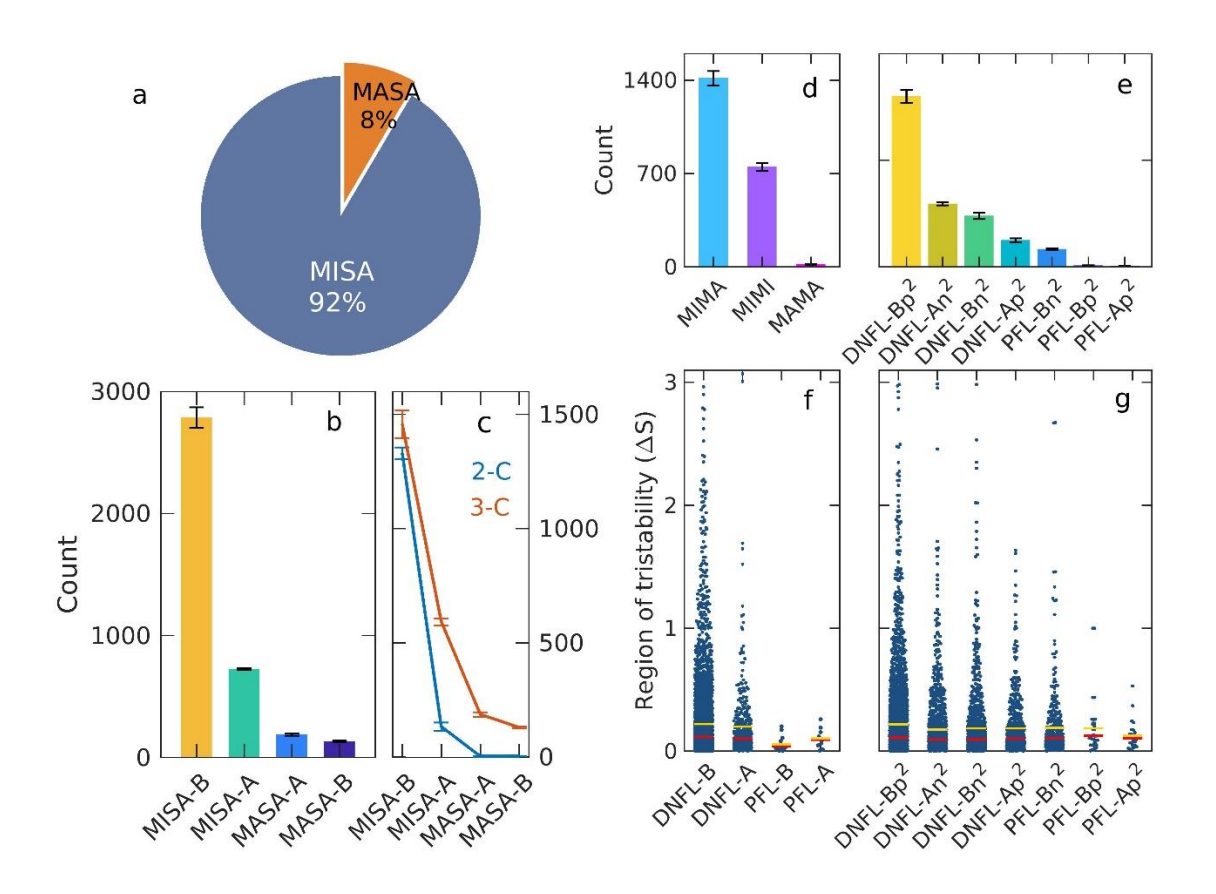


Figure 2.5: Robustness of the networks with two fused PFLs: (a) A pie chart depicting the mean percentage of tristable responses generated by the MISA and the MASA networks. The average tristable responses generated by the four sub categories of motifs for 2-C and 3-C

networks taken together (b) and (c) taken separately. (d) The average tristable responses generated by the three different types of 3-C networks MIMA (mutual inhibition mutual activation), MIMI (mutual inhibition mutual inhibition) and MAMA (mutual activation mutual activation). (e) The average number of tristable responses generated by all the individual 3-C networks. The average tristable region (ΔS) for the 2-C (f) and 3-C (g) networks.

Our calculations also show that networks having fused mutual activation loops are not at all robust in generating tristable responses. Among the individual 3-C network motifs, here too, the motifs having mutual inhibition (DNFL) are more robust in producing tristable responses compared to the motifs having mutual activation (PFL) (Figure 2.5e). Further, the robustness score increases if the self-activation is on the far side of the input signal (DNFL-Bp² and DNFL-Ap²). We also found that the robust networks produced larger tristable region (Figure 2.5f and 2.5g) suggesting that the tristable regions for the MISA networks are bigger than the MASA networks.

Using the automation energy based method, we were able to categorise different types of tristable bifurcations during the run. Among the four different types, Type-IV and Type-I were found to be most and least prevalent, respectively (Figure 2.6a) in the four categories of the network motifs. Type-II and Type-III had similar values of robustness scores across all the motifs. The robustness of four different bifurcation types are in the order Type-IV > Type-III > Type-II > Type-I in the most robust 2-C and 3-C networks DNFL-B and DNFL-Bp², respectively (Figure 2.6b).

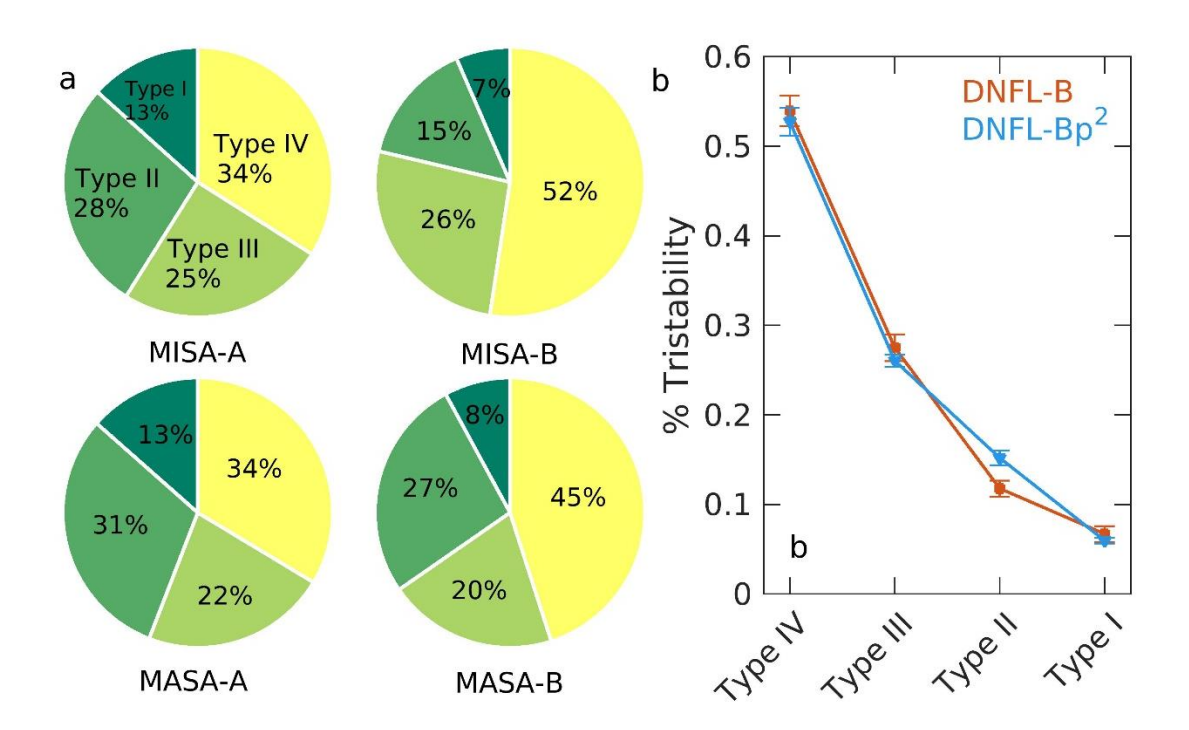


Figure 2.6: Robustness of types of tristable responses: (a) Mean percentage of four types of tristable responses for four sub categories of the networks. (b) Average percentage of four types of tristable responses for DNFL-B and DNFL-Bp² networks.

Similar robustness score for other networks were also realised (not shown). Type-IV is most robust tristable due to the fact that the system can be tristable even with a small stable branch sandwiched in between one ON and one OFF threshold (see **Figure 2.3** for the bifurcations). Type-I has two ON and two OFF thresholds indicating that this might have formed due to fusion of two independent bistable switches from two feedback loops. This highlights the fact that in the particular parameter space, the two feedback loops independently must be bistable before their fusion to give rise to a tristable with two ON and two OFF thresholds. The probability of simultaneously satisfying all these criterion is small and hence Type-I is the least prevalent.

2.3.2. Robustness of SATS

In order to broaden the scope of our method, we next investigated the robustness of selfactivating toggle switches (SATS) that are known to drive epithelial-to-mesenchymal transitions (EMT) during cancer progression ^{143,159}. Careful observation of the SATS topology on the EMT suggest that they are MISA motifs with input signal on both the nodes. Based on the nature of input signal on the two nodes, the SATS are classified into four types (Figure 2.7a). We found that all the EMT motifs are capable of generating tristable responses (Figure **2.7b).** Out of the four motifs, EMT-B₁ is several fold robust in generating tristable responses than the others. EMT-B₁ has a MISA-B motif with an additional inhibition from S to B which increases its robustness compared to EMT-B2 which has MISA-A motif with inhibitory input signal on A. This is in accordance with the result that 2-C MISA-B is more robust than 2-C MISA-A motif. Comparison of the robustness scores for the MISA-B (1330 \pm 9), EMT-B₁ (2881 \pm 40), and EMT-B₃ (320 \pm 9), we found that an inhibitory signal on the node with selfactivation increases the robustness of MISA-B networks. The robustness of different types of tristable responses follow a similar trend as was observed in 2-C and 3-C network motifs (Figure 2.7c). The different robustness score of the tristable types might have a significant impact in the outcome of cellular fates in the EMT. The different robustness scores are associated with the percentage of cells that would exhibit the corresponding bifurcation types or phenotypes under cell-to-cell variations due to various extrinsic factors. The frequent occurrence of Type-IV TS suggest that in a population, a major percentage of the cells (~ 55%) will not exhibit the pEMT state neither during the EMT nor during the reverse mesenchymalto-epithelial transition (MET) in a typical single-cell dose response experiment. In Type-III TS, a significant population of cells (~ 25%) will exhibit the pEMT state during the EMT but not during the MET. The cells can be in pEMT state both during EMT and MET only in case of Type-I and Type-II TS. However, such possibilities are quite low because the prevalence of Type-I and Type-II are quite low in the robustness score. This highlights the fact that the cell-to-cell variability due to extrinsic noise has significant effect on the phenotypic outcome during EMT or MET.

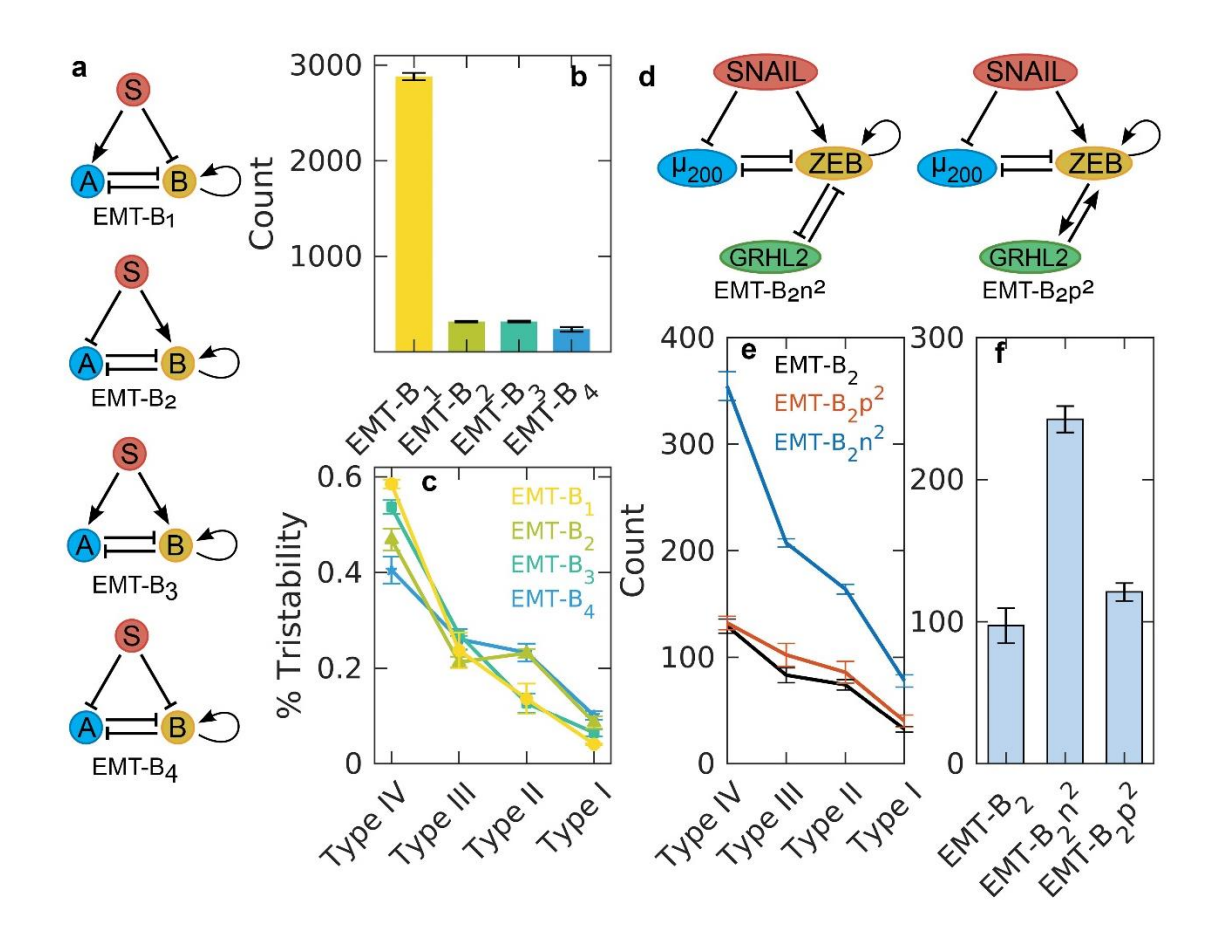


Figure 2.7: Robustness of SATS motifs relevant to EMT: (a) Network diagrams of the four SATS motifs relevant to EMT. (b) Average tristable counts for the four networks. (c) Average percentage of four types of tristable responses for the four networks. (d) The core regulatory network of EMT. An additional PFL loop with mutual inhibition between GRHL2 and ZEB generated the network EMT- B_2n^2 . The additional loop with mutual activation between GRHL2 and ZEB generated the network EMT- B_2p^2 .

Previously, it was shown that and additional DNFL between the TFs Zeb-Ovol and also between Zeb-Grhl2 in the EMT network stabilizes the pEMT state through a dual-bistable switch 159,160 . In a dual-bistable switch, the upper branch of one bistable becomes the lower branch of the other bistable switch. Following this, we investigated on two different EMT networks EMT-B₂n² and EMT-B₂p², where we incorporated an additional DNFL and PFL to the respective networks (Figure 2.7d) to determine the role of DNFL in stabilizing the pEMT state. From the robustness counts of the tristable responses, we found that EMT-B₂n² produced 2.5 fold increase in tristable responses compared to EMT-B₂ (Figure 2.7e). On the other hand,

there was marginal increase of tristable responses in EMT- B_2p^2 . These results highlight the importance of mutual inhibition in producing robust tristable responses in EMT network¹⁵⁸. We also found that EMT- B_2n^2 produced greater number of dual-bistable responses compared to EMT- B_2p^2 and EMT- B_2 (Figure 2.7f). Therefore, under fluctuating parameter space, an additional DNFL between Zeb-Grhl2 or between Zeb-Ovol stabilizes the pEMT state compared to addition of a PFL.

2.3.3. The origin of robustness

Our results suggest that mutual inhibition (DNFL) is important in generating robust tristable responses. However, it is important to understand the dynamical origin of the robustness of these networks. To determine the origin of the robustness in MISA networks, we compared the tristable response from the unperturbed network and bistable response from the perturbed network. To perturb the network, we removed the self-activation keeping all other parameter values unchanged (Figure 2.8). We found that in MISA-B network, both the TS and BS resulted in similar levels of B at low and high S values. This is due to the fact that at low S, the addition of the self-activation on B did not cause any further increase in B because the basal activation is sufficient for full induction of B. At high S, B is completely shut down by the negative regulation from A even with the self-activation on B. However, addition of the selfactivation on B created an intermediate level of B thus stabilising the TS in the DNFL-B network. In the MISA-A network (DNFL-A), at low S, the levels of A in BS and TS is similar due to negative regulation on A by fully active B. At high S, the self-activation on A further increases the level of A in TS compared to BS. Thus, the self-activation helps in stabilizing the intermediate level of A in the TS in the DNFL-A network. In addition to this, the mutual inhibition (DNFL) in the MISA motifs, prevent full induction of the genes, thus allowing to stabilize the intermediate levels of the regulators and ultimately functioning as the stabilizer for the TS. In the motifs with mutual activation, at high S values, the gene is fully active therefore even adding the self-activation did not further increase the levels of the genes in MASA-A (PFL-A) and in MASA-B (PFL-B). Addition of the self-activation only decreases the threshold values as the SN bifurcations shifted to lower S values in the TS. Therefore, in motifs with mutual activation, the possibility of having an intermediate level of the genes is low as compared to the motifs with mutual inhibition.

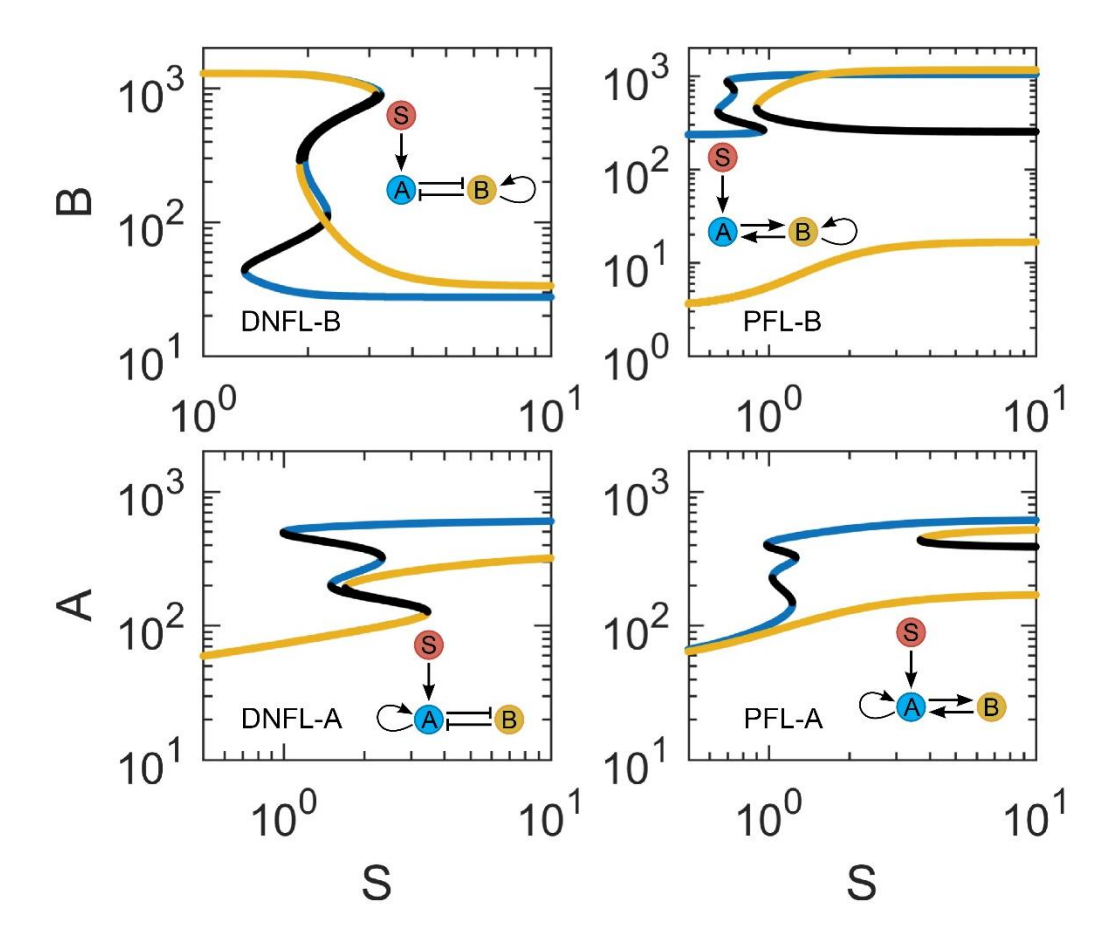


Figure 2.8: Comparison of the multistability from the perturbed and the unperturbed networks: Each of the MISA and MASA networks were perturbed by removing the selfactivation and keeping all the parameters unchanged. Bistable and tristable bifurcations were generated and were compared. The blue-black and yellow-black lines are the tristable and bistable responses, respectively.

2.3.4. Sensitivity of model parameters

Multistability in non-linear chemical systems largely depends on the parameter values. So far, we have analysed the robustness of the motifs based on the tristable responses under random variation of the parameter space. However, robustness score did not provide much information about the key parameters in generating tristable responses. To address this problem, we performed a local parameter sensitivity analysis of the 2-C network motifs. Here, we started with a parameter set that resulted in tristability and then we randomly varied a particular parameter keeping all other parameters fixed to see how many times the change leads to tristable responses. We repeated this method for every parameter in the model to determine their sensitivity in producing tristable responses. Consistent with the robustness results, we found that the MISA motifs (DNFL-A and DNFL-B) were less sensitive to parameter variations (Figure 2.9). The threshold parameters $(B_{B,0}, A_{B,0}, B_{A,0})$, the degradation rates (k_A, k_B) and the Hill coefficients $(n_{A,B}, n_{B,B}, n_{A,A})$ were found to be highly sensitive compared to other parameters.

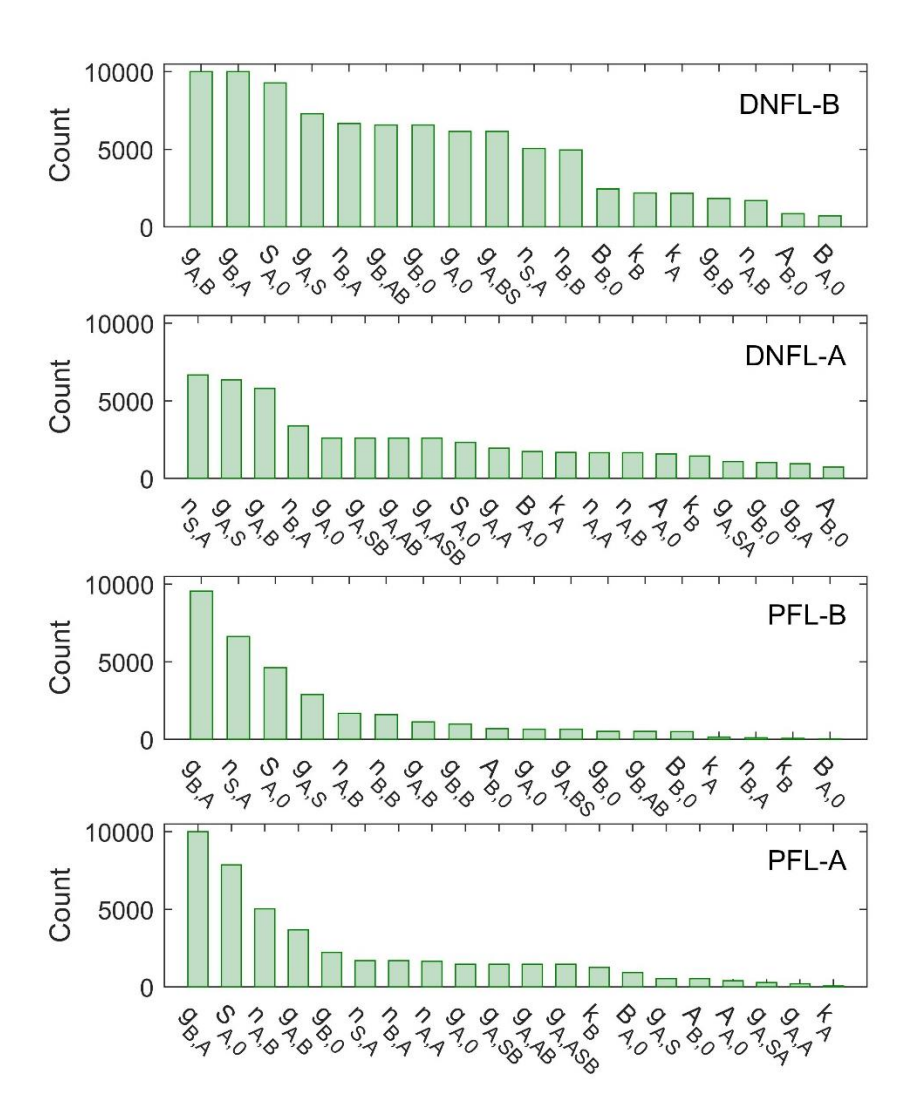


Figure 2.9: Sensitivity of parameters: Average tristable counts generated by perturbing each parameter by keeping the other parameters fixed for the different MISA and MASA networks.

2.4. Summary and conclusions

Cell fate decisions are crucial physiological processes that accounts for diverse nature of cellular identities in multicellular organisms^{161–163}. Cell-fate decisions are governed by gene regulatory networks that must perform with high accuracy for appropriate results. Therefore, the networks must be robust enough to achieve desired outcomes under continuous influence of cellular variabilities due to intrinsic and extrinsic factors. In this chapter, we investigated the robustness of 2-C and 3-C network motifs having fused PFLs in generating tristable bifurcations under random parameter variations. In order to do this, we developed a new method of bifurcation analysis using the effective potential energy landscape where the local minima-maxima represents the stable and unstable SSs, respectively. With change in the bifurcation parameter, the qualitative nature of the effective potential landscape changed with the birth and death of a pair of local extrema whose dose monitoring allowed us to generate 1-parameter bifurcation diagrams of the system. Using this method, for every network motif, we ran bifurcation analysis for 1.5 million random parameter sets. We calculated the robustness score by counting the total number of tristable responses each network generated.

We found that that the networks having mutual inhibition with self-activation (MISA) are most robust in producing tristable responses as compared to the networks having mutual activation with self-activation (MASA) motifs. Further investigations into individual 3-C networks suggested that mutual inhibition is prominent in producing robust tristable responses. We also showed that the robust networks produced bigger tristable regions. Additionally, we also showed that if the self-activation and the input signal are on different nodes, it increases the robustness of the network. Using the energy based method, we were able to categorise the tristable response into four different types based on the relative locations of the SN bifurcation points. We showed that Type-IV tristable (one ON and one OFF thresholds) is the most abundant and Type-I tristable (two ON and two OFF thresholds) is the least abundant across various networks. We applied our method to four different SATS networks to determine their robustness in generating tristable responses. We found that an inhibitory input signal on the node with self-activation is more robust compared to activatory input signal on the same node. We also showed that addition of a mutual inhibition loop to

the TF Zeb in the core regulatory network motif of EMT made the pEMT state accessible as compared to that of adding a mutual activation loop to Zeb. The pEMT state was stabilised by a dual-bistable switch. This conclusion is in accordance with the recent findings that mutual inhibition between Zeb-Ovol and Zeb-Grhl2 stabilises the pEMT state.

Many networks that are found naturally in the context of cell-fate decisions have mutual inhibition with self-activation motif¹⁶⁴. For example, the core regulatory networks in differentiation programs of trophectoderm-inner cell mass (Cdcx2-Oct3/4)¹⁶⁵, primitive endoderm epiblast (Gata6-Nanog)¹⁴⁶, differentiation of HSCs into myeloid and erythroid (PU.1-Gata1)¹⁶¹, Th1-Th2 (Tbet-Gata3)^{139,140}, Th17-Treg (Roryt-Foxp3)^{74,75}, EMT (miR34-Snail, miR200-Zeb)^{143,166,167} and endocrine-acinar differentiation (Nkx6-Ptf1a) all consist of MISA motifs. Regulatory networks controlling cell-fate decisions are continuously influenced by chemical noise that has the potential to change the dynamics and outcome of the decision making systems. Therefore, the regulatory networks must be robust and tunable to limit the effects of chemical noise. Our findings suggest that it is the system's strategy to naturally select the most robust MISA motifs over MASA motifs for accurate performance under the chemical noise. We believe that our work will be helpful in designing network motifs with greater tunability and robustness.

Previous studies explored searching of parameter space for multistability in the context of EMT¹⁵⁸. These studies were able to determine only the SS values via numerical integration of the model equations with random variation in initial conditions. In contrast to this, our method can generate a complete 1-parameter bifurcation diagram by detecting the stable and unstable SSs. Our energy based method is significantly faster and is independent of initial conditions compared to the numerical integration method. Since the potential based method is independent of initial conditions, it has the ability to detect all the SS values whereas the initial condition dependent numerical integration method has difficulty in detecting a SS having weak basin of attraction. Further construction of bifurcation diagrams using the effective potential landscape is a new paradigm of analysing non-linear systems. The numerical continuation method where a particular solution of the dynamical system is followed to construct the bifurcation can face difficulty in detecting broken SSs. Such broken SSs have recently been shown to occur in early T-cell lineage commitment¹⁶⁸. Broken

branches can also generate atypical bifurcations, like the isola bifurcations, that were proposed to be relevant in long-term memory¹⁶⁹ and neural stem cell differentiation mediated by BMP2 protein¹⁷⁰. The potential based method is able to detect the broken branches since it determines the SS based on the local extrema of the potential landscape.

Our potential energy based method can also be applied to find multistable bifurcation diagrams. However, it depends on the accurate calculation of the effective potential function. For a multi-dimensional system, calculation of the potential energy landscape becomes challenging. Recent studies have proposed new methods of calculating potential energy landscapes for multi-dimensional systems^{171,172} in context of cellular differentiation¹⁷³ and therefore can be used for the construction of bifurcation diagrams for larger network systems. In all our networks that we have investigated here, the multivariate system was reduced to a univariate system such that the effective potential is calculated. However, for more complex networks, such reduction of multivariate to univariate systems may not always be possible. Recently, Ye *et al.*¹⁶⁸ have investigated network topologies that have the potential to generate irreversible tetrastability with sequential activation of genes. They found that certain networks were enriched and were responsible for such qualitative behaviour in the SSs in early T cell development. Consistent with our findings, the occurrence frequency of MISA motifs in these subnetworks is quite large highlighting the importance of mutual inhibition in dictating the robustness in many cell-fate decisions.

Chapter 3

Robustness of Networks with Positive Feedback Loops Fused to Feedforward Loops

3.1. Introduction

A typical bistable switch has a continuous S- or Z-shape signal response curve. Studies on the molecular network of the long-term memory (LTM) of *Aplysia*¹⁶⁹ revealed that in addition to the typical continuous S- and Z- shape curves of the BS, there exist 'mushroom'-type and 'isola' type BS responses. Using systematic analysis of 2-parameter bifurcations, the authors showed that different regions in the 2-parameter bifurcation diagram represent different 'types' of the BS responses. Further analysis of the heat-shock protein network dynamics under different stress levels¹⁷⁴ also featured similar 'mushroom' and 'isola' type BS switches. Recent studies on the differentiation of neural stem cells mediated by bone morphogenetic protein 2 (BMP2) in the central and peripheral nervous systems¹⁷⁰ also suggested the existence of mushroom and isola type bistable bifurcations. These findings suggest that apart from the typical BS switch, the 'atypical' mushroom and isola bifurcations also play crucial roles in cell-fate decisions. It is therefore important to understand the dynamical features of these atypical bifurcations in order to understand the underlying cellular functions. However,

the origin of the atypical bifurcations and the role of network topology in generating these atypical bifurcations still remains elusive. In this Chapter, we address the origin and the dynamical features of the atypical bifurcations by investigating the robustness of network motifs in generating such responses.

In order to understand the role of network motifs in developing typical and atypical BS signal response curves, we designed networks with a single PFL in the form of self-activation and the component with the PFL is under the influence of external input signal via a feed-forward signalling. Therefore, the entire motif represents a fusion between a PFL and a FFL. The FFL has regulations through two different arms, direct and indirect via an intermediate component. By modifying the regulations in the two different arms, we generated eight different network motifs, depending on the different types of regulations (positive or negative) in the FFL. We categorised these networks into two major groups as incoherent and coherent networks. Since all these motifs consist of one PFL, these networks have potential to generate BS switches, however, with disparate abilities. We, therefore investigated the robustness of these networks in generating 1-parameter bistable bifurcations under random parameter perturbations using the potential energy based bifurcation analysis method discussed in Chapter 2.

Systematic analysis of the robustness of these networks reveal that the incoherent networks are capable of producing both typical and atypical bistable responses whereas the coherent networks produced only typical bistability. By perturbing the regulations in the incoherent networks, we found that the mushroom and isola bifurcations are formed by the congregation of two disparate S- and Z-shaped bistable bifurcations. Using phase-plane analysis of these bifurcations, we show that the positive and negative arms of the FFL work in two different signalling regimes as determined by the average signalling thresholds. We show that in the OR gate configuration of the multiple input signals on the target node, the inverted isola (II) and inverted mushrooms (IM) are more robust as compared to the normal isola (NI) and normal mushrooms (NM) and it reverses for the AND and MIXED gate configurations. Finally, we extended the scope of the work by investigating fusion of two PFLs with a FFL where it produces tristable typical and atypical signal response curves.

3.2. Modelling and methodology

3.2.1. The model networks

Consider a component B that self-activates itself thus forming a PFL. S is an input node that regulates B through two different signalling pathways where S directly regulates B and S also indirectly regulates B through A, thus forming a feed-forward loop (FFL) between S and B. The regulations from S to B via the direct and indirect arms can either be positive (activation) or negative (inhibition). Based on the different combination of regulations on the two arms of the FFL, there are eight different networks possible (Figure 3.1). If both the arms in the FFL have different regulations (either positive or negative) it is an incoherent FFL (Figure 3.1, top panel) and if both the arms have same regulations it is a coherent FFL (Figure 3.1, bottom panel).

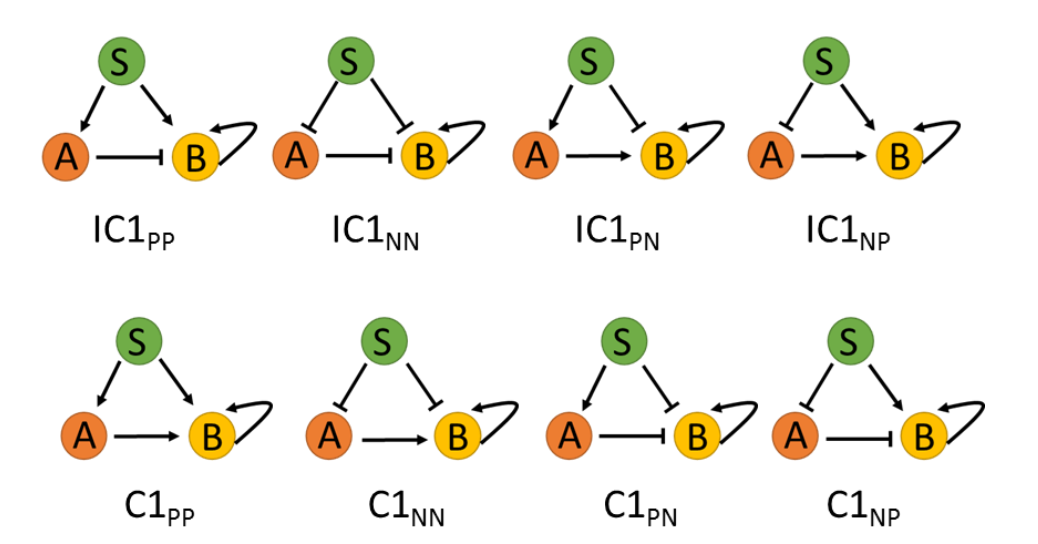


Figure 3.1: Model networks: Network motifs with fusion between a PFL (self-activation on B) and a FFL. Two classes of the networks motifs: Incoherent (top row) and coherent (bottom row). The name of the networks are mentioned below the network diagram. In the name, 'IC' stands for incoherent and 'C' stands for coherent. The number '1' in the name indicates the presence of a PFL. The 'N' and 'P' in the subscript stands for negative and positive regulation, respectively. The first and second letter in the subscript indicate the type of regulation from S to A in the indirect arm and S to B in the direct arm, respectively.

We have used three different modelling methodologies to account for AND, OR and MIXED logic configurations of the regulation of B by the A, S and B itself. Our aim was to determine the robustness of the model networks in generating bistable signal responses including the atypical mushroom and isola bifurcations under random variation of parameter space. To perform this large scale analysis of bifurcations, we resorted to the automation method of bifurcation analysis based on the potential energy landscapes introduced in Chapter 2.

Modelling using AND gate configurations

We used Hill functions to represent the regulatory interactions in the networks. The dynamical equations for the model networks in the AND gate input configurations of node B are written as

$$\frac{dA}{dt} = g_{A,0} + g_{A,1} \cdot H_{A,1}(S) - \gamma_A \cdot A \tag{3.1}$$

$$\frac{dB}{dt} = g_{B,0} + g_{B,1} \cdot H_{B,1}(B) \cdot H_{B,2}(S) \cdot H_{B,3}(A) - \gamma_B \cdot B$$
(3.2)

where, in the case of activation the Hill function is represented as $H_{Y,i}(X) = \frac{\left(\frac{X}{X_{Y,0}}\right)^{n_{XY}}}{1+\left(\frac{X}{X_{Y,0}}\right)^{n_{XY}}}$ and

in the case of inhibition it is
$$H_{Y,i}(X) = \frac{1}{1 + \left(\frac{X}{XY,0}\right)^{n_{XY}}}$$

The parameters of the type $X_{Y,0}$ and n_{XY} represent the threshold value of X required to activate/inhibit Y and Hill coefficient, respectively. In the Eqs. 3.1 and 3.2, $g_{A,0}$ and $g_{B,0}$ are the basal synthesis rates, and $g_{A,1}$ and $g_{B,1}$ are the maximal expression rates of A and B, respectively. γ_A and γ_B are the degradation rate constants of A and B, respectively.

Modelling using OR gate configuration

We have used OR logic of modelling different regulations on B to see if the robustness of the networks depend on the modelling methodologies. In OR gate configurations, the different regulations regulate B in an additive manner thereby suggesting independent regulations on

B. The general form of the dynamical equations for the model networks with OR logic is written as

$$\frac{dA}{dt} = g_{A,0} + g_{A,1} \cdot H_{A,1}(S) - \gamma_A \cdot A \tag{3.3}$$

$$\frac{dB}{dt} = g_{B,0} + g_{B,1} \cdot H_{B,1}(B) + g_{B,2} \cdot H_{B,2}(S) + g_{B,3} \cdot H_{B,3}(A) - \gamma_B \cdot B$$
(3.4)

where, $g_{B,1}$, $g_{B,2}$ and $g_{B,3}$ are the maximal expression rates of B due to B itself, S and A, respectively.

Modelling using MIXED gate configuration

We have incorporated a third type of methodology where the regulations on B are through a MIXED gate configurations of OR and AND gates. In the MIXED gate, the regulations on B from S and A are in AND configuration and this combine regulation is in OR gate configuration with the self-activation. The general form of the dynamical equations for the networks with MIXED gate configurations is written as

$$\frac{dA}{dt} = g_{A,0} + g_{A,1} \cdot H_{A,1}(S) - \gamma_A \cdot A \tag{3.5}$$

$$\frac{dB}{dt} = g_{B,0} + g_{B,1}.H_{B,1}(B) + g_{B,2}.H_{B,2}(S).H_{B,3}(A) - \gamma_B.B$$
(3.6)

Since all the model networks (**Figure 3.1**) have a PFL, we anticipate that all the networks have the potential to generate bistable bifurcations which includes both the typical BS and atypical isola and mushrooms. For all the model networks modelled using AND, OR and MIXED gate configurations, we investigated the robustness of the network motifs in generating typical as well as atypical bistable signal response curves under random parameter variations. The parameters were randomly chosen from independent distributions (**Table 3.1**) and the

threshold parameters $(S_{A,0}, S_{B,0}, A_{B,0}, B_{B,0})$ were determined using the half-functional rule discussed in Chapter 2.

Table 3.1: The parameters and their ranges

Parameters	Ranges
$g_{A,0}$ and $g_{B,0}$	1-10
$g_{A,1},g_{B,1},g_{B,2},g_{B,3}$	1-100
$S_{A,0}, S_{B,0}, A_{B,0}, B_{B,0}$	Using half-functional rule
$n_{SA}, n_{SB}, n_{AB}, n_{BB}$	1-10
γ_A, γ_B	0.01-0.1

3.3. Results and discussions

3.3.1. Bifurcation analysis using the potential energy landscapes

The potential energy landscape based bifurcation analysis is an efficient tool in analysing large number of bifurcation diagrams without the need of manual interventions. For a multi-dimensional system, however, it is difficult to express the effective potential energy function. We therefore reduce the multivariable system into a univariate system using transfer function. In this section, we discuss the method of arriving at the effective potential energy function for a multivariate system. For simplicity purpose, we discuss the method for the model networks with AND gate configuration.

Eq. 3.2 is a dynamical equation of B involving multiple variables. The dynamical equations involving multiple variables is reduced to an equation with a single variable using transfer function. In the model networks, B is regulated by S, A and B itself and can be expressed as a function of these variables. Similarly, A can be expressed as a function of S. Therefore, to

reduce Eq. 3.2 into a single variable, we use the concept of transfer function. Using Eq. 3.1, the SS equation of A can be written as

$$A = (g_{A,0} + g_{A,1}, H_{A,1}(S))/\gamma_A \tag{3.7}$$

Substituting Eq. 3.7 in Eq. 3.2, we get

$$\frac{dB}{dt} = g_{B,0} + g_{B,1} H_{B,1}(B) H_{B,2}(S) H_{B,3}(H_{A,1}^1(S)) - \gamma_B B$$
(3.8)

where
$$H_{A,1}^1(S) = (g_{A,0} + g_{A,1}, H_{A,1}(S))/\gamma_A$$

Eq. 3.8 is the dynamical equation of B with a single variable B. Note that S is an input signal and used as a parameter in the equations.

The effective force of the system, therefore, can be written as

$$F(B,S) = G_B(S,B) - \gamma_B.B \tag{3.9}$$

where, $G_B(S, B) = g_{B,0} + g_{B,1}$. $H_{B,1}(B)$. $H_{B,2}(S)$. $H_{B,3}(H_{A,1}^1(S))$. Using the effective force, the effective potential function can be obtained as

$$V(B,S) = -\int_0^B [G_B(S,x) - \gamma_B.x] \ dx \tag{3.10}$$

Using Eq. 3.10, the potential landscapes were generated at different values of the input signal S. By monitoring the local minima-maxima in the potential landscape at different values of S the bifurcation diagrams were generated. The local minima and maxima in the potential landscapes are associated with stable and unstable SSs. The S value associated with the birth and death of a pair of local minima-maxima represents the SN bifurcation points. Following this method, a large number of bifurcations were generated where we randomly varied the parameter space. Similar method was followed for generating the bifurcation diagrams for the models with OR and MIXED gate configurations.

Apart from the typical bistable bifurcations, the potential energy based method can also identify mushroom bifurcations and bifurcations with broken branches such as isola (Figure 3.2). In Figure 3.2a-b the bistable bifurcation diagrams are overlaid on top of the potential

energy contours. The normal isola (NI) and the inverted isola (II) are presented in **Figure 3.2c** and **Figure 3.2d**, respectively. Both NI and II have two SN points denoted by SN_1 and SN_2 . In the normal mushroom (NM) (e) and the inverted mushroom (IM) (f) there are four SN points represented by SN_1 , SN_2 , SN_3 and SN_4 . The bistable, NI and II bifurcations have one bistable region between SN_1 and SN_2 , whereas in the NM and IM bifurcations, there are two separate bistable regions, one between SN_1 and SN_2 and the other between SN_3 and SN_4 .

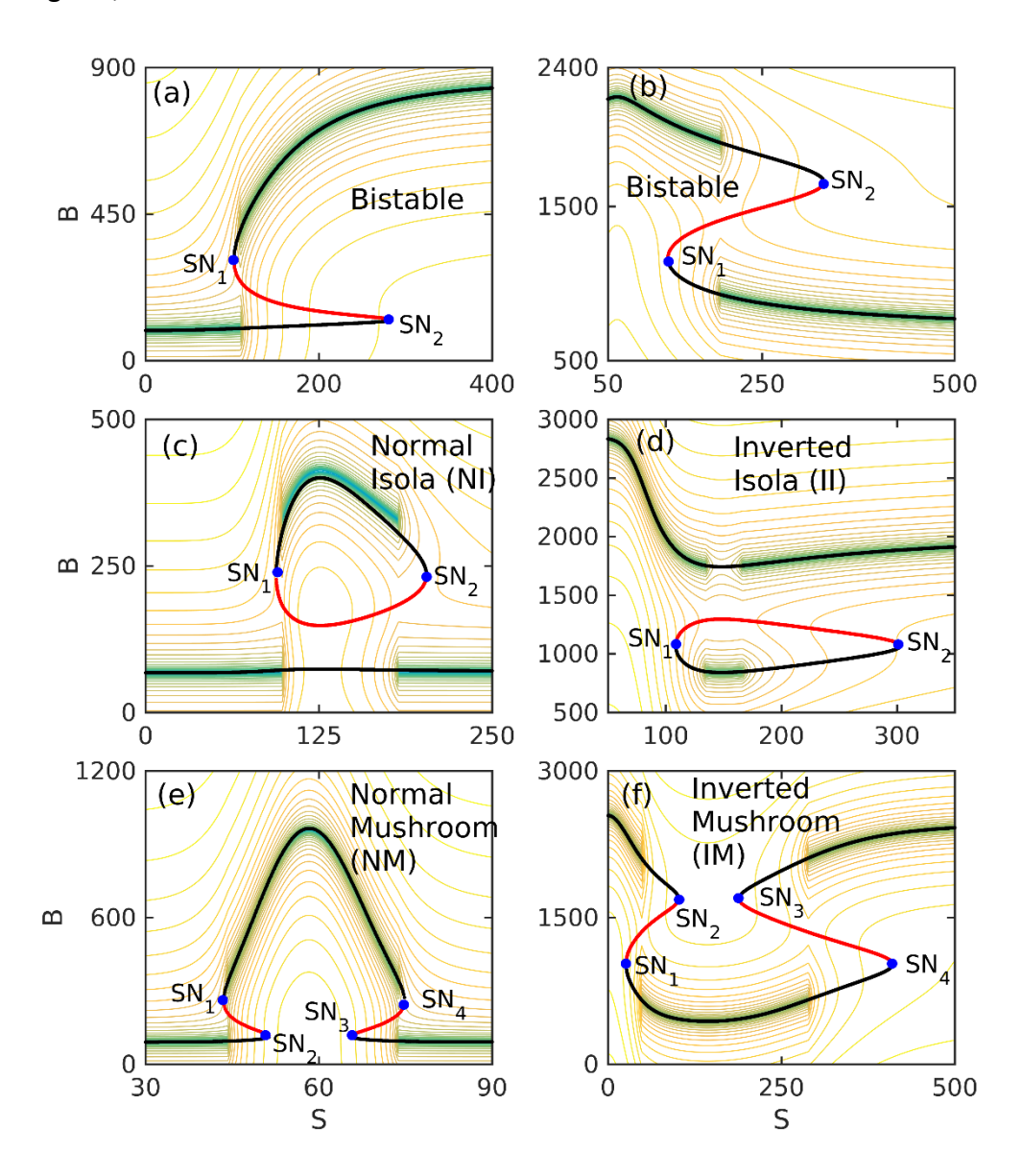


Figure 3.2: The bistable bifurcations generated by the potential energy method: The 1-parameter bifurcations are laid over the contours of the potential energy $(\log(V(B)))$. Continuous bifurcations with two SN points consist of the typical bistable bifurcations (a-b). Bifurcations with broken branches consist of normal isola (NI) (c) and inverted isola (II) (d).

Continuous bifurcations with four SN points consist of normal mushroom (NM) (e) and inverted mushroom (IM) (f). The black and red lines in the bifurcations represent stable and unstable SSs, respectively. The blue filled circles indicate the saddle-node (SN) bifurcation points. The color gradient in the contour plots represent the depth of the potential landscapes with green being the deepest.

3.3.2. Robustness of networks with AND gate configuration

For all the models with AND gate, using the potential energy method, we ran bifurcation analysis for 100,000 random parameter sets. We repeated these calculations 5 times to obtain a quintuplet set. From these runs, we determined the average robustness score for each network motif by counting the number of bistable bifurcations the network generated for 100,000 random parameters averaged over 5 runs. We also categorised each of the bifurcations into typical bistable, normal isola (NI), inverted isola (II), normal mushroom (NM) and inverted mushroom (IM) using the potential energy based method run in MATLAB. We found that the incoherent networks generated a larger number (60%) of total bistable (both typical and atypical) responses as compared to the coherent networks (40%) (Figure 3.3a). However, the incoherent networks are least potent (24%) in generating the typical bistable switches as compared to the coherent networks (76%) (Figure 3.3b). Surprisingly, only the incoherent networks generated atypical bistable responses whereas none of the coherent networks produced any atypical switches (Figure 3.3c). Among the different types of atypical responses generated by the incoherent networks, the NI and NMs are the most robust as compared to the II and IMs (Figure 3.3d). Furthermore, the NI are more robust than the NM in all of the incoherent networks. All the incoherent networks are equally robust in generating the atypical isola and mushroom bifurcations.

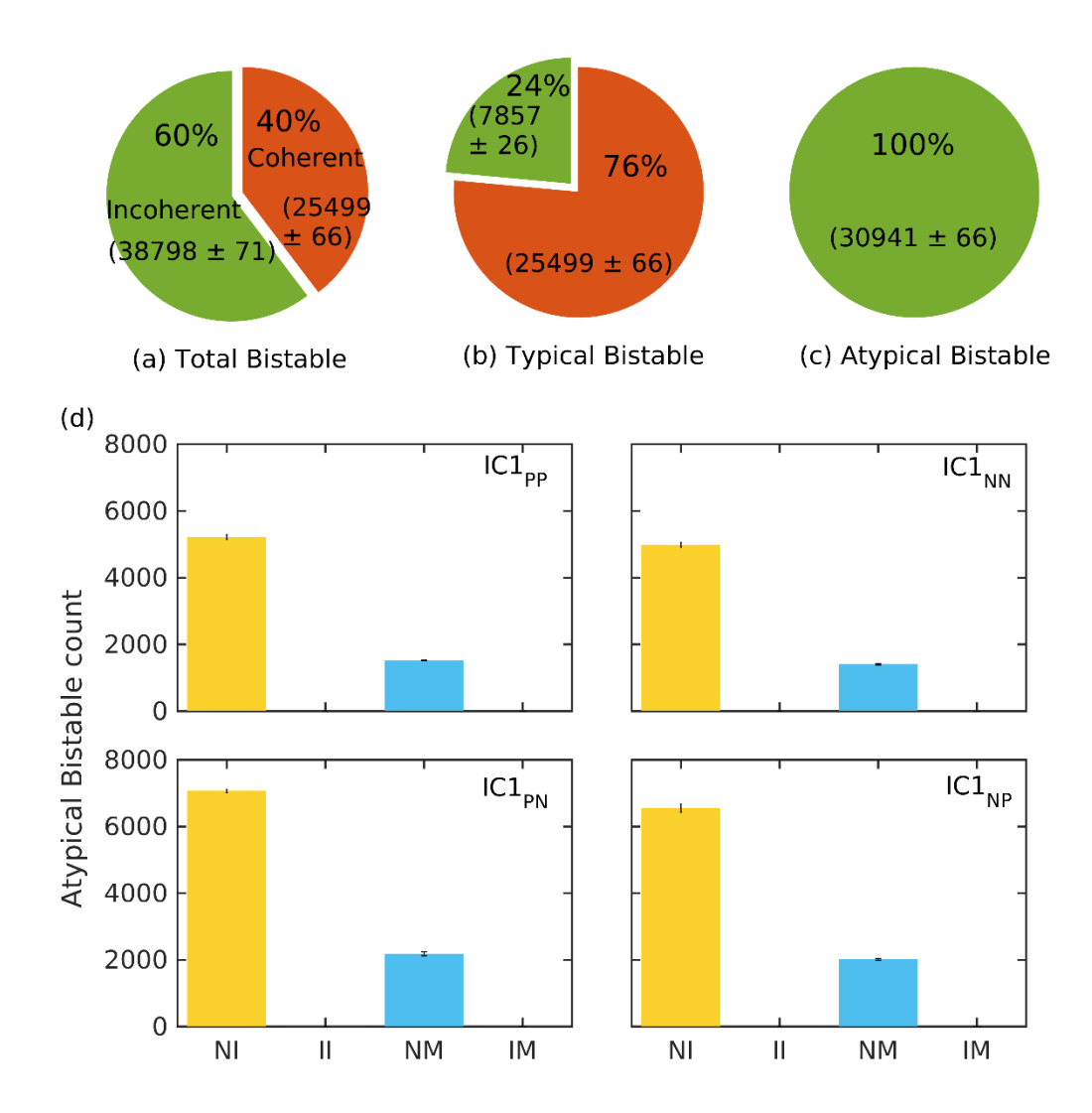


Figure 3.3: The average count of the bistable responses for AND gate: (a) Average percentage of total bistable count (typical and atypical) by the incoherent (green) and coherent (orange) networks. The numerical figure in the parenthesis represent the average count. The average percentage of typical bistable (b) and atypical bistable (c) by incoherent and coherent networks. (d) Average counts of atypical bifurcations generated by the incoherent networks. NI: Normal Isola, II: Inverted Isola, NM: Normal Mushroom and IM: Inverted Mushroom. The error bars represent ±1 standard error of mean.

3.3.3. The origin of the isola and mushroom bifurcations

To understand the rationale behind coherent networks not generating any atypical isola or mushroom bifurcations, we systematically analysed the origin of isola and mushroom bifurcations by the incoherent networks. To begin with, we looked into the origin of isola bifurcation. We considered the incoherent network $IC1_{PP}$ and systematically perturbed it by removing the regulation from the two arms without changing the parameter values. We first removed the regulation from A to B in the indirect arm. This perturbed network generated a typical bistable response (Figure 3.4a). The bistable bifurcation showed an increasing response with increase in input signal S due to the fact that S positively regulates B. Next, we removed the regulation from the direct arm which also resulted in a typical bistable response (Figure 3.4b). However, this bistable bifurcations showed a decreasing response with increase in S because of the negative regulation from S to B. Hence the two bistable bifurcations generated by the two different perturbations are qualitatively opposite in nature. The congregation of these two qualitatively opposite bistable bifurcations resulted in an isola bifurcation for the full unperturbed network (Figure 3.4c-d).

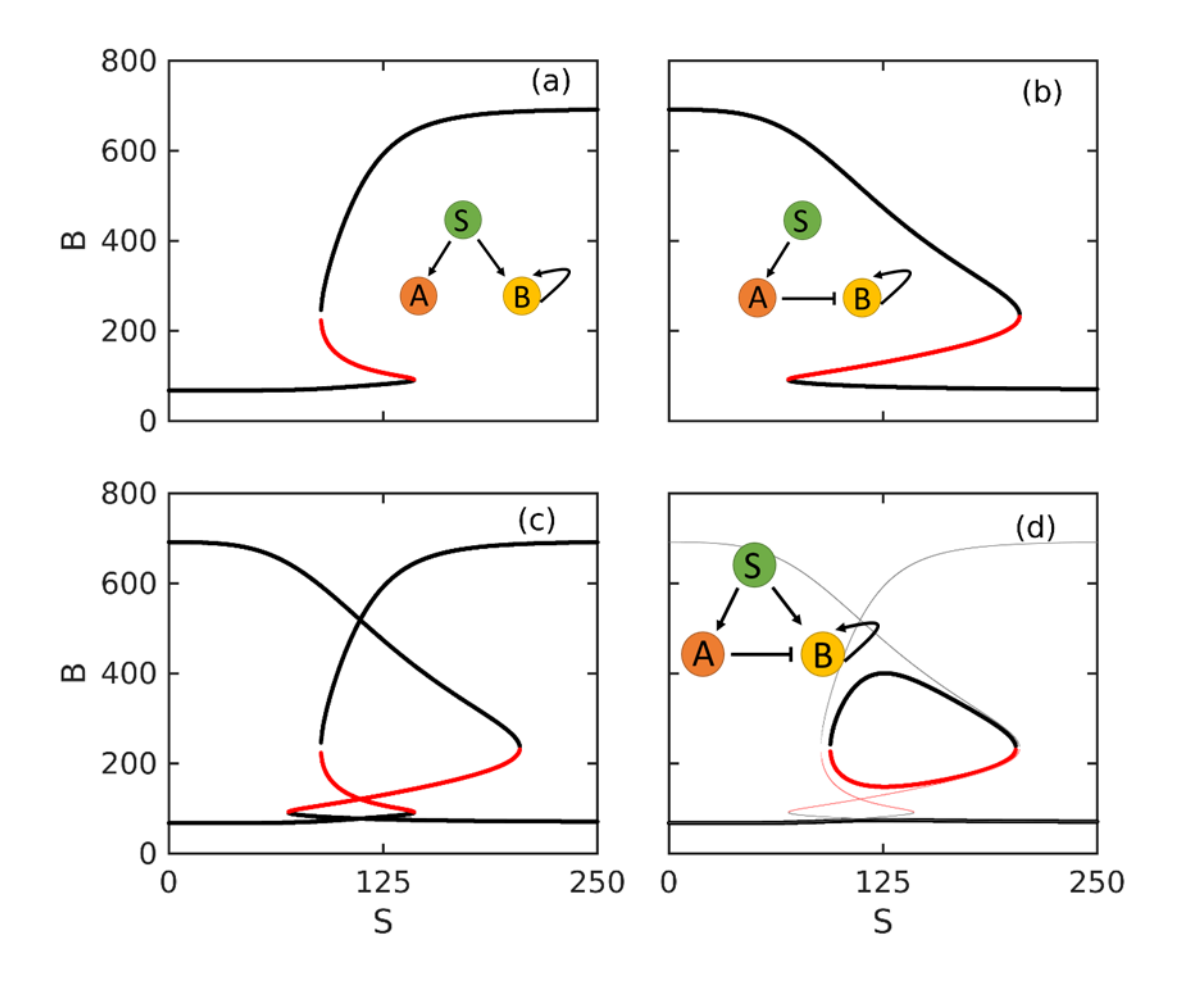


Figure 3.4: The origin of the isola bifurcations: The network IC1_{PP} was perturbed by removing the regulations from the two arms. Bistable response on removing the regulation from A to B

in the indirect arm (a) and from S to B in the direct arm (b). (c) The congregation of the two distinct bistable responses. (d) The formation of isola due to the congregation of the two distinct bistable bifurcations for the full network. The parameters used to plot the NI are: $g_{A,0}=8.0346, g_{A,1}=85.4358, g_{B,0}=4.8210, g_{B,1}=44.9532, S_{A,0}=135.3604, S_{B,0}=94.4814, B_{B,0}=201.0295, A_{B,0}=599.6196, n_{SA}=2, n_{SB}=6, n_{BB}=4, n_{AB}=3, \gamma_A=0.0995, \gamma_B=0.0714$. To plot the bistable response in (a) and (b), the interaction $H_{B,3}(A)$ and $H_{B,2}(S)$ was removed, respectively, without altering the parameter values.

Similar analysis was performed to understand the origin of the mushroom bifurcations. Here too, the congregation of two qualitatively opposite bistable bifurcations from the two differently perturbed networks resulted in a mushroom bifurcation for the full unperturbed network (Figure 3.5).

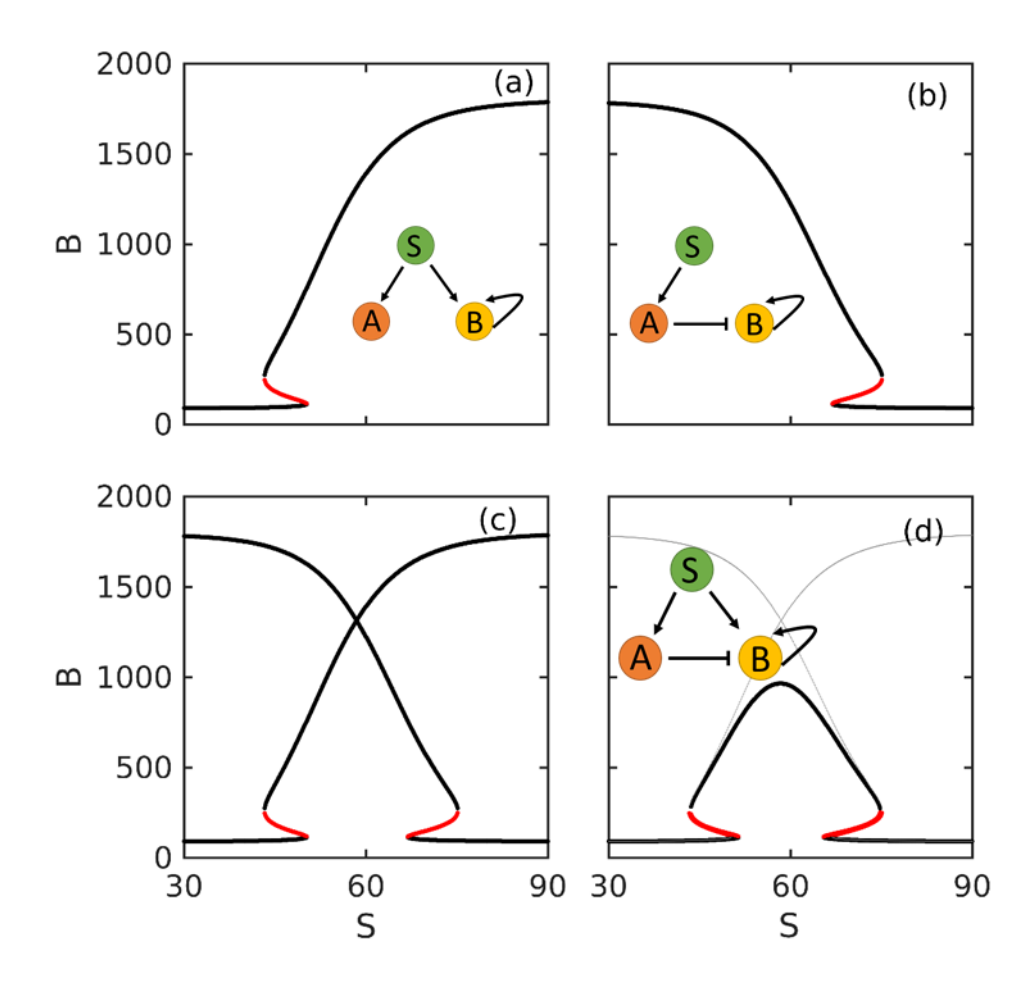


Figure 3.5: The origin of the mushroom bifurcations: The network IC1_{PP} was perturbed by removing the regulations from the two arms. Bistable response on removing the regulation

from A to B in the indirect arm (a) and from S to B in the direct arm (b). (c) The congregation of the two distinct bistable responses. (d) The formation of mushroom due to the congregation of the two distinct bistable bifurcations for the full network. The parameters used to plot the NI are: $g_{A,0}=3.8761, g_{A,1}=74.6160, g_{B,0}=2.7198, g_{B,1}=51.4442, S_{A,0}=162.1356, S_{B,0}=52.7809, B_{B,0}=220.9353, A_{B,0}=688.9720, n_{SA}=3, n_{SB}=9, n_{BB}=5, n_{AB}=7, \gamma_A=0.0119, \gamma_B=0.0301.$ To plot the bistable response in (a) and (b), the interaction $H_{B,3}(A)$ and $H_{B,2}(S)$ was removed, respectively, without altering the parameter values.

Similar perturbation analysis performed on other incoherent networks also resulted in similar conclusions. We conclude that the congregation of two qualitatively opposite bistable bifurcations give rise to atypical isola and mushroom bifurcations. The qualitatively opposite nature of the bistable bifurcations is an important criteria in the formation of the atypical isola and mushroom bifurcations. The opposite nature of the two bistable responses is due to the fact that the regulation from S to B in the incoherent networks are different in the two different arms. Whereas, in the coherent networks, the regulations are identical in two different arms, hence, cannot produce opposite bistable responses. Therefore, coherent networks do not produce any atypical isola and mushroom bifurcations.

AND gate configurations of the input signal on B generated a large number of NI and NM bifurcations and rarely produced II and IM bifurcations (**Figure 3.3d**). For the AND logic gate the Hill functions for different regulations on B are represented in a multiplicative manner $[H_{B,1}(B).H_{B,2}(S).H_{B,3}(A)]$ because of which all the regulations are significant. Due to the contrasting nature of the regulations in the incoherent FFL, the effective regulation on B is low at low and high S input values. Therefore, the average counts of NI and NMs are significantly higher as compared to the II and IMs. One important feature of the NI and NM bifurcations is that the positive and the negative arms are initiated at low and high values of S, respectively in the incoherent networks. This feature can also be supported by analysing the phase-plane diagrams (**Figure 3.6**) corresponding to the NI bifurcation shown in **Figure 3.2c**, for the incoherent network IC1_{PP}. In the phase-plane diagrams, A and B-nullclines are plotted at different S values. At low input signal S (S=80,90,120,150), the A-nullcline changes a little while the B-nullcline changes in shape and values significantly (**Figure 3.6a-d**)

suggesting the onset of the positive regulation. Whereas at high values of S (S = 180, 200, 220, 250), the B-nullcline becomes static but the A-nullcline changes significantly (Figure 3.6d-h) suggesting the onset of the negative regulation. Similar results were observed in the phase-plane diagrams for the NM bifurcations generated by the same network (Figure 3.7).

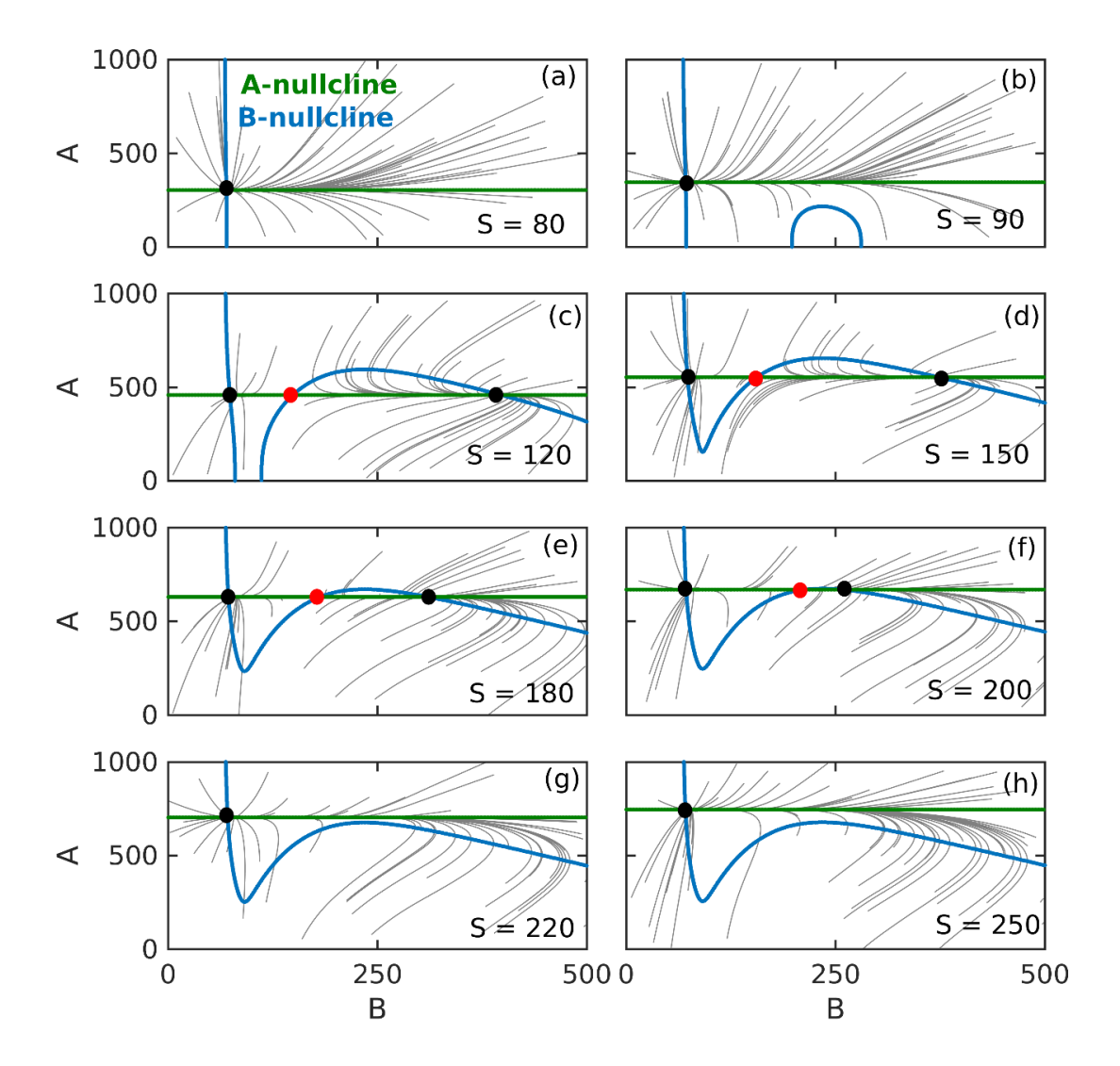


Figure 3.6: The phase-plane analysis for the normal isola bifurcation: The normal isola (Figure 3.2c) is generated by the incoherent network IC1_{PP}. The blue and green curves represent B and A nullclines, respectively. The intersection of the two nullclines indicate a SS. The black and the red solid circles represent stable and unstable SSs, respectively. The S indicates the input signal. The grey lines represent the trajectories obtained from various initial conditions. The parameter values reported in **Figure 3.4** are used here.

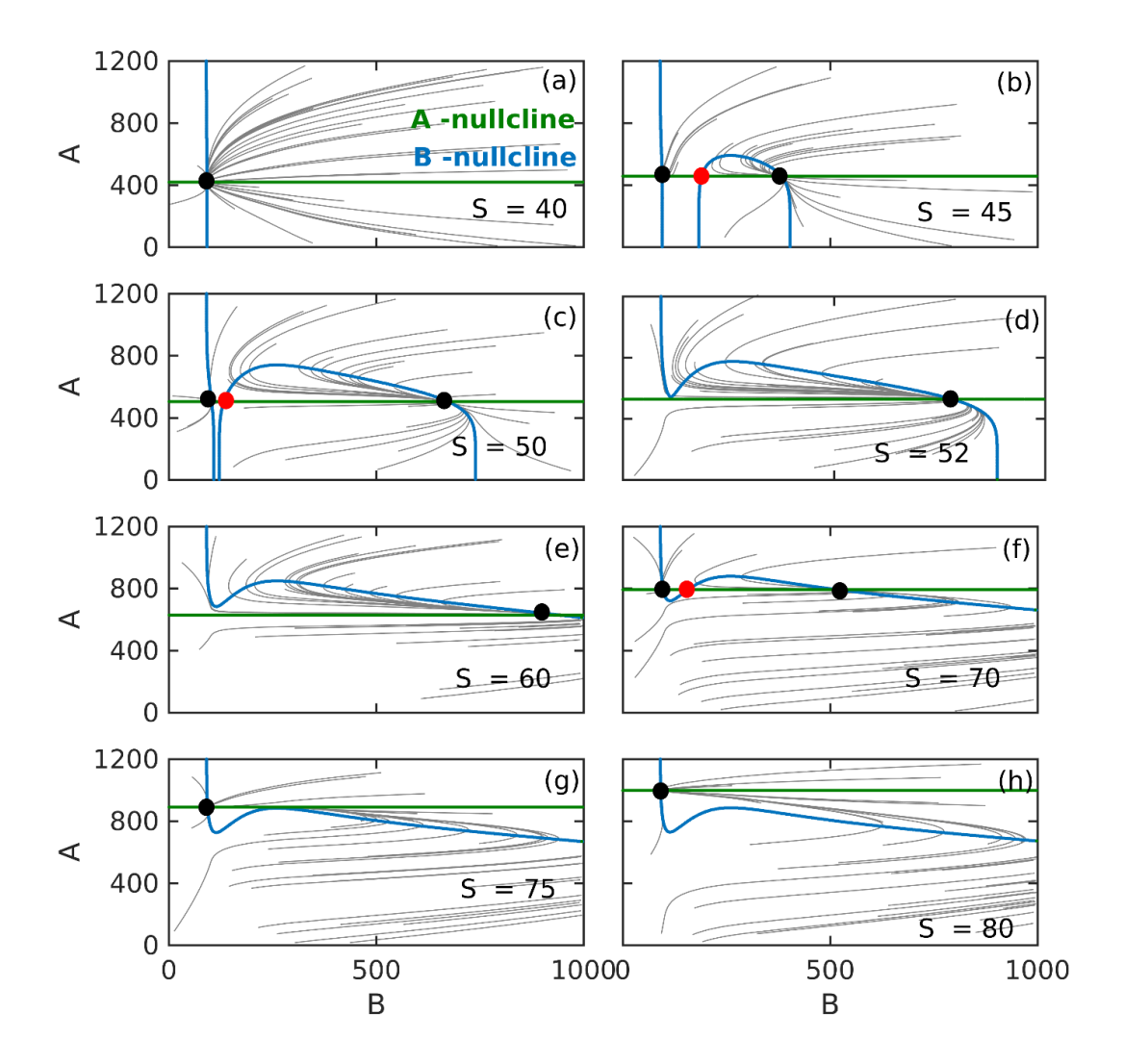


Figure 3.7: The phase-plane analysis for the normal mushroom bifurcation: The normal mushroom (Figure 3.2e) is generated by the incoherent network IC1_{PP}. The blue and green curves represent B and A nullclines, respectively. The intersection of the two nullclines indicate a SS. The black and the red solid circles represent stable and unstable SSs, respectively. The S indicates the input signal. The grey lines represent the trajectories obtained from various initial conditions. The parameter values reported in Figure 3.5 are used here.

In order to establish the generality of the finding that for the NI and NMs, the positive and the negative arms must trigger at low and high signal strengths, respectively, we recorded the threshold of the regulations of these two arms for normal atypical bistable responses for all the incoherent networks. In **Figure 3.8** we present the average of these thresholds for all the incoherent networks.

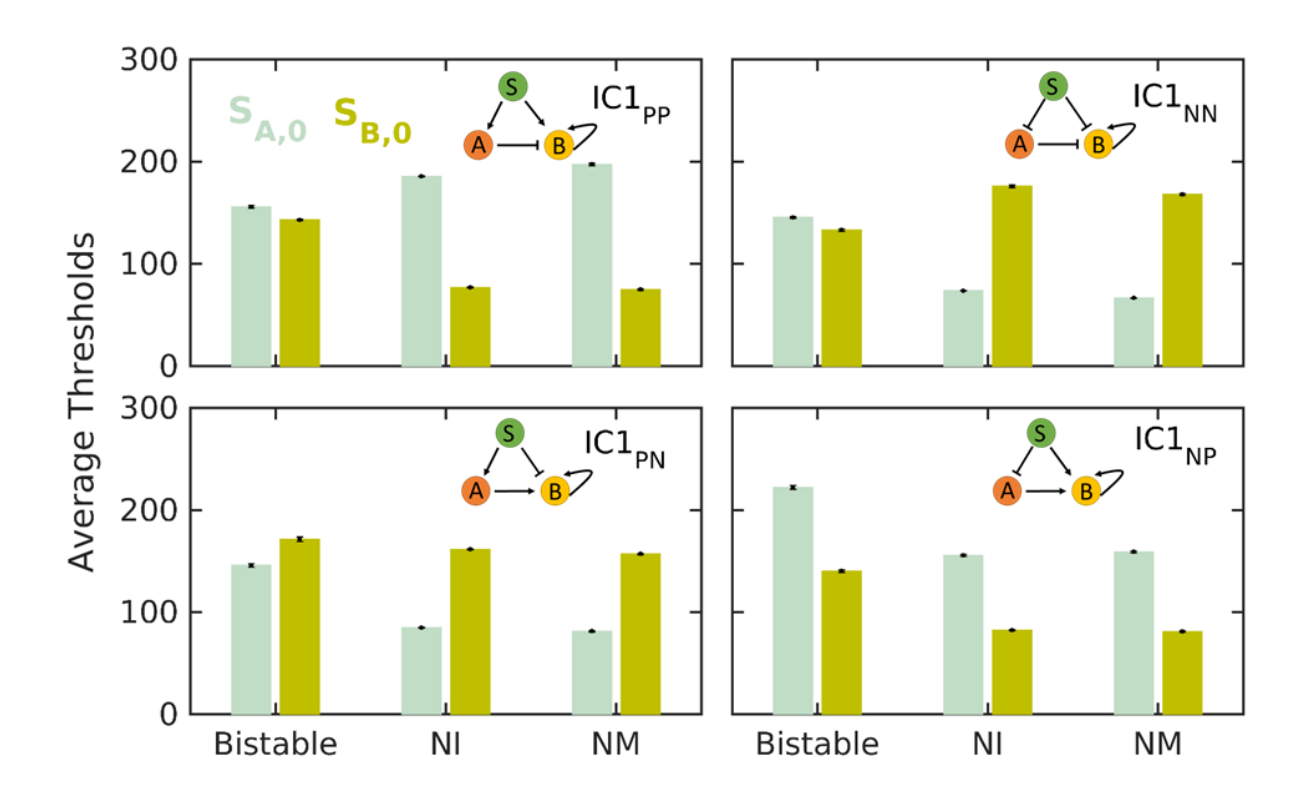


Figure 3.8: The average threshold values of S for the incoherent networks with AND gate: $S_{A,0}$ and $S_{B,0}$ are the threshold values of S for the indirect and the direct arm, respectively. The error bars represent ± 1 standard error of mean.

In all the incoherent networks, for the NI and NM bifurcations, the average threshold value of the positive arm is much lower compared to the average threshold value in the negative arm. For the typical bistable bifurcations, the average threshold values in the two different arms are of comparable values. The low threshold value in the positive arm indicate that at low values of the input signal S, the positive arm is initiated while the high threshold value in the negative arm indicate that at high S, the negative arm is initiated, thus giving rise to a normal atypical bistable response.

3.3.4. Robustness of networks with OR gate configuration

We again made use of the potential method to generate 1-parameter bifurcation diagrams for 100,000 random parameter combinations ran in quintuplet. We used Eq. 3.3 and Eq. 3.4 in this case. We found that the coherent networks are most robust (60%) in producing total bistable responses as compared to the incoherent networks (40%) (Figure 3.9a). This is opposite to what we found in case of AND gate configuration. Furthermore, in OR gate configurations, the coherent networks are once again more robust (71%) in generating typical bistable responses as compared to the incoherent networks (29%) (Figure 3.9b). Similar to the AND gate, here too, the coherent networks did not produce any atypical bifurcations (Figure 3.8c). Among the various atypical responses, the robustness of II and IMs are higher than that of the NI and NMs. This finding is opposite to the responses observed in the AND gate configurations where the NI and NMs were most robust than II and IMs.

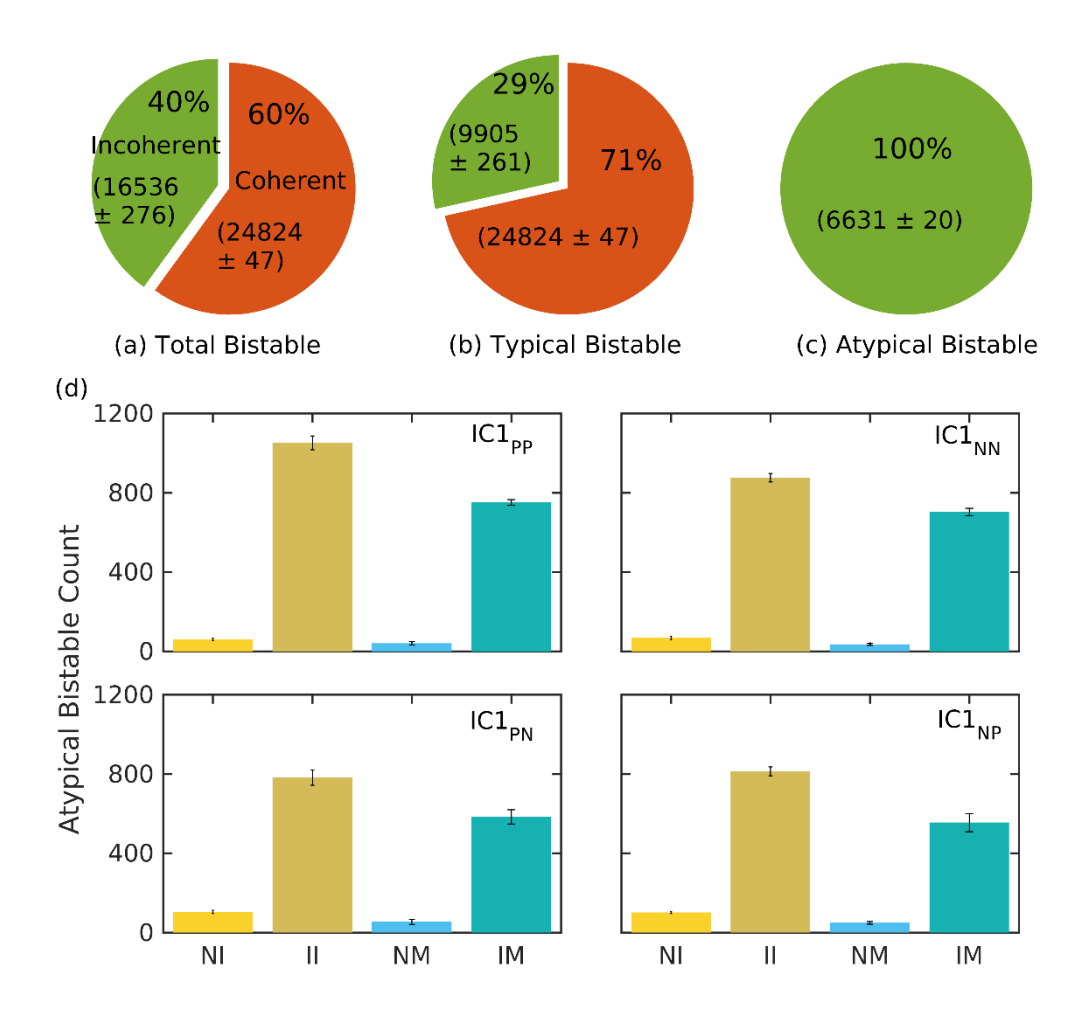


Figure 3.9: The average count of the bistable responses for OR logic: (a) Average percentage of total bistable count (typical and atypical) by incoherent (green) and coherent (orange) networks. The numerical figure in the parenthesis represent the average value of the count. The average count of typical bistable (b) and atypical bistable (c) by incoherent and coherent networks. (d) Different types of atypical bifurcations generated by the incoherent networks.

NI: Normal Isola, II: Inverted Isola, NM: Normal Mushroom and IM: Inverted Mushroom. The error bars represent ± 1 standard error of mean.

Since in the OR logic all the different regulations are independently regulating B in an additive manner $[H_{B,1}(B) + H_{B,2}(S) + H_{B,3}(A)]$, there is a possibility of getting both inverted and normal atypical bifurcations. However, because of the contrasting regulations of the incoherent FFL, the effective regulation on B is high at low and high S values. Therefore, the counts for II and IMs are more than NI and NMs for OR logic since the II and IMs have high induction of the gene at low and high signal values.

The average threshold values $S_{A,0}$ and $S_{B,0}$ for the two different arms in the incoherent networks suggest that in case of II and IMs, the negative arm is initiated at lower values of S whereas the positive arm is initiated at higher values of S (Figure 3.10).

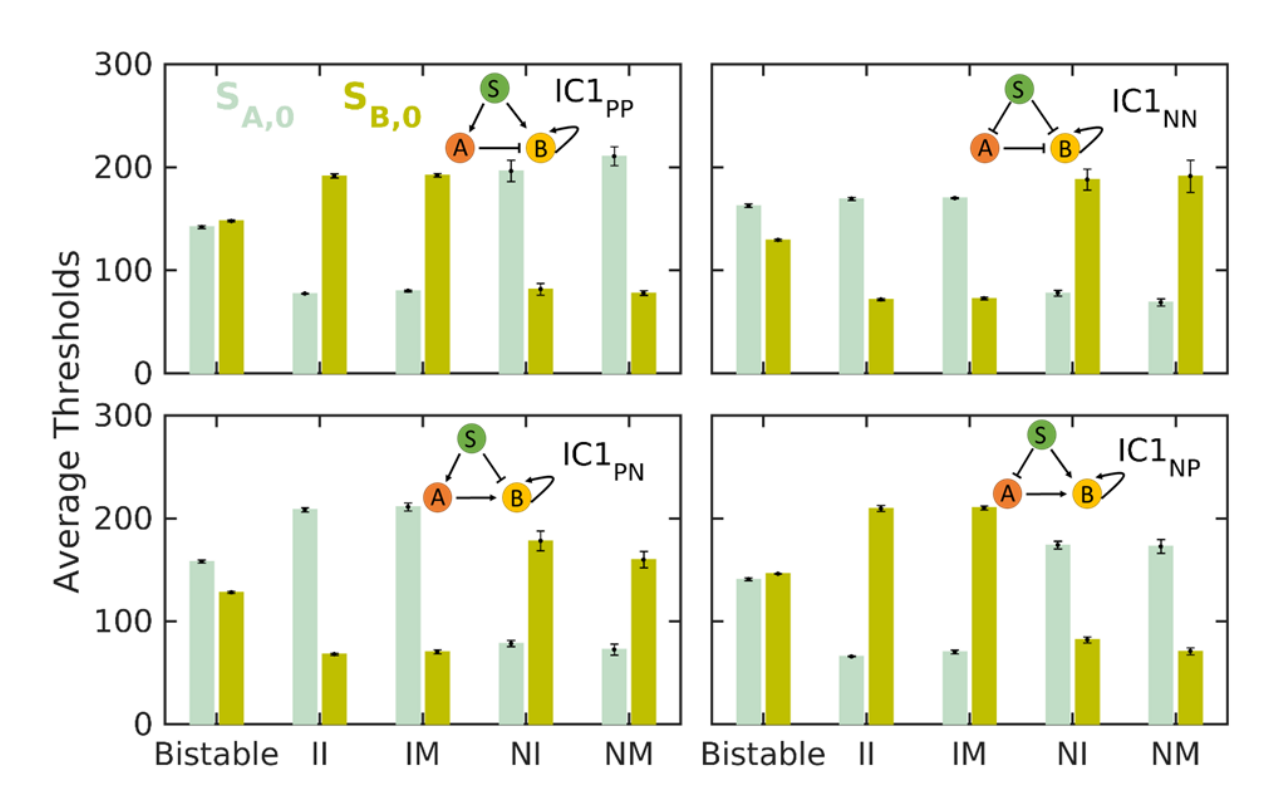


Figure 3.10: The average threshold values of S for the incoherent networks with OR gate: $S_{A,0}$ and $S_{B,0}$ are the threshold values of S for the indirect and the direct arm, respectively. The error bars represent ± 1 standard error of mean.

The smaller threshold value of the negative arm for the II and IM bifurcations in all the incoherent networks suggest that at lower S input signals, the negative arm is initiated. Similarly the threshold values for the positive arm for the same bifurcations are larger indicating that at higher S values, the positive arm is initiated. Whereas, for NI and NM bifurcations, the threshold values for the positive arm are smaller than the threshold values for the negative arm suggesting that at lower S values, the positive arm is initiated and at higher S values, the negative arm is initiated. These are the characteristic features of the threshold values for different bistable responses.

3.3.5. Robustness of networks with MIXED gate configuration

Much like the OR gate configurations, in the MIXED gate we found that the coherent networks are most robust (63%) in producing total bistable responses as compared to the incoherent networks (37%) (Figure 3.11a). Similar to the AND and OR gate configurations, we found that in the MIXED gate also the coherent networks produced more number (77%) of typical bistable switches than the incoherent networks (23%) (Figure 3.11b). Once again, the coherent networks are not at all capable of generating any type of atypical isola and mushroom bifurcations (Figure 3.11c). Among the different types of the atypical switches, the NI and NMs are more robust in all the incoherent networks as compared to the II and IMs (Figure 3.9d). These findings are similar to that of in AND gate (Figure 3.3d) but opposite to that of in OR gate configuration (Figure 3.9d).

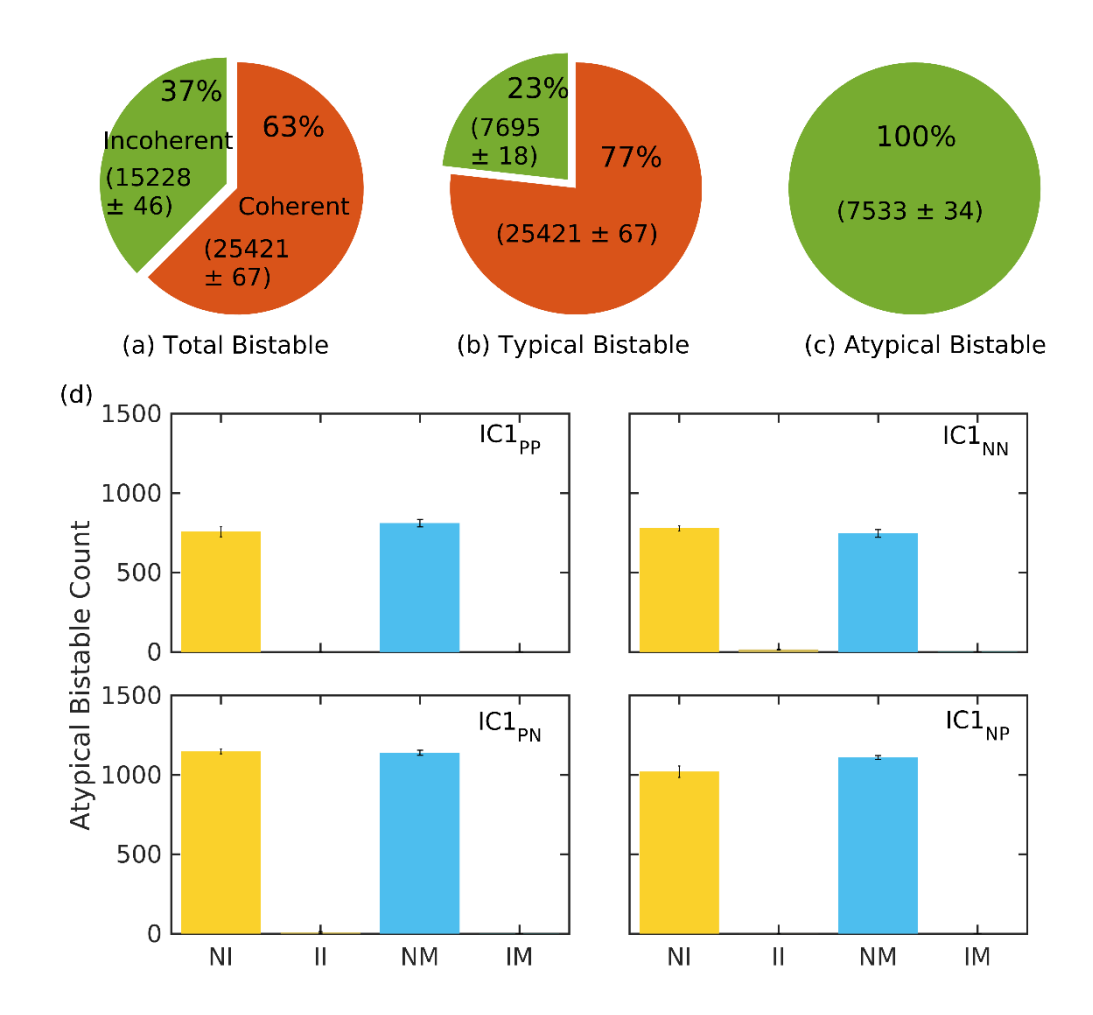


Figure 3.11: The average count of the bistable responses for the MIXED logic: (a) Average percentage of total bistable count (typical and atypical) by incoherent (green) and coherent (orange) networks. The average count is denoted in the parenthesis. The average count of typical bistable (b) and atypical bistable (c) by incoherent and coherent networks. (d) Different types of atypical bifurcations generated by the incoherent networks. NI: Normal Isola, II: Inverted Isola, NM: Normal Mushroom and IM: Inverted Mushroom. The error bars represent ± 1 standard error of mean.

Again, for the same reasons that the two contrasting regulations ($(H_{B,2}(S))$ and $H_{B,3}(A)$) are in multiplicative manner, the SS value of B is low at low and high S input signal values. Therefore, in MIXED gate configurations, the number of NI and NMs are more compared to the number of II and IMs, similar to in AND gate.

3.3.6. Addition of a second PFL to the model networks

We extended the model networks by adding an additional PFL by introducing an interaction from B to A (Figure 3.12). The model networks now have two fused PFLs and S regulate both the components A and B. Based on the regulations from S to B via the two different arms, these networks can be categorised into two classes, incoherent and coherent. Since two PFLs are present in the networks, all the networks have the potential to produce tristable responses. We used the potential energy based method to carry out the tristable bifurcation analysis. We found that all the incoherent networks are able to produce both typical as well as atypical tristable bifurcations (Figure 3.13).

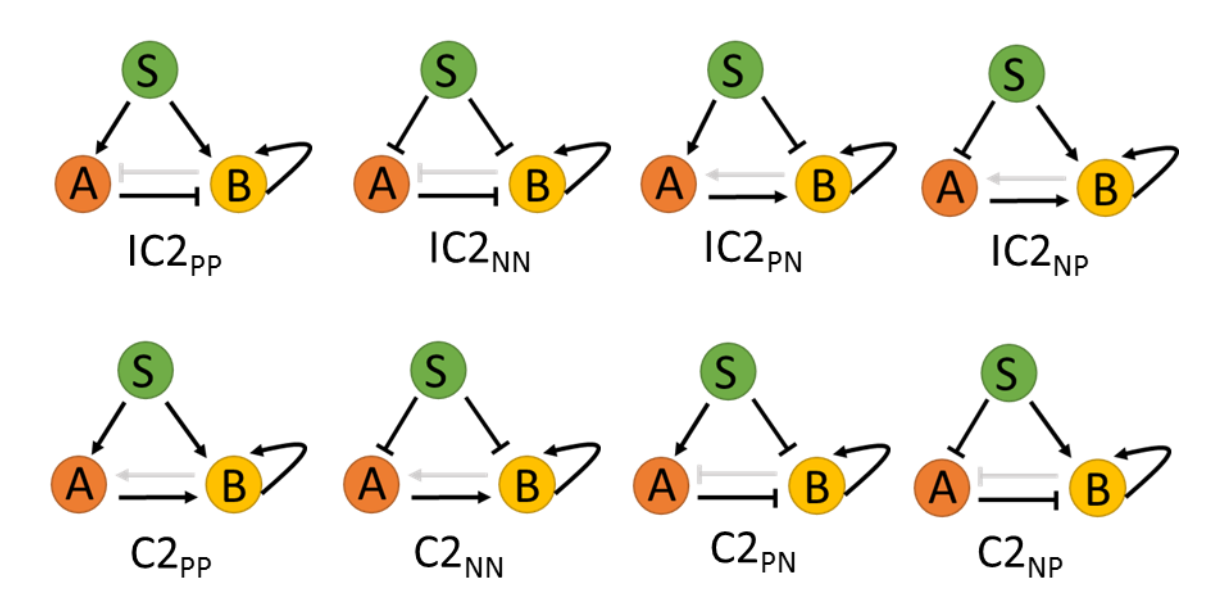


Figure 3.12: Networks with added PFL: A regulation from A to B (grey) is added to the network motifs in Figure 3.1, thus incorporating an additional PFL. Two classes of the networks motifs: Incoherent (top row) and coherent (bottom row). The name of the networks are mentioned below the network diagram. The grey lines represent the trajectories obtained from various initial conditions. The number '2' in the name stands for two PFLs. The 'N' and 'P' in the subscript stands for negative and positive regulation, respectively. The first and second letter in the subscript indicate the type of regulation from A to B in the indirect arm and S to B in the direct arm, respectively.

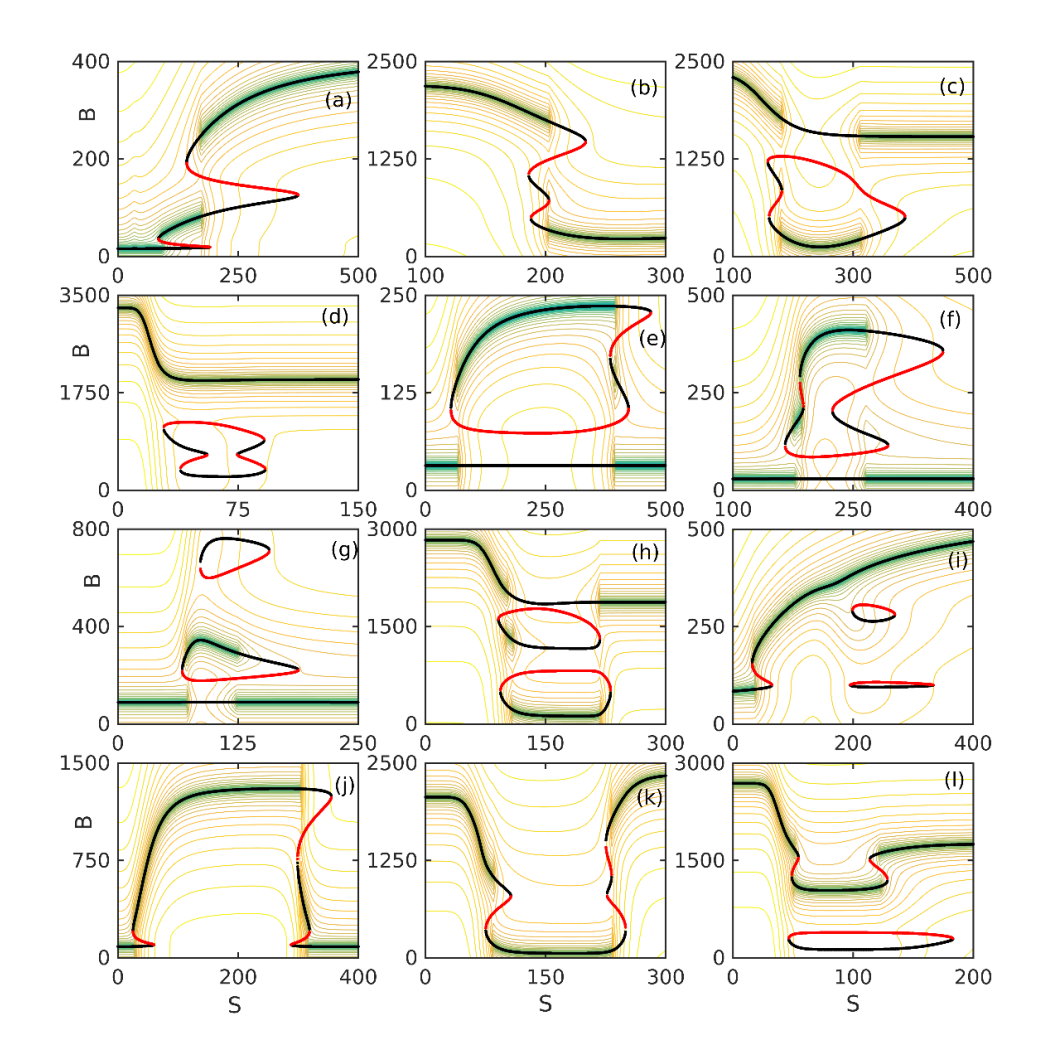


Figure 3.13: The tristable bifurcations overlaid on top of the contours of the potential energy: Different tristable bifurcations generated by the incoherent tristable networks. (a-b) are the typical tristable bifurcations whereas the remaining (c-l) are the atypical tristable bifurcations. The black and red lines represent the stable and unstable SSs, respectively.

3.4. Summary and conclusions

Bistable switch is employed by many cell-fate decision making systems to convert a graded response into a digital 'all-or-none' response. A typical bistable response consists of a continuous S- or Z-shape loci of the SSs of the variable of interest as a function of input signal. However, not all BS responses are continuous. Previous works suggest the existence of bistable responses with 'broken' branches of the SSs and are known as isola bifurcations. Furthermore, previous investigations also suggest the presence of bistable switches which

have a combined S- and Z- shape signal response curves and are known as mushroom bifurcations. The isola and mushroom bifurcations can be termed as 'atypical' bistable bifurcations.

The typical bistable and atypical mushroom are continuous curves whereas the atypical isola has a discontinuous curve or 'broken' SSs. The conventional method of analysing bifurcations using XPPAUT or Oscil8 uses numerical continuation method which rely on initial conditions to generate the SS values from the differential equations. Therefore, the numerical continuation method has the ability to analyse the continuous bifurcations such as the typical bistable and atypical mushrooms, whereas, it is difficult to identify bifurcations with discontinuous or broken branches such as the isola. We here, used the potential energy landscape method discussed in Chapter 2 to identify the broken SSs thereby analysing the atypical isola bifurcations and also various other bistable bifurcations.

Isola and mushrooms are known to regulate the differentiation of neural stem cells, and the dynamics of heat shock proteins. Chemical noise can interfere with the cell-fate decisions and change its dynamics and outcomes. The cell-fate decisions, therefore, adapt to certain topology of the regulatory motifs to limit the effects of the chemical noise. In this Chapter, we investigated the robustness of networks with PFL fused to FFL (Figure 3.1) that have the potential to generate both typical as well as atypical bifurcations under variation of random parameter space. The networks are classified into incoherent and coherent based on the regulations on the two different arms of the FFL. In case of incoherent networks, the regulations are different whereas in case of coherent the regulations are same. Using the potential based bifurcation analysis method, we found that these model networks are able to generate typical as well as atypical bistable bifurcations (Figure 3.2). We modelled the dynamical equations for the networks with AND, OR and MIXED gate configurations of the input signals on B to determine if the robustness of the bistable bifurcations depend on the modelling methodologies.

To investigate the robustness of the networks, we generated 100,000 random parameter combinations in quintuplet sets and ran bifurcation analysis for each network. We then calculated the average number of bistable bifurcations generated by each network to

determine the robustness score. The bistable bifurcations are categorised into typical and atypical using the potential based method. We found that all the incoherent networks are able to generate both typical as well as atypical bistable bifurcations whereas the coherent networks generated only typical bistable responses. Among the different atypical bifurcations, with OR gate, II and IMs are most robust as compared to the NI and NMs (Figure 3.9). Whereas with AND and MIXED gate configurations, the NI and NMs are most robust compared to II and IMs (Figure 3.3 and Figure 3.11). With OR gate, since the different interactions on B are added in the dynamical equations (Eq. 3.4), the effective regulation can generate either normal or inverted atypical bistable responses. On the other hand with AND and MIXED gate configurations, the interactions are multiplied (Eq. 3.2 and Eq. 3.6) which lowers the effective regulation on B at low and high input signals, thus generating mostly normal atypical responses.

What makes the incoherent network more robust than coherent networks in generating isola and mushroom bifurcations? To address this question, we investigated the origin of the isola and mushroom bifurcations. With systematic perturbations of the incoherent networks, we found that the isola and mushroom bifurcations are formed by the congregation of two qualitatively opposite bistable bifurcations (Figure 3.4 and Figure 3.5). We observed that the two qualitatively opposite bistable bifurcations are formed due to the two different regulations in the incoherent networks. Similar opposite behaviour of the bistable bifurcations are not observed in the coherent networks due to the presence of similar regulations on the two different arms. Therefore, coherent networks do not have the potential to generate atypical isola and mushroom bifurcations.

Furthermore, we observed that the NI and NM bifurcations are formed when the positive arm of the FFL is initiated at low signal and the negative arm is initiated at high signal (Figure 3.6 and Figure 3.7). However, the II and IM bifurcations are formed when the negative arm acts as low signal and positive arm acts at high signal. These observations are supported by the mean threshold values of the component S for the two different regulations (Figure 3.8 and Figure 3.10). We extended the networks by incorporating an additional PFL that resulted in tristable networks (Figure 3.12). The incoherent tristable networks generated typical as well as atypical tristable bifurcations (Figure 3.13)

Chapter 4

Arrangements of Multiple Positive Feedback Loops and the Robustness of Bistable Switches

4.1. Introduction

A clonal population of cells in identical environmental conditions exhibit significant cell-to-cell variations thus creating cellular heterogeneity. Cellular heterogeneity is a natural phenomenon where in an isogenic population a cell differs from other cells in terms of its size, shape, protein and mRNA contents, cell cycle duration and response to stimuli 102,175. Cellular heterogeneity is caused due to the presence of the two types of chemical noise: intrinsic 91,176 and extrinsic noises 83,84,177–180. Intrinsic noise is inherent to a cell and arises because of fluctuations of low copy numbers of the chemical species undergoing chemical reactions in the cell and extrinsic noise has global effect on all the chemical reactions in the cell. While in some cellular processes such as cell cycle 181, p53 dynamics 182, apoptosis 183, HIV virus latency/replication 184,185, aneuploidy 186, the cellular noise creates nuisance whereas in others the cellular noise helps the cells to adapt to continuously fluctuating environment 187,188. An intriguing question that arises here is how does a living cell minimizes the effects of chemical noise that can cause hindrance to the cellular functions?

From earlier findings, it is known that NFL might minimize the effects of stochastic fluctuations¹²⁷. Since then, a number of researchers in both theoretical/computational^{176,189}– ¹⁹⁴ and experimental ^{195–197} fields shifted their focus on the role of negative feedback in cellular noise. Negative feedback indeed has the potential to attenuate noise but are more sensitive to external signals^{128,129}. Hornung et al., based on calculations on simple network motifs, predicted that PFLs can filter noise and are not sensitive to external signals 128. A PFL also has the potential to convert a graded signal into a digital 'all-or-none' response by creating bistability⁷⁰. Bistability is a common phenomenon found in many biological systems such as cellular differentiation^{36–38}, memory^{39,40}, cell cycle transitions^{43–45}, and maturation of frog eggs^{41,42}. Using system-level stochastic model of budding yeast cell cycle¹²³, it was found that PFLs filter noise in various cell cycle events.

Cellular differentiation processes such as epithelial-to-mesenchymal transitions (EMT)³⁷, adipocyte differentiation³⁶, myogenic and osteogenic differentiation⁴⁷ are regulated by bistable switches. For a cell to be locked in its differentiated state, the system must be able to reduce the effects of noise such that the cells are not reverted to their initial states and vice versa. This is important in cases where from a large pool of precursor cells only a small fraction of cells are differentiated in presence of weak signalling regime. Coupling of a NFL to a bistable response will only generate excitability, hence this is not a feasible solution to minimize the noise in bistable systems^{58,59}. Contrary to this it was shown that two fused PFLs functioning individually in disparate time scales have the potential to reduce the chemical noise^{82,198}. Thus fusion of two or more PFLs might be a possible solution to the problem. However, the way the PFLs are fused can have altering effects on the noise propagation in the system. In a recent study, Ahrends et al., showed that preadipocyte to adipocyte differentiation uses a bistable switch which is generated by seven PFLs arranged in a consecutive manner around a master regulator peroxisome proliferator-activated receptor y (PPARG)⁶¹. This consecutive arrangement of PFLs around a master regulator PPARG can also be named as parallel arrangement of PFLs. They showed that addition of PFLs reduces noise more efficiently compared to a single PFL with high cooperativity.

At this point, a question that is needed to be answered is how the arrangement of multiple PFLs regulate the noise in bistable systems. Just like parallel arrangement, multiple PFLs can also be arranged in a sequential chain-like fashion that we call serial arrangement of PFLs. Here, the parallel and serial arrangement of PFLs are analogous to the parallel and serial arrangement of resistors in electrical circuits. Both the parallel and serial topologies can produce bistable switches with identical average properties, the SS values and the region of bistability. In this chapter, using mathematical modelling and stochastic calculations, we investigated the role of parallel and serial topologies in reducing extrinsic and intrinsic noises. We found that compared to serial arrangements, the cells in parallel PFLs are more stable and less sensitive to chemical noise and are able to maintain their respective differentiated states. Thus, parallel PFLs efficiently reduces the noise compared to serial arrangement of PFLs. Our investigations and calculations suggest that the SN bifurcation points are less sensitive to extrinsic noise and the distribution of SN points are less skewed in parallel PFLs. Also, using mean residence time calculations we found that the stable SSs in parallel arrangement are more stable to intrinsic fluctuations compared to the same in serial PFLs. We have also shown that our results are consistent for both AND or OR-gate configurations of input signals and are independent of modelling methodologies.

4.2. Modelling of the networks

We fused multiple PFLs in two different ways namely parallel and serial arrangements, where, both classes of network topologies have the potential to generate bistable responses. In parallel arrangement, the PFLs are independently fused to a central regulator X_0 and in serial arrangements the PFLs are linked to one another head-to-tail in a chain like manner (Figure 4.1). To begin with, we first created a PFL between X_0 and X_1 where X_0 and X_1 mutually activate each other. This is a single PFL (1L) and serves as a repeating unit for multiple PFLs. Adding another component X_2 via a PFL to X_0 will create a two-loop (2L) parallel motifs whereas if X_2 is fused with X_1 via a PFL it becomes a 2L serial motifs. In parallel motifs, all the new components are added as independent PFLs to X_0 (Figure 4.1a, left) whereas in serial motifs all the new components are added to the preceding component as PFLs (Figure 4.1a, right). This way we generated up to five loops (5L) of both parallel and serial PFLs.

In a signalling system, input signals can be redundant or non-redundant in a way to trigger response. In signal transduction pathways non-redundant input signals behave as AND logic gates and redundant signals functions as OR gate signals much like in electrical circuits²⁴. In this work we have considered both AND and OR gate signalling configurations whenever or wherever required. For example, in parallel motifs, production of X_0 is positively regulated by X_1 , X_2 , etc. either by AND or OR logic gates configuration. In serial motifs, the production of X_1 is positively regulated by X_{1-1} and X_{1+1} , again either by AND or OR gate configurations except for the terminal components.

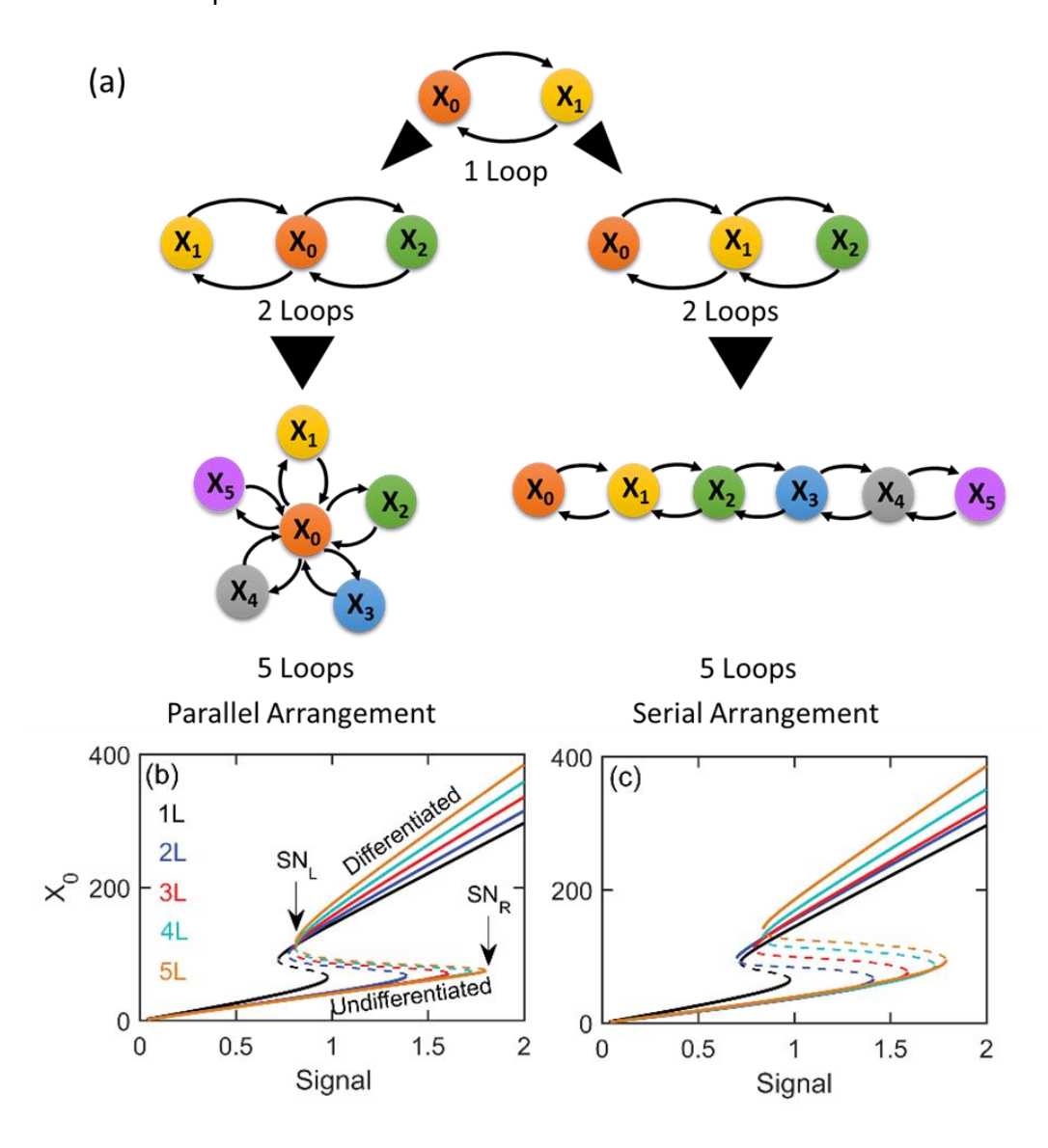


Figure 4.1: Network circuit diagrams and the bistable bifurcation diagrams for the models: (a) PFL between X_0 and X_1 creates a 1L PFL and several of these are fused together either in a parallel (left) or serial arrangements (right). One-parameter bistable bifurcation diagrams for

different number of loops for parallel (b) and for serial (c) motifs. The solid lines represent the stable SSs and the broken lines represent the unstable SSs. The right and left SN points (SN_R and SN_L) are indicated by the arrows. The upper and the lower stable branches represent the differentiated and undifferentiated (dedifferentiated) states respectively.

In the basic repeat unit of a PFL, the production rate of X_0 is directly proportional to the amount of X_1 present and X_0 in turn helps the production of X_1 through enzymatic activation of the TF (T_1) for X_1 . The TF (T_1) has two states, active ($T_{1,A}$) and inactive ($T_{1,I}$), and T_1 0 catalyzes the transcription activation (**Figure 4.2**). The synthesis rate of the component T_1 1 is directly proportional to the amount of active TF ($T_{1,A}$). This represent a single PFL (1L) and is capable of generating bistable response in presence of enough non-linearity or ultrasensitivity¹⁹⁹.

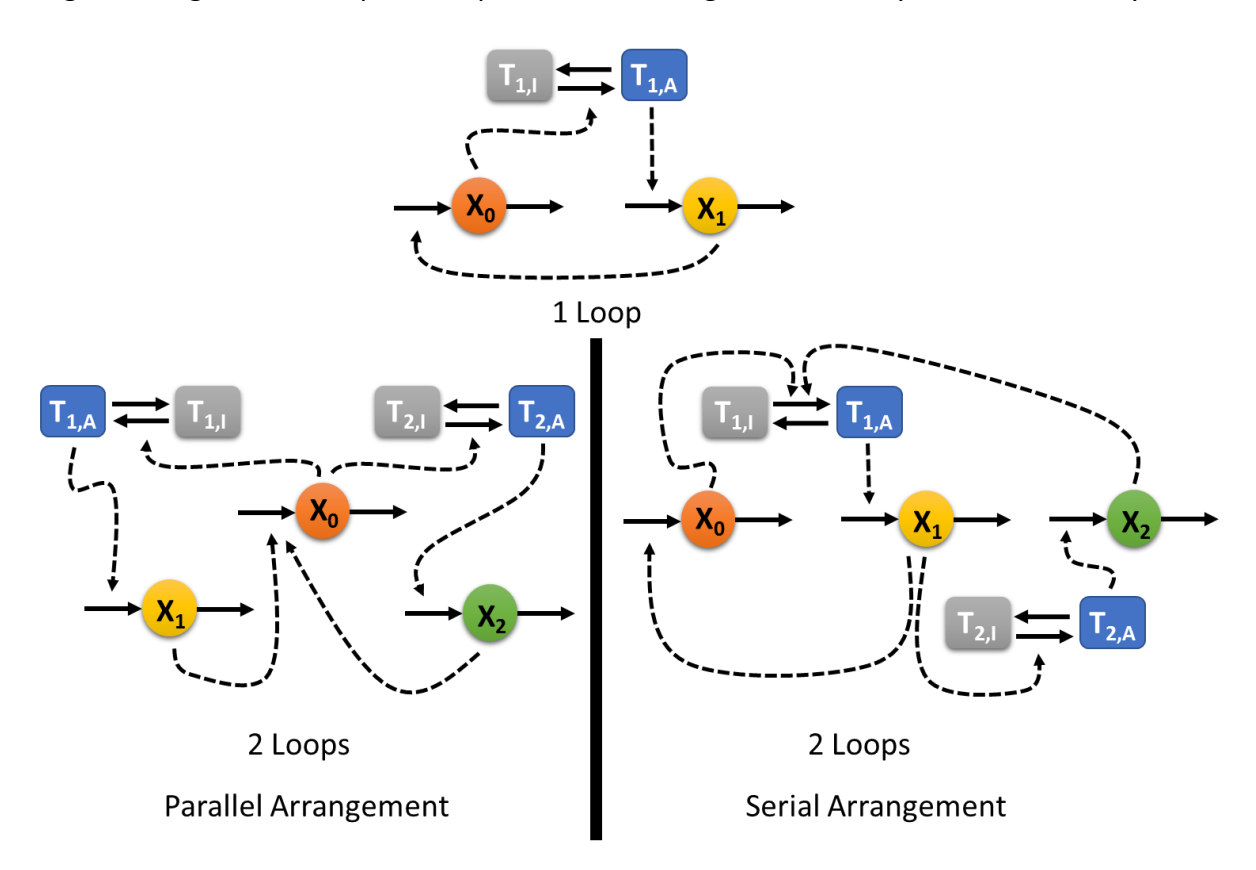


Figure 4.2: Mechanistic details of the networks. X_is are the main regulators. T_{i,A} and T_{i,I} are active and inactive TFs, respectively. The solid arrows associated with the regulators represent synthesis and degradation. The solid arrows associated with the TFs represent interconversion between active and inactive states of the TFs. The broken arrow represents enzymatic regulation on a certain chemical reaction.

To introduce ultrasensitivity into the PFL, we used Goldbeter-Koshland's (GK) zero-order ultrasensitivity in the activation-deactivation of the TF^{200} . To satisfy the requirement of GK switch, we assumed that the total amount of TF ($T_T = T_A + T_I$) is constant and that the state change of the TF follows Michaelis-Menten enzyme kinetics. In parallel motifs, the TF (T_i) of any component X_i is enzymatically activated by X_0 and in turn the synthesis rate of X_0 is positively regulated by all other components X_i s either through AND or OR gate configurations. Similarly for serial motifs, the TF (T_i) of any component X_i is enzymatically activated by two neighbouring components X_{i-1} and X_{i+1} either by AND or OR gate configurations (Figure 4.2).

The dynamical equations for the models are listed in the **Table 4.1**

Table 4.1: List of dynamical equations for the parallel and serial models.

Parallel	Serial
$\frac{dX_0}{dt} = s(k_0V + k_1\mathcal{P}_0) - \gamma X_0$	$\frac{dX_0}{dt} = s(r_0V + r_1X_1) - \gamma X_0$
$\frac{dX_i}{dt} = k_2 V + k_2' T_{i,A} - \gamma X_i$	$\frac{dX_i}{dt} = r_2 V + r_2' T_i - \gamma X_i$
$\frac{dT_{i,A}}{dt} = \frac{k_f X_0 (V.T_T - T_{i,A})}{K_M V + (V.T_T - T_{i,A})} - \frac{k_b V.T_{i,A}}{K_M V + T_{i,A}}$	$\frac{dT_{i,A}}{dt} = \frac{r_{f,i}G_i(V.T_T - T_{i,A})}{K_MV + (V.T_T - T_{i,A})} - \frac{r_bV.T_{i,A}}{K_MV + T_{i,A}}$
For AND-gate $\mathcal{P}_0 = \frac{1}{V^{N-1}} \prod_{i=1}^N X_i$ and for OR-gate	For AND-gate $G_i = \frac{1}{V}X_{i-1}X_{i+1}$ and for OR-gate
$\mathcal{P}_0 = \sum_{i=1}^N X_i$	$G_i = X_{i-1} + X_{i+1}$; for $N = 1$, $G_1 = X_0$ and for
	$i = N, \ \mathcal{G}_N = X_{N-1}$

For i=1,2,...N, where N=number of loops, V is a scaling factor to change the number of molecules of chemical species

The dynamical equations for X_0 and X_i s are written as mass action kinetics that has synthesis part and degradation part whereas the dynamical equations of the TFs are written using GK function. For all the different loops (1L, 2L, ..., 5L) in parallel motifs, we have used the same set of parameter values. For serial motifs, the activation rate constant of the TF for X_1 ($r_{f,1}$) and the regulated synthesis rate constant of X_0 (r_1) are carefully adjusted so as to generate similar bistable bifurcation diagrams as in the corresponding parallel motifs. We have also

introduced a cell-volume parameter V, to alter the number of molecules of various species without altering the qualitative dynamics of the system.

4.3. Results and discussions

4.3.1. Modelling using AND-gate input signal configuration

We first investigated the SS deterministic responses of both parallel and serial motifs in the absence of intrinsic or extrinsic noise using XPPAUT software 156 in order to generate 1parameter bifurcation diagrams. All of these PFLs generate reversible bistable bifurcation diagrams with respect to the parameter s which acts as external signal that regulates the preadipocyte-to-adipocyte differentiation process. The choice of parameter s as the bifurcation parameter is supported by the fact that the external stimulus rosiglitazone initiates the differentiation in mouse OP9 cells³⁶ in preadipocyte differentiation. The parameter s is termed as 'signal' in the rest of this chapter. The parameters k_0 and r_0 represent the 'effectiveness' of the signal. As the number of PFLs are increased, the region of bistability also increases for both parallel (Figure 4.1.b) and serial (Figure 4.1c) arrangements. For both parallel and serial motifs, we managed to generate similar bistable bifurcation diagrams including the region of bistability and the SS values. This forms an important criteria in comparing these topologies for noise propagation. The effectiveness of the serial and parallel PFLs can be determined by quantifying the deviation from the average SS values in presence of noise. For cellular differentiation process, the lower stable SS represent the undifferentiated or de-differentiated state while the upper stable SS represent the differentiated state of the cells. It has been proposed that two different types of bifurcations, a SN and a pitchfork, drive the cell fate decision making processes. The much celebrated Waddington's epigenetic landscape¹⁵⁴ recruits supercritical pitchfork bifurcations while adipocyte differentiation happens through SN bifurcations. In the SN bifurcation points, the alternate states are present well before the critical points whereas in pitchfork bifurcations the alternate states emerge only after the critical point. This difference has important consequences when the intrinsic noise interferes with the decision making processes. In

presence of intrinsic noise, the alternate stable SSs can coexist before the critical point in case of SN bifurcations whereas there is no possibility of coexistence of alternate states before the critical point in pitchfork bifurcations. Also, the cell fate decision making is always reversible in Waddington's epigenetic landscape model whereas in SN bifurcations, the differentiation processes can be irreversible as well.

In absence of any chemical noise, every cell in a genetically identical population will behave identically, hence, there will be a clear switch-like transitions of the entire population from undifferentiated (or dedifferentiated) state to the differentiated state after the right critical point (SN_R). Similarly all the cells will revert back to the undifferentiated (or dedifferentiated) state from the differentiated state if the signal is lowered below the left critical point (SN_L). In absence of any noise, the population is 'pure' in terms of its differentiation-meaning the entire population of cells is either differentiated or undifferentiated (or dedifferentiated). Therefore, a bistable switch represent 'all-or-none' digital switch-like response. However, in presence of intrinsic noise, each cell behaves differently even in a genetically identical cell population and hence results in a non-switch like response which leads to mixed population of differentiated and undifferentiated cells. To estimate the extent of mixed population due to chemical noise, we calculated the percentage of differentiated (high X_0 , Upper stable SS) and undifferentiated (low X_0 , Lower stable SS) cells with varying doses of signal S.

4.3.1.1. Control of population heterogeneity in presence of extrinsic noise

In our models, the extrinsic noise was introduced by choosing the unregulated synthesis rates (k_0, r_0, k_2, r_2) from independent log-normal distributions with a coefficient of variation (CV) of 30%. The choice of 30% variation was due to the fact that similar variations have been observed in many protein expression levels. Our aim here was to see among parallel and serial motifs which one filters out extrinsic noise more efficiently. We calculated the fraction of cells that gets differentiated or dedifferentiated as we change the signal s in presence of extrinsic noise. To calculate the fraction of differentiated cells we first initialized the population in undifferentiated state (low s0, Lower stable s1) and calculated the fraction of population that gets differentiated (high s2, Upper stable s3) with increase in signal doses. Likewise, to

calculate the fraction of dedifferentiated cells, we started with the assumption that all the cells are differentiated (high X₀, Upper stable SS) and calculated the fraction of population that gets dedifferentiated (low X₀, Lower stable SS) with decrease in signal values. Our objective here was to find out the fraction of cells that gets differentiated at a given signal and out of the differentiated cells the fraction of cells that gets dedifferentiated back at the same signal. For a single PFL (1L) we found that the differentiation and dedifferentiation curves intersect each other at intermediate signal value thus giving rise to a mixed population (Figure 4.3a and 4.3b). This indicates that at intermediate signal values, a fraction of the differentiated cells will undergo dedifferentiation. For parallel motifs, with increase in feedback loops, these two curves moves away from each other thus reducing the extent of mixed population (Figure 4.3a). In case of serial motifs, with increase in feedback loops these two curves does not move away much from each other thus retaining the mixed population throughout (Figure 4.3b).

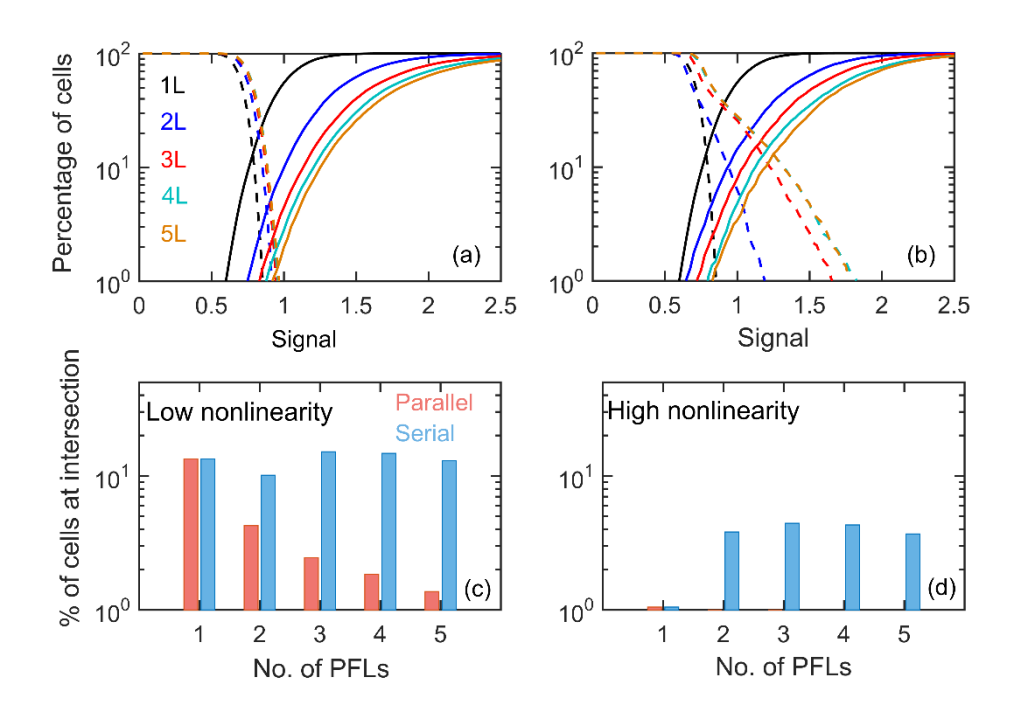


Figure 4.3: Differentiation with AND-gate in presence of extrinsic noise: (a-b) The percentage of differentiated (solid lines) and dedifferentiated (broken lines) cells with varying signal doses for parallel (left) and serial (right) motifs for different number of PFLs having low non-linearity ($K_M = 0.05$). (c-d) The percentage of cells at the intersection of differentiated

and dedifferentiated curves with different number of PFLs for low (c; $K_M=0.05$) and for high (d; $K_M=0.01$) nonlinearity in parallel (cyan) and serial (orange) motifs.

To estimate the extent of population heterogeneity, we calculated the percentage population at the intersection point of differentiation and dedifferentiation curves for both parallel and serial arrangements. We found that in parallel motifs, the percentage population at the intersection decreased with increase in number of feedback loops whereas in serial motifs it did not (Figure 4.3c). Therefore, it is safe to conclude that serial motifs are less efficient in minimizing or filtering out the extrinsic noise compared to parallel motifs although their bistable bifurcation diagrams are almost identical. To find out whether the efficacy of parallel motifs in reducing the extrinsic noise has to do anything with non-linearity or ultrasensitivity of the system, we reduced the Michaelis constant (K_M) by five times from 0.05 to 0.01. Decreasing the K_M value leads to increase in the non-linearity or ultrasensitivity of the system. Even with increased ultrasensitivity, we found that parallel PFLs reduced extrinsic noise more efficiently than serial PFLs however, serial motifs performed better in reducing noise in this as compared to with low non-linearity (Figure 4.3d).

4.3.1.2. Control of population heterogeneity in presence of intrinsic noise

We explored the effect of intrinsic noise on the differentiation dynamics both in parallel and serial arrangements of PFLs by simulating the chemical reactions of the model networks using Gillespie's stochastic simulation algorithm¹⁰⁸. Depending upon the amount of stochastic (intrinsic) noise present in the system, the value of the variable (X₀) of the system may jump between the two stable SSs. In the bistable region, the system transitions between the two stable SSs and ultimately at equilibrium some fraction of the cells will reside in the upper stable SS and the remaining will settle down in the lower stable SS. As the number of feedback loops increases, the percentage of mixed population with intrinsic noise decreases in parallel PFLs (Figure 4.4a) whereas there is no significant change in mixed population in serial PFLs (Figure 4.4b). The percentage of cells at the intersection reduces more effectively in parallel arrangements and in serial arrangements they do not change much (Figure 4.4c). With increased non-linearity, the parallel motifs were able to reduce the effect of noise significantly

but the heterogeneity in serial motifs did not change much. Therefore, based on our calculations, we conclude that parallel arrangement of PFLs reduce both extrinsic and intrinsic noise more efficiently than serial arrangement.

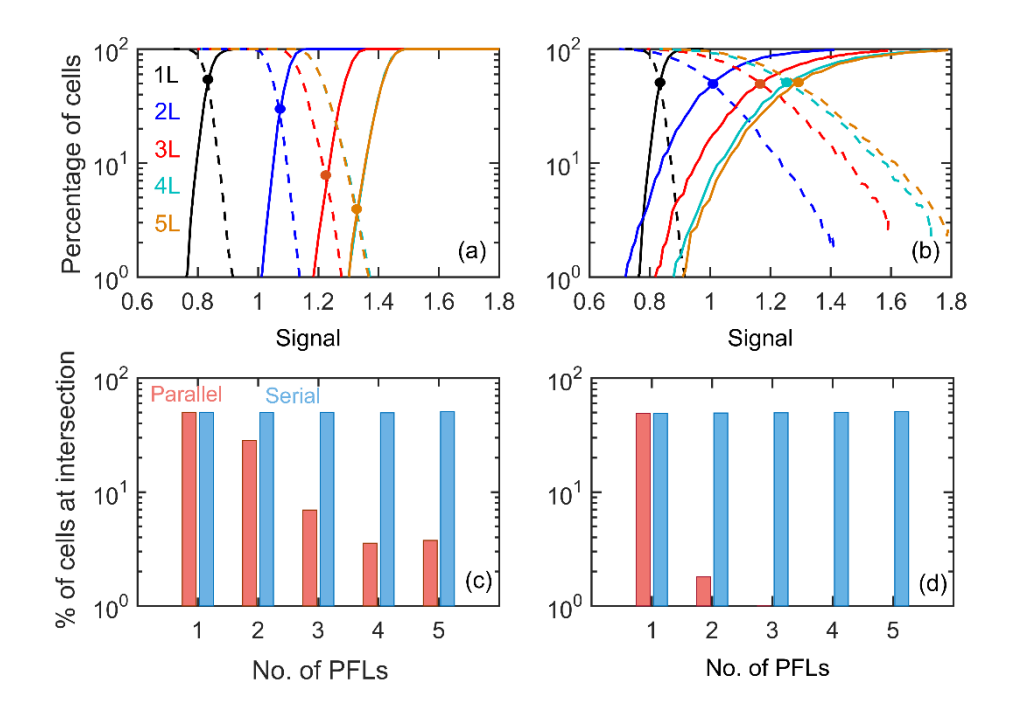


Figure 4.4: Differentiation with AND-gate in presence of intrinsic noise: (a-b) The percentage of differentiated (solid lines) and dedifferentiated (broken lines) cells with varying signal doses for parallel (left) and serial (right) motifs for different number of PFLs having low non-linearity ($K_M = 0.05$). (c-d) The percentage of cells at the intersection of differentiated and dedifferentiated curves with different number of PFLs for low (c; $K_M = 0.05$) and for high (d; $K_M = 0.01$) nonlinearity in parallel (cyan) and serial (orange) motifs.

4.3.1.3. Sensitivity of SN bifurcation points in presence of extrinsic noise

While performing calculations using extrinsic noise, we observed that the SN bifurcation points of the bistable switch moved left and right. Therefore, we hypothesized that the SN points might be sensitive to extrinsic noise and might play a role in regulating the extrinsic noise in both parallel and serial motifs. To validate this hypothesis, we calculated the signal s values corresponding to left and right SN bifurcation points for 10000 cells in presence of extrinsic noise. We calculated the CV of the distribution of both left and right SN points and

found that the CV in serial motifs are higher than that of in parallel motifs (Figure 4.5a). We found that the higher amount of noise in serial motifs is due to the skewness of the distribution of the SN points (Figure 4.5b). While the distribution of the right SN points is similar in parallel and serial motifs, the distribution of left SN points are highly positively skewed in serial motifs as compared to parallel motifs (Figure 4.5c).

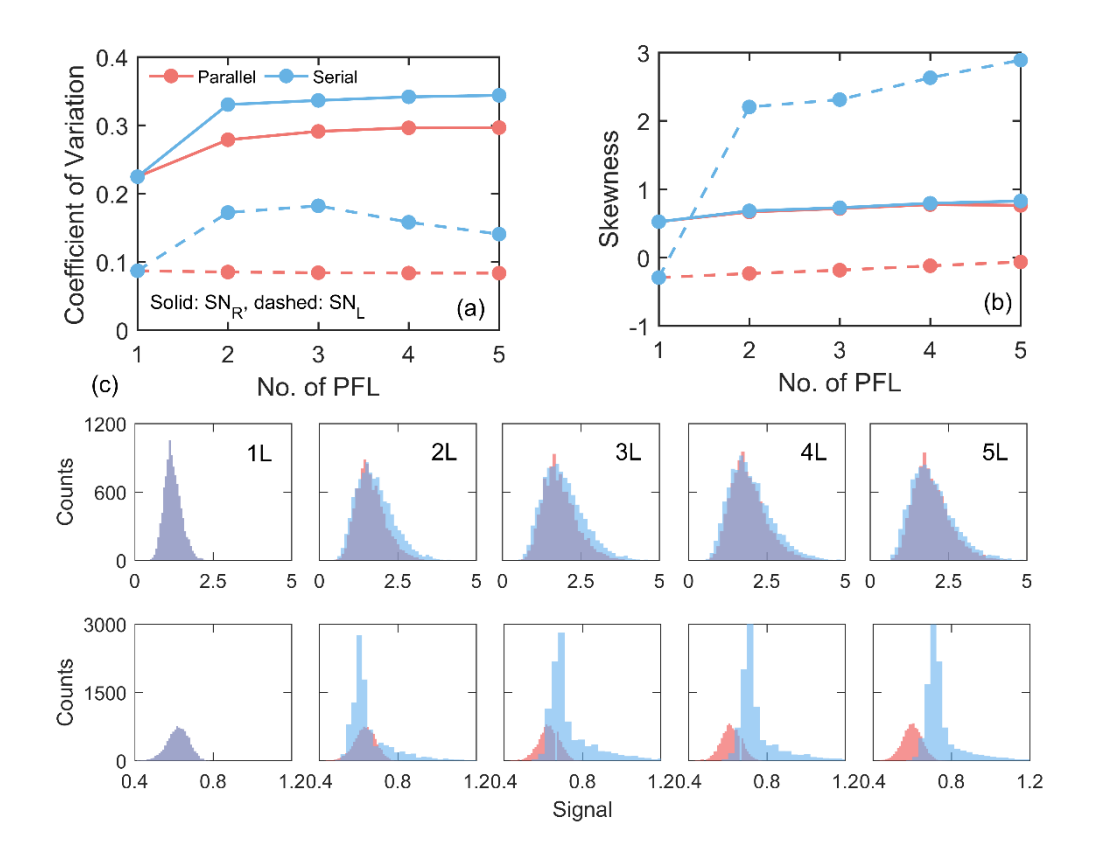


Figure 4.5: Sensitivity of SN bifurcation points to extrinsic noise in models with low non-linearity ($K_M = 0.05$): The variation in CV (a) and skewness (b) of the distributions of right and left SN points in presence of extrinsic noise for different number of PFLs. (c) Comparison of distribution of right (c; top panel) and left (c; bottom panel) SN bifurcation points for the parallel and serial motifs.

Consistent with the skewness of the left SN points, the dedifferentiation curves in serial motifs have long tails (Figure 4.3b). We repeated the calculations with increased non-linearity and found similar results as well. Therefore, in serial motifs, the left SN bifurcation points that dictates the transition from differentiation to dedifferentiation are very susceptible to extrinsic noise compared to the same in parallel motifs.

4.3.1.4. Sensitivity of the steady states in presence of intrinsic noise

The extent of fluctuations in an ensemble of SS values in presence of intrinsic noise is determined by how stable the SSs are²⁰¹. Mean residence time (MRT) of the SSs can determine the stability of the SSs in a bistable system under intrinsic noise. We calculated the MRT of upper and lower stable branches in the bistable region and found that in both the branches the MRT is higher in parallel motifs compared to the same in serial motifs (Figure 4.6). This is a clear indication of the fact that because of the high MRT in parallel motifs, the stable SSs are less susceptible to intrinsic noise as compared to the same in serial motifs. In serial motifs, the chain-like architecture contributes to the noise amplification because of which the SSs might be more susceptible to intrinsic noise as compared to the parallel motifs where the PFLs are independent.

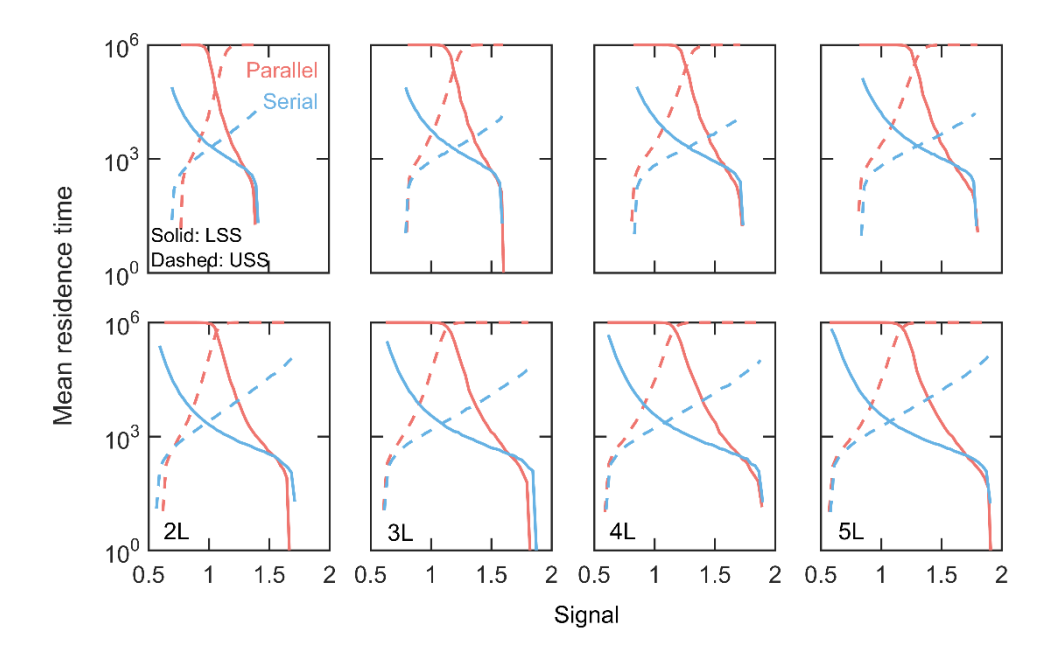


Figure 4.6: Stability of steady states in presence of intrinsic noise determined by mean residence time (MRT): Comparison of mean residence time for upper (USS) and lower (LSS) SSs for parallel and serial motifs with AND gate. The top panel is for low non-linearity ($K_M = 0.05$) and bottom panel is for high non-linearity ($K_M = 0.01$) of the models.

4.3.2. Modelling using OR-gate input signal

The above results were for AND-gate configurations, but we also performed calculations using OR-gate configurations of the input signals. Using OR configurations we generated almost-identical bistable bifurcation diagrams (Figure 4.7a and 4.7b) both for parallel and serial topologies and performed similar calculations as done in AND configurations. In OR configurations, parallel motifs, again reduced both extrinsic and intrinsic noise efficiently compared to serial motifs although serial motifs did a better job in reducing noise in OR gate compared to in AND gate (Figure 4.7c-f). Using mean residence calculations, we again found that the stable branches in parallel motifs are more stable than the same in serial motifs. From these calculations we found that OR-gate signalling input show less variability compared to AND gate due to the noise getting amplified in a multiplicative manner in AND gate.

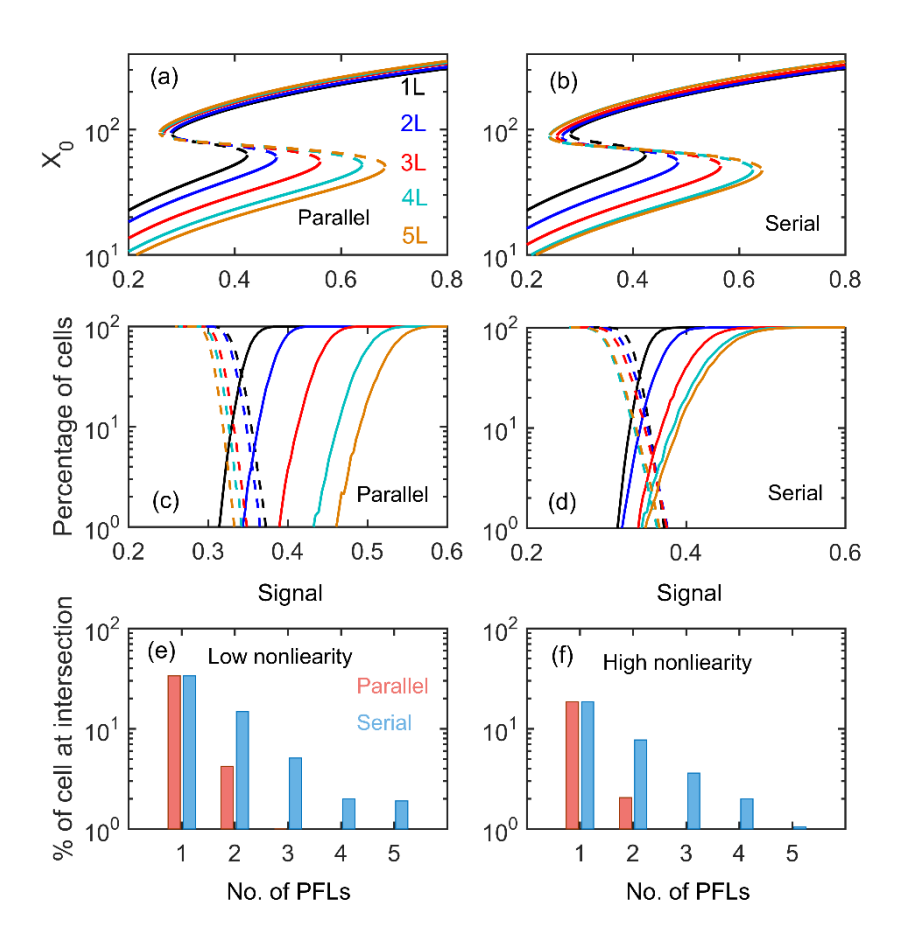


Figure 4.7: Differentiation with OR-gate configuration: (a-b) One-parameter bistable bifurcation diagrams for parallel (left) and serial (right) motifs. (c-d) The percentage of differentiated (solid lines) and dedifferentiated (broken lines) cells in presence of intrinsic

noise and with low non-linearity ($K_M=0.05$) for parallel (left) and serial (right) models. The extent of mixed population for low (e) and for high (f) non-linearity in the models.

4.3.3. Modelling using Hill functions

We also modelled our system with Hill functions instead of Goldbeter-Koshland's switch to determine if the results depend on modelling methodologies (Table 4.2). We performed similar calculations and found that even using Hill functions, parallel motifs reduce noise more efficiently than serial motifs (Figure 4.9).

Table 4.2. Dynamical equations for the models with Hill function. List of dynamical equations for models with Hill function.

Parallel	Serial
$\frac{dX_0}{dt} = \varepsilon_0 s \left(V + \frac{\alpha V \prod_i^N X_i^M}{V^{NM} + \prod_i^N X_i^M} \right) - \gamma X_0$	$\frac{dX_0}{dt} = s(k_0V + p_0X_1) - \gamma X_0$
$\frac{dX_i}{dt} = \varepsilon_i X_0 - \gamma X_i$	$\frac{dX_i}{dt} = k_i V + \frac{p_i V X_{i-1}^M X_{i+1}^M}{b_1 V^{2M} + X_{i-1}^M X_{i+1}^M} - \gamma X_i$

N is the number of PFLs and M is the cooperativity, $X_{N+1} = 1$

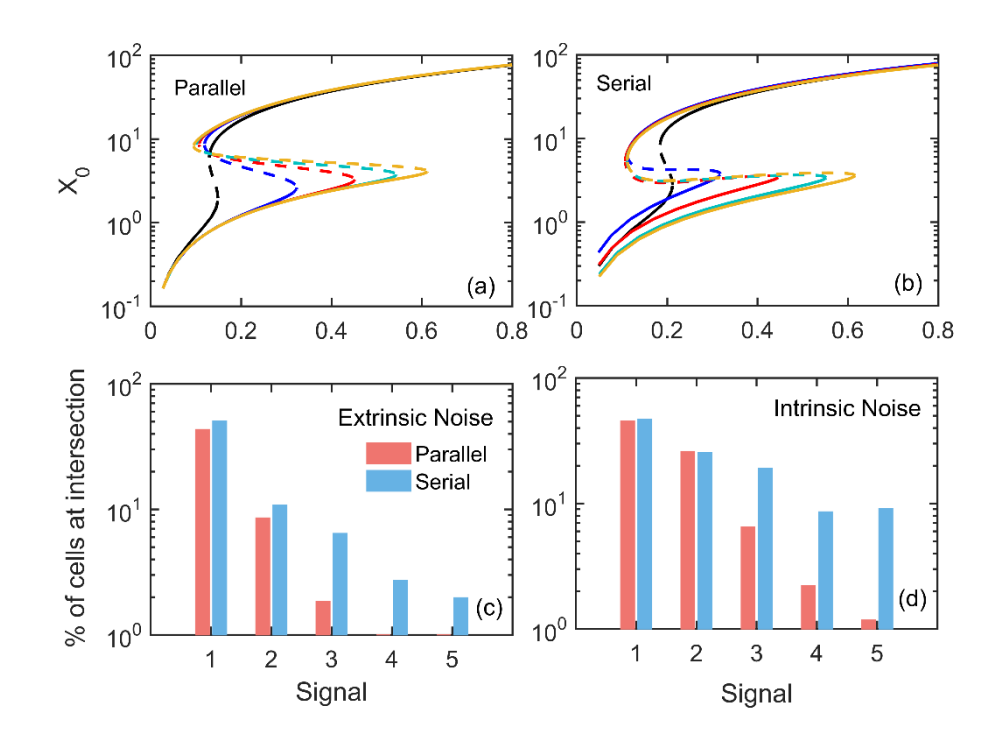


Figure 4.9: Differentiation using AND-gate Hill functions in presence of extrinsic and intrinsic noise: The one-parameter bistable bifurcation diagrams for parallel (left) and serial (right) models using AND-gate Hill function for different number of PFLs with cooperativity 2. Comparison of the percentage of mixed population at the intersection of the differentiation and dedifferentiation curves for parallel and serial motifs in presence of extrinsic (c) and intrinsic (d) noise.

4.4. Methodologies and calculations

4.4.1. Calculation of differentiation-dedifferentiation percentages

We estimated the percentages of cells in a population of 10000 cells that have differentiated or dedifferentiated in presence of extrinsic and intrinsic noise with varying signal doses s. In single cell quantification of proteins in eukaryotic cells, it was reported that protein distributions usually are asymmetric and are positively skewed that resembles log-normal distributions^{179,183,202}. Extrinsic noise in cellular population arises due to difference in cell size, shape, cellular contents, matrix density, cell cycle stages and pH. This extrinsic noise greatly contributes to population heterogeneity in protein numbers that results in positive skewness

in protein distributions. Therefore, in order to mimic this distribution we picked the unregulated rate constant values (k_0 and k_2 for parallel motifs and r_0 and r_2 for serial motifs) from independent log-normal distributions with 30% variation around the mean. Unregulated proteins were found to have log-normal distributions with a typical CV of 30%.

We started with 10000 cells being in lower stable SS (undifferentiated state) and numerically solved the coupled differential equations listed in **Table 4.1** using MATLAB at different values of signal s. We numerically integrated the dynamical equations for sufficient long time to ensure the system reached SS. To estimate the fraction of differentiated cells, we initialised the system at lower stable SS and at each signal value we calculated the number of cells whose SS value was greater than X_0 corresponding to the right saddle-node (SN_R) bifurcation point. Similarly, to estimate the fraction of dedifferentiated cells, we initialised the system at upper stable SS and at each signal value we calculated the cells whose SS value was less than X_0 value corresponding to the left saddle-node (SN_L) bifurcation point.

To estimate the percentage of differentiated-dedifferentiated cells in presence of intrinsic noise, we used Gillespie's stochastic simulation algorithm¹⁰⁸ and simulated the chemical reactions for both the network models (Figure 4.8). To estimate the percentage of differentiated cells, we initialised the system at lower stable SS and at each signal value we calculated the number of cells whose SS value was greater than the separatrix (corresponding unstable SS) value. Similarly, to estimate the fraction of dedifferentiated cells, we initialised the system at upper stable SS and at each signal value we calculated the number of cells whose SS value was less than the corresponding separatrix value.

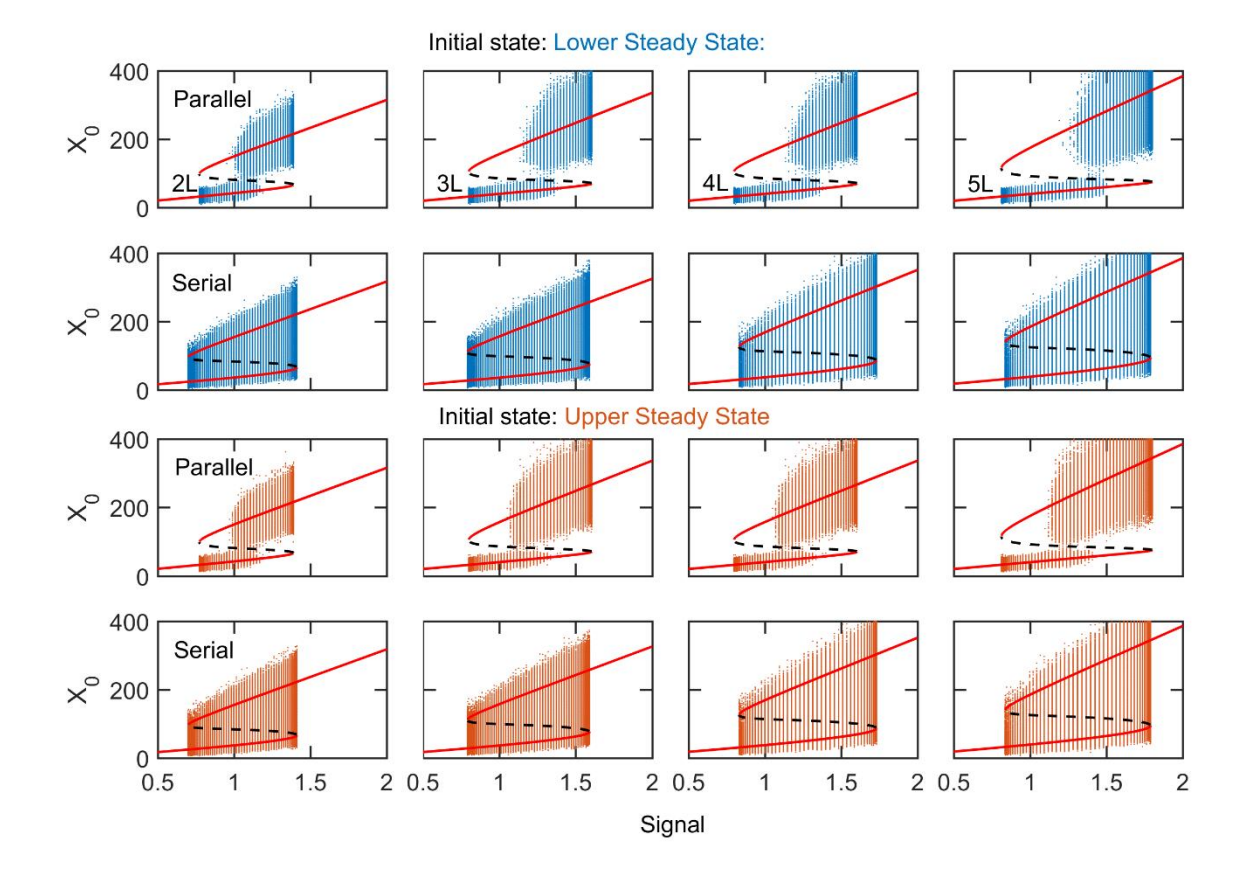


Figure 4.8: The steady state distribution in presence of intrinsic noise in models with low non-linearity ($K_M = 0.05$): The distribution of SS values of X_0 for 10000 cells distributed over the bifurcation diagram in presence of intrinsic noise for different number of PFLs with low non-linearity and with AND-gate configuration. The upper two panels (blue) and the lower two panels (orange) represent cells initialized in the lower and upper SSs, respectively.

4.4.2. Calculation of sensitivity of bifurcation points

In presence of extrinsic noise, the SN bifurcation points for different cell will be different. Under the influence of extrinsic noise, we recorded both left and right SN bifurcation points for 10000 different cells. We then calculated the CV and the skewness of the left and right SN points for different number of PFLs for both serial and parallel topologies. We also plotted the population distributions of the two SN points for the two different arrangements of PFLs.

4.4.3. Calculation of mean residence time (MRT)

In presence of intrinsic noise, we calculated the mean residence time of the stable SSs (undifferentiated and differentiated states) in the bistable region. We started from lower stable SS (undifferentiated state) and simulated the chemical reactions using Gillespie's SSA and recorded the time the SS value of X_0 crossed the separatrix for the first time to get the first passage time or residence time of the lower stable SS. To estimate the residence time of the upper stable SS, we started from the upper stable SS (differentiated state) and followed similar procedure mentioned above. We repeated these calculations for 10000 times to get the mean residence time (MRT) for both lower and upper stable SSs. The maximum time of calculation was 1×10^6 arbitrary time units.

4.5. Summary and conclusions

Cellular functions such as differentiation are regulated by network motifs that are capable of generating distinct SSs and dynamical properties. The properties of regulatory networks crucially depend on the architectural design or the topology of these networks. For example, a PFL generates multistable SSs and a NFL generates oscillations and excitability²⁰³. The average properties of some of these regulatory networks could be similar however in presence of chemical noise the properties might get perturbed differently. In many biological systems, chemical noise acts as a nuisance and cause hindrance to the functioning of the system. Therefore, the system's natural tendency would be to adapt to a network architecture that has the potential to minimize the effect of chemical noise for smooth functioning of the system. In this context, PFLs are known to reduce the fluctuations in various cellular phenomena^{44,45,123,128}. Also, multiple PFLs create bistable switches that are known to regulate many cellular differentiation processes 36,37,40. Multiple PFLs helps the system to generate robust bistability, however the arrangements of these PFLs might have some crucial role in minimizing the effects of chemical noise in the system. Therefore, investigating the architecture of regulatory networks might help in understanding how the system lock the cells either in differentiated or undifferentiated states even in presence of chemical noise.

Ahrends *et al.*, showed that preadipocyte to adipocyte differentiation is regulated by a bistable switch and the low rate of differentiation is maintained by the stochastic fluctuations of chemical species within a weak signalling regime. However, this same stochastic fluctuations might lead to the loss of differentiated state, thus locking the cells in the differentiated state is a crucial task the system has to achieve. This indicates that there must be some mechanism in place using which the system might be able to reduce the effect of this stochastic fluctuation so as to avoid the loss of differentiated state. As discussed before, the architecture of the regulatory network might have some relevance in noise filtration ^{82,198}. They found out that the adipocyte differentiation process is regulated by seven independent PFLs arranged in a consecutive manner around a master regulator PPARG, thus creating a parallel topology of the PFLs. This raises a question as to why these PFLs are arranged in a parallel manner only while a serial arrangement of these PFLs may as well serve the purpose.

In order to address the concern of how different arrangement of PFLs control noise, we generated bistable switches with almost similar region of bistabilities and SS properties from both parallel and serial arrangements. We calculated the percentage of cells that gets differentiated or dedifferentiated at different signal values both in case of parallel and serial topologies. We found that both in AND-gate and OR-gate input signalling configurations, parallel arrangement of PFLs reduce both extrinsic and intrinsic sources of noise much effectively as compared to the same in serial arrangement. Our calculations suggest that the left SN bifurcation points in serial motifs are more sensitive to extrinsic noise compared to that of the same in parallel motifs and this leads to highly skewed distribution of SN points in serial motifs indicating high amount of noise. In case of intrinsic noise, the stability of the two SSs in the bistable region measured by the mean residence time is much higher in parallel motifs than in serial motifs. This indicates that the cells residing in either of the stable SSs in parallel motifs are less susceptible to stochastic fluctuations thus locking their states.

In absence of any type of chemical noise, parallel and serial motifs would not make any difference in differentiation dynamics. However, based on our results, in presence of both types of noise, parallel motifs reduce noise much better than serial motifs. Therefore, the choice of parallel arrangement of PLFs over serial arrangement in differentiation process might be an evolutionary strategy of the system to adapt to the most robust network in order

to minimize the effect of noise and work efficiently. Parallel architecture of PFLs are not only limited to cellular differentiation systems but also found in other biological systems. In cell cycle network of *Saccharomyces cerevisiae* (budding yeast), activation of b-type cyclins Clb1, 2 are regulated by three PFLs through independent involvement of Cdh1, Sic1 and Fkh2 in ORgate configuration¹²³. Stochastic model of the cell cycle predicted that if one of these PFLs are removed, the variability in the system increases and that hampers the properties such as cell cycle time, size at birth and division etc. Similar architecture of PFLs are also present in activation of maturation promoting factor (MPF) in cell cycle network of *Saccharomyces pombe* (fission yeast)²⁰⁴.

All the parameters that we used in our models fall under biologically relevant ranges. For proteins, we have chosen ~70 min as the half-life which is typical average half-life of many proteins. The synthesis rate constants that we chose in our models also falls in the molecular abundance in the physiological range of few hundred molecules per cell. We have performed simulations where rate constants were picked from log-normal distributions with 30% CV which takes into account the reasonable range in parameter values. Further, we have studied two different configurations of input signals (AND and OR-gate) using two different modelling methodologies (Goldbeter-Koshland's switch and Hill function) to generate bistable switches that regulate the differentiation dynamics. In all of these case, our calculations provide similar conclusion indicating the generality of our findings.

Chapter 5

Negative Cooperativity and Bistability in Receptor-Ligand Binding

5.1. Introduction

A vast majority of cellular responses to external stimuli are due to binding of the signalling molecules or ligands to their cognate cell surface receptors. Receptor-ligand interaction dynamics play a crucial role in signal transduction pathway as binding of ligands to cell surface receptors triggers intracellular signalling pathways to allow the cell to carry out various physiological functions. For example, TGF- β receptor²⁰⁵, class I and class II cytokine superfamily^{206–209}, receptor tyrosine kinases^{210,211} and G-protein coupled receptors^{212,213} control cellular functions such as cell-division, proliferation, apoptosis, differentiation, metabolism etc. The binding of ligands to multimeric receptors often leads to cooperativity in receptor-ligand binding dynamics. In a multimeric receptor, binding of a ligand alters the dynamics of binding of subsequent ligands to the same receptor. This leads to allosteric interactions among the binding sites which is often recognized as the mechanism of cooperativity^{214,215}. If the binding of a ligand increases the affinity of binding of subsequent

ligands, it is known as positive cooperativity and if it dampens the binding of subsequent ligands it is known as negative cooperativity 216,217 . In subsequent binding of ligands to a multimeric receptor, the definition of cooperativity can be best explained by the Gibb's free energy change (ΔG) of binding. In positive cooperativity, ΔG in the subsequent binding steps becomes more negative, in negative cooperativity it becomes less negative and in non-cooperativity ΔG value does not change 218 . The cooperative nature of the binding kinetics can be extracted from the typical sigmoidal ligand binding curve and fitting the curve by the Hill function 219,220 . The Hill coefficient (n_H) associated with the cooperativity represents positive, negative and non-cooperativity binding with $n_H > 1, n_H < 1$ and $n_H = 1$, respectively. Positive cooperativity generates a stiff sigmoidal response consisting of a threshold in the required amount of ligand for full engagement of the receptor 221 . Thus, positive cooperativity produces an ultrasensitive switch in the activity of the receptor. Owing to its ultrasensitive nature, positive cooperativity plays important roles in generating system level phenomena such as bistability, multistability and oscillations in feedback regulated networks 203,222,223 .

Unlike positive cooperativity, negative cooperativity generally produces hyperbolic responses without any signalling threshold^{216,224}. Epidermal growth factor receptors^{225–227}, insulin receptor^{228–230}, and glycoprotein hormone receptors²³¹ are a few example of receptor-ligand system where negative cooperativity has been observed. Both the positive and negative cooperativities are common in biology yet, negative cooperativity was never really explored much. A detailed mathematical model was developed by Kiselyov *et al.*²³² based on the concept of harmonic oscillator to account for several experimental observations and includes negative cooperativity for a dimeric insulin receptor. In dimeric receptor-ligand binding it was shown by Ha *et al.*²³³ that negative cooperativity can generate ultrasensitive response with a threshold if the ligand has strong affinity towards the receptor. This shows that negative cooperativity can be a source of non-linearity which is required to generate bistability in a PFL.

5.2. Modelling and methodology

The basic structure of our model has a dimeric receptor with a single ligand binding spot on each monomer. The fully ligated receptor is the active form of the receptor and regulates downstream signalling pathway. We have considered two different models of downstream regulation of the signalling pathways. In the first one, the active receptor-ligand complex upregulates the gene that produces the ligand and in the second one the active receptor-ligand complex also upregulates the receptor. The former case creates a single PFL and the latter case creates a fusion of two PFLs.

5.2.1. Mechanism of the binding dynamics

In both the models discussed above, the mechanism of binding is same. Each monomer in the dimeric receptor (R_2) is capable of binding only one ligand (L) molecule. The binding of a ligand to the receptor is a two-step sequential process. In the first step, the ligand binds to one of the monomers of the unoccupied receptor (R_2) and in the second step, another ligand molecule binds to the remaining monomer of the singly-occupied receptor (R_2L_1) to form the active receptor-ligand complex (R_2L_2) . Similarly, the unbinding of the ligands from the engaged receptors also follows two-step sequential process.

5.2.1.1. Module 1: Positive feedback in the ligand upregulation

Figure 5.1 shows the schematic representation of the binding-unbinding mechanism of the ligand and receptor in the system with a single PFL.

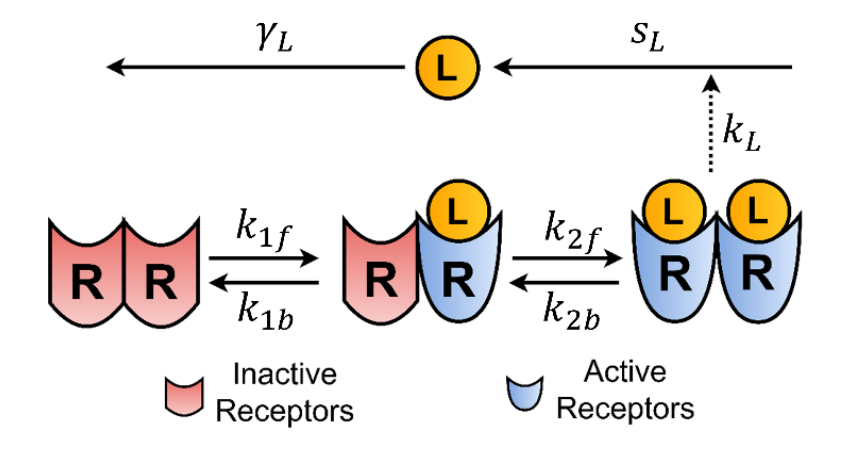


Figure 5.1: Schematic representation of the receptor-ligand binding model: The ligand (L) binds to the dimeric receptor (R_2) in a sequential manner. The fully occupied receptor is responsible for synthesis of the ligand thereby creating a PFL between the ligand and the active receptor. The solid arrow represents chemical binding whereas the dashed arrow represents catalytic effect on a chemical reaction. The degradation reaction is represented by an open-ended arrow. The rate constants of the binding/unbinding reactions are mentioned on the top of the respective arrows.

The active cell surface receptor triggers gene regulation by activating or deactivating the cytoplasmic signalling molecules. These cytoplasmic molecules transmit information from cell surface to the nucleus. In our model, we reduced the complex signalling pathway by considering that the active receptor directly activates the synthesis of ligands, without the loss of generality. Apart from the regulated synthesis of the ligands by the active receptor, we have also considered the unregulated basal synthesis of the ligands (s_L) to initiate the signalling feedback. Therefore, this module is a simple representation of an autocrine signalling module^{234,235}. k_L is the rate constant of the regulated ligand production which also serves as the strength of the PFL in the model. γ_L is the degradation rate of the ligands that degrades exponentially with a mean life-time of $1/\gamma_L$. In this model, we assumed that the total amount of receptors are constant and follows the expression $R_T = R_1 + R_2 L_1 + R_2 L_2$.

All the chemical reactions in the module follow mass action rate laws and the dynamical equations are presented in **Table 5.1**.

We have considered both ordered and disordered binding of the ligand to the receptor. In the disordered binding, the free ligand can bind to any of the two available sites on the dimeric receptor. The resulting 'conformers' are not distinguishable from one another. In general, the disordered binding of ligands to multimeric receptors with N binding sites, the number of ways i-th binding can happen is given by the binomial factor $\binom{N}{i}$. For a dimeric receptor, the value of this factor is 2 (N=2 and i=1) for the first binding event. Similarly, for the unbinding event from the fully engaged receptor (R_2L_2), there are two ways by which a single ligand can unbind. Therefore, the rate of binding of a ligand to a dimeric unoccupied receptor and the rate of unbinding of a ligand from the fully engaged receptor increases by a factor of 2. **Table 5.1** consists of the kinetic equations of the model with the binomial factor represented as ν (= 2) for disordered binding. For the ordered binding, the ligand binds to the unoccupied receptor at a specific site and hence the value of the factor is 1 (ν = 1). We, here report the results for the disordered binding case.

Table 5.1: The dynamical equations for the receptor-ligand binding model with PFL in ligand upregulation

$$\frac{dL}{dt} = s_L + k_L R_2 L_2 + k_{1b} R_2 L_1 + \nu R_{2b} R_2 L_2 - \nu R_{1f} R_2 L - k_{2f} R_2 L_1 L - \gamma_L L$$
(5.1)

$$\frac{dR_2}{dt} = k_{1b}.R_2L_1 - \nu.k_{1f}.R_2.L \tag{5.2}$$

$$\frac{dR_2L_1}{dt} = \nu. k_{1f}. R_2. L + \nu. k_{2b}. R_2L_2 - k_{1b}. R_2L_1 - k_{2f}. R_2L_1. L$$
(5.3)

$$\frac{dR_2L_2}{dt} = k_{2f}.R_2L_1.L - \nu.k_{2b}.R_2L_2 \tag{5.4}$$

$$R_T = R_2 + R_2 L_1 + R_2 L_2 (5.5)$$

5.2.1.2. Module 2: Positive feedback in both ligand and receptor upregulation

In the previous module (**Figure 5.1**), we had a PFL in ligand upregulation by the fully engaged receptor R_2L_2 . However, in many receptor-ligand systems, the receptor abundance is upregulated by the active receptor, thus, forming a PFL^{235–239}. In this section, we introduced a second PFL where the active receptor complex R_2L_2 upregulates the receptor synthesis (**Figure 5.2**).

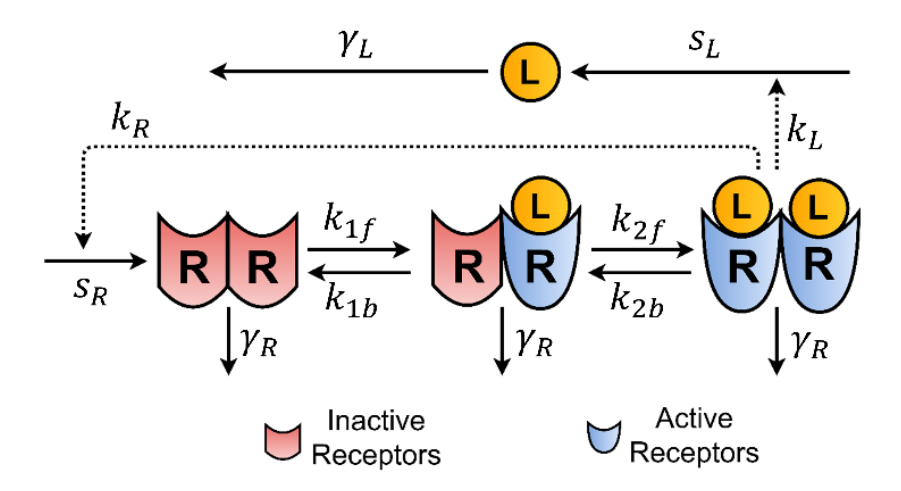


Figure 5.2: Schematic model of the receptor-ligand binding model with an additional positive feedback loop: In addition to the PFL in ligand upregulation, a second PFL is added where the active receptor R_2L_2 upregulates receptor synthesis.

We included the production and degradation of the receptor complexes where s_R represents the basal production rate and k_R represent the upregulation from the active receptor R_2L_2 . γ_R is the degradation rate of the free and ligated receptors. During the degradation process, only the receptors degrade but the ligands gets replenished. This mechanism represents the internalization of cell surface receptors. The list of dynamical equations are presented in **Table 5.2.**

Table 5.2: The dynamical equations for the model with two PFLs

$$\frac{dL}{dt} = s_L + k_L R_2 L_2 + k_{1b} R_2 L_1 + \nu k_{2b} R_2 L_2 - \nu k_{1f} R_2 L - k_{2f} R_2 L_1 L - \gamma_L L + \gamma_R R_2 L_1 + 2 \gamma_R R_2 L_2$$
(5.6)

$$\frac{dR}{dt} = s_R + k_R \cdot R_2 L_2 + k_{1b} \cdot R_2 L_1 - \nu \cdot k_{1f} \cdot R_2 \cdot L - \gamma_R \cdot R_2$$
(5.7)

$$\frac{dR_2L_1}{dt} = \nu. k_{1f}. R_2. L - \nu. k_{2b}. R_2L_2 - k_{1b}. R_2L_1 - k_{2f}. R_2L_1. L - \gamma_R. R_2L_1$$
(5.8)

$$\frac{dR_2L_2}{dt} = k_{2f}.R_2L_1.L - \nu.k_{2b}.R_2L_2 - \gamma_R.R_2L_2$$
(5.9)

In a receptor-ligand binding, the binding affinity of the ligand to the receptor is typically measured by the dissociation constant. In the model, the dissociation constant of the first and second steps are given by K_1 and K_2 respectively. The dissociation constants are further defined as the ratio of the rate constants of the unbinding and the binding reactions $(K_1 = k_{1b}/\nu k_{1f})$ and $K_2 = \nu k_{2b}/k_{2f}$. The measure of cooperativity is defined as $C = K_1/K_2$. The numerical value of C determines the measure of cooperativity in the receptor-ligand binding. Based on the value of C, the three different regimes of cooperativity can be identified. For the positive, negative and non-cooperative binding the regimes of C are C > 1 ($K_1 > K_2$), C < 1 ($K_1 < K_2$) and C = 1 ($K_1 = K_2$), respectively. By adjusting the values of binding (k_{1f}) and k_{2f} and unbinding (k_{1b}) and k_{2b} rate constants, different cooperativities can be achieved as $C = k_{1b} \cdot k_{2f}/(4 \cdot k_{1f} \cdot k_{2b})$. The factor 4 is the binomial factor ($\nu = 2$) which is due to the disordered binding of the ligands to the dimeric receptor.

5.3. Results and discussions

5.3.1. Positive feedback in ligand upregulation: Single PFL

We first carried out 1- parameter bifurcation analysis of the model using XPPAUT software (http://www.math.pitt.edu/~bard/xpp/xpp.html). The 1-parameter bifurcation diagrams of the model with different values of cooperativities C are presented in the **Figure 5.3** with unregulated basal synthesis rate of ligands (s_L) as the bifurcation parameter.

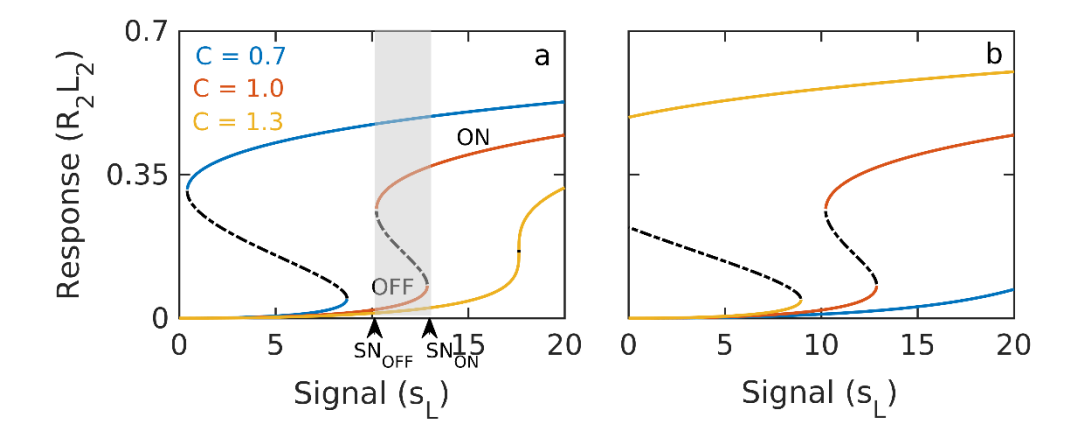


Figure 5.3: The one-parameter bifurcation diagrams: (a) Bistable bifurcation diagrams with basal rate of ligand synthesis s_L as the bifurcation parameter. The solid and the broken lines represent the stable and unstable SSs, respectively. The 'ON' and 'OFF' thresholds are indicated as SN_{ON} and SN_{OFF} for the bifurcation for C=1.0. The shaded region indicates the bistable region for C=1.0. The different colors of the bifurcations plots represent different values of C achieved by changing K_1 with a fixed K_2 value. (b) Bistable bifurcation diagrams for different cooperativities achieved by changing K_2 with a fixed K_1 . The parameter values are $k_{1b}=0.2, k_{2b}=0.25, k_{1f}=0.1, k_{2f}=0.5, k_L=2.66, \gamma_L=1.0$. k_{1b} was modified keeping k_{1f} fixed at 0.1 to achieve different cooperativities at constant K_2 . Similarly different cooperativities were achieved by varying K_2 by modifying k_{2b} with $k_{2f}=0.5$ and keeping K_1 fixed.

We found that the module exhibit bistability with two stable SSs separated by an unstable SS. Our aim here was to see the effect of cooperativity on the bistability. To change the cooperativity C, the values of K_1 and K_2 were modified accordingly. In the **Figure 5.3**, the

cooperativity $\mathcal C$ was initially kept at 1 with $K_1=K_2=1$. The cooperativity of the system can be modified either by changing K_1 or by changing K_2 . First, the cooperativity C was changed by changing K_1 keeping K_2 (= 1) fixed. We found that the negative cooperativity ($\mathcal{C}=0.7$) regime leads to bigger region of bistability (SN_{ON}-SN_{OFF}) as compared to the non-cooperativity (C=1) or positive cooperativity (C=1.3) regimes (**Figure 5.3a**). The two SN bifurcation points moved to the right (high s_L) in both positive and non-cooperativity relative to the negative cooperativity and at higher positive cooperativities (C > 1.3), the model did not exhibit bistability. On the other hand, increased negative cooperativity (C < 0.7) exhibited bigger region of irreversible bistability with SN_{OFF} in the negative region. Note that the 'ON' signalling threshold in the negative cooperativity is much lower as compared to the positive cooperativity. This is due to the fact that as K_1 is reduced to get negative cooperativity, the singly occupied receptor (R_2L_1) is stabilized requiring less ligands (s_L) to achieve the fully engaged receptor (R_2L_2) that kick starts the positive feedback cycle. Whereas in the positive cooperativity, K_1 is increased destabilizing the singly occupied receptor (R_2L_1) and hence SN_ON is pushed to higher s_L because more amount of ligands are required to start the feedback cycle. Due to large abundance of R_2L_1 , when the signal was removed, more amount of ligands are needed to be removed to get back to the OFF state and hence the SN_{OFF} moved to the left in the negative cooperativity. In case of positive cooperativity, the abundance of R_2L_1 was less and hence removal of small amounts of ligands reverted the system back to the OFF state causing SN_{OFF} to move to high value of s_L resulting in a narrow bistable region. Further, the SS value of the ON state representing the extent of response was much higher in the negative cooperativity as compared to the positive cooperativity. Therefore, negative cooperativity when achieved by adjusting K_1 , can cause stronger response at low signal concentration region.

Next, we changed K_2 to achieve different cooperativities keeping K_1 fixed at 1. This resulted in an opposite trend to that of when K_1 was changed with K_2 fixed. In this, K_2 was increased to get negative cooperativity and that resulted in a smaller region of bistability as compared to non-cooperativity and positive cooperativity (**Figure 5.3b**). When K_2 was increased to get negative cooperativity, the doubly engaged receptor (R_2L_2) became less abundant due to shift of equilibrium to the left. Thus more ligands are required to kick start the feedback cycle

and as a result the SN_{OFF} moved to the far right in negative cooperativity. Similarly, when small amounts of ligands were removed the system fell back to the OFF state and hence the SNoN was also at high s_L value. When K_2 was decreased to get positive cooperativity, the abundance of R_2L_2 increased which needed less ligands to trigger the feedback cycle and also more amounts of ligands were needed to be removed to come back to OFF state. Therefore, here both SN_{ON} and SN_{OFF} moved to the left resulting in a bigger bistable region. Thus, negative cooperativity generates robust bistability when R_2L_1 is stabilized by reducing K_1 and positive cooperativity generates robust bistability when R_2L_2 is stabilized by reducing K_2 .

To examine the bistable behaviour of the model for different K_1 and K_2 values, we carried out 2-parameter bifurcation analysis using the XPPAUT software.

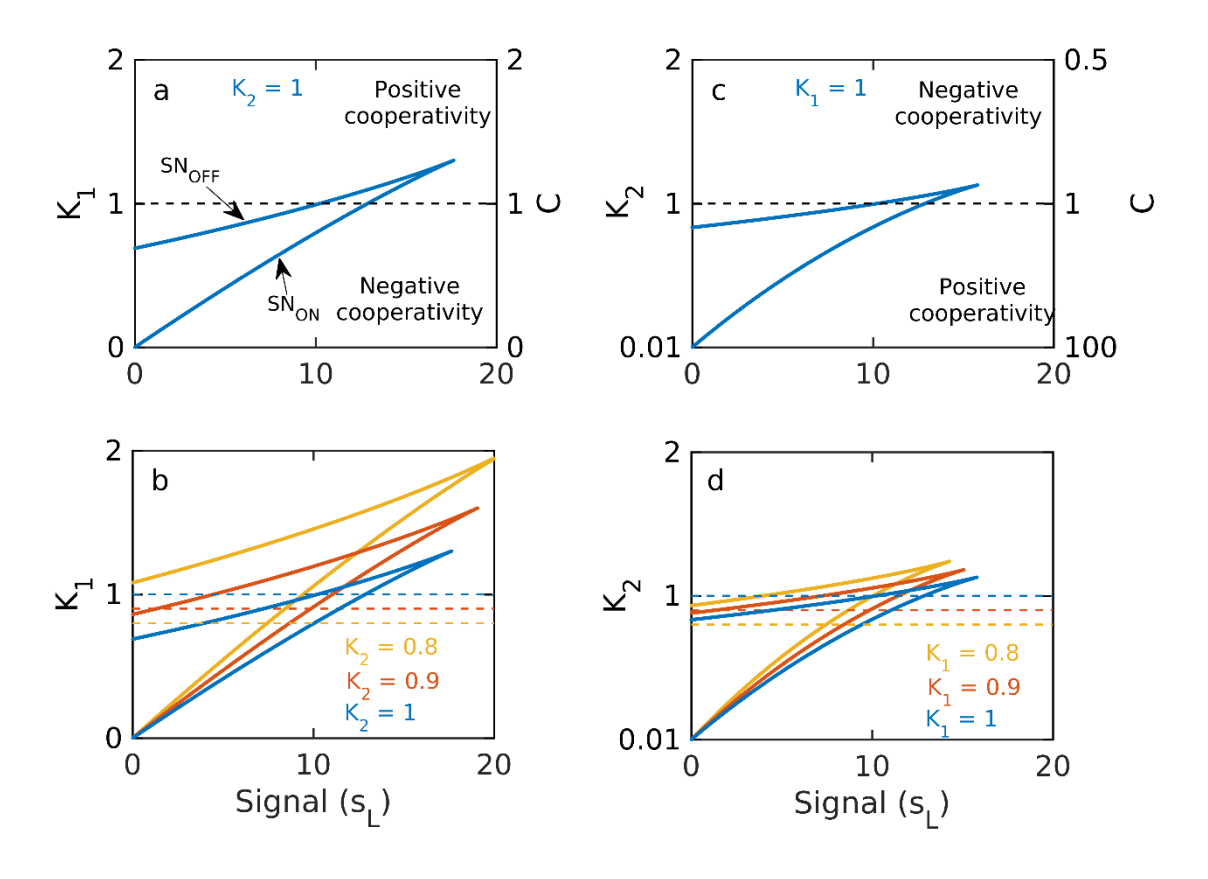


Figure 5.4: The two-parameter bifurcation analysis for the model: the solid colored lines are the loci of the SN bifurcation points. The region bounded by these lines represent bistable region and outside region represents monostability. The non-cooperativity, C=1, is represented by the dashed horizontal lines that separates the positive (C > 1) and negative

(C < 1) cooperativity regions. Two-parameter bifurcations with fixed value of K_2 (left) and K_1 (right), respectively.

In **Figure 5.4a**, we present the 2-parameter bifurcation analysis with varying K_1 and fixed K_2 . The region bounded by the two lines represents the bistable region and the region outside of it represents the monostable region. The lower and the upper lines represent the loci of $\mathsf{SN}_{\mathsf{ON}}$ and $\mathsf{SN}_{\mathsf{OFF}}$, respectively. The horizontal broken line at C=1 divides the space into two regions-positive (C>1) and negative (C<1) cooperativities. **Figure 5.4a** suggests that a bigger region of bistability occurs in the negative cooperativity and as the two lines approach the positive cooperativity space, the bistable region decreases. We repeated this calculation for different values of K_2 and here too negative cooperativity leads to bigger bistable region that increases with decrease in K_2 value (**Figure 5.4b**). This highlights the fact that the ligand must strongly bind to the receptor to achieve strong ultrasensitivity with the negative cooperativity²³³. Similar calculations were carried out where K_2 was changed with fixed K_1 (**Figure 5.4c-d**). In these figures, bigger bistable region existed in the positive cooperativity and the bistable region decreases as the two lines moves towards negative cooperativity. Overall **Figures 5.4c-d** has completely opposite results compared to **Figure 5.4a-b**.

The strength of the PFL is important in understanding the bistability in any PFLs. We carried out 2-parameter bifurcation analysis of the model with different cooperativities and different feedback strength (k_L) (Figure 5.5a). With the feedback strength increased, the bistable region increased. Further, in negative cooperativity, a lower feedback strength is required for robust bistability compared to that in positive cooperativity. Figure 5.5b represent a 2-parameter bifurcation analysis of bistability with respect to total receptor concentration (R_T). Bistability can be observed in negative cooperativity at smaller receptor concentrations than in positive cooperativity. Overall, Figure 5.5 indicates that bistability in negative cooperativity can be achieved with small positive feedback strength and low receptor concentrations.

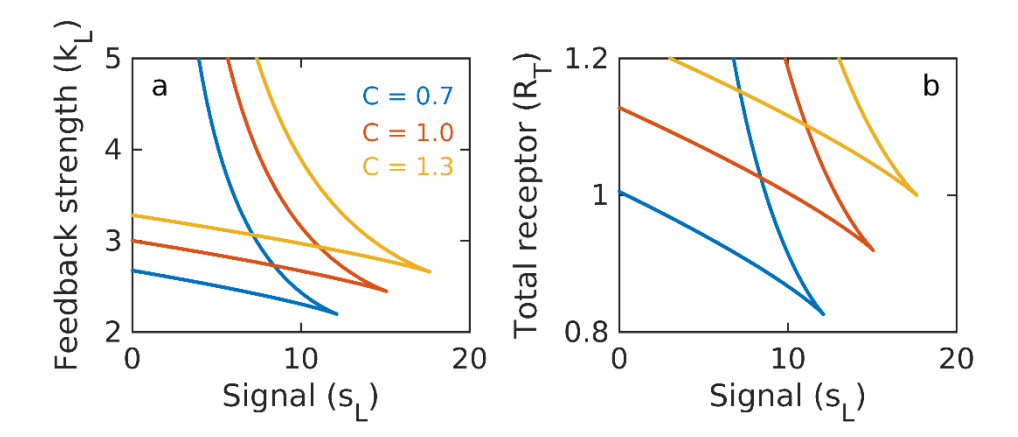


Figure 5.5: Two parameter bifurcation analysis showing the effect of feedback strength (k_L) and total receptors (R_T) : The different colored lines are for different cooperativity values as indicted in the legends. The cooperativity C was changed by varying K_1 while K_2 was fixed at 1.

Until now, we have considered the amount of ligand s_L as the main bifurcation parameter. In this section we present the bifurcation analysis with total receptor concentration (R_T) as the bifurcation parameter (Figure 5.6). Similar to that with s_L as the bifurcation parameter, here too we analysed the bistable region in negative and positive cooperativities by changing either K_1 and K_2 . Figure 5.6 resulted in a complete opposite trend to what we observed with s_L as the bifurcation parameter. Here, when K_1 was changed with fixed K_2 (Figure 5.6a,c), positive cooperativity generated robust bistability and when K_2 was changed with fixed K_1 , negative cooperativity resulted in robust bistability (Figure 5.6b,d). Here, the variation of right SN point (SN_{ON}) with K_1 is similar to that of with s_L as the bifurcation parameter. This is due to the fact that as K_1 was decreased to get negative cooperativity, the intermediate R_2L_1 complex gets stabilized which requires less ligands (s_L) and also less receptors (R_T) to shift the system to the ON state. Hence, in negative cooperativity the SN_{ON} is at low value of R_T as compared to the same in positive cooperativity (Figure 5.6a,c). On the other hand, when K_2 was decreased to get positive cooperativity, R_2L_2 gets stabilised and hence less ligands (s_L) and less receptors (R_T) are required for ON threshold (Figure 5.6b,d). However, the behaviour of SN_{OFF} with K_1 or K_2 depends crucially on the bifurcation parameters s_L and R_T . In **Figure 5.6a**, the bistable region increased in positive cooperativity because the SN_{OFF} moved left. This is because R_2L_2 helps start the PFL due to which there is an increase in number of ligands that

allowed the 'ON' state to survive even though when receptors were removed. This resulted in smaller value of SN_{OFF} and consequently bigger bistable region. Similarly when K_2 was increased to get negative cooperativity, the stability of R_2L_2 decreases but again, the large amounts of ligands allowed the system to maintain the 'ON' state even though large amounts of receptors were removed.

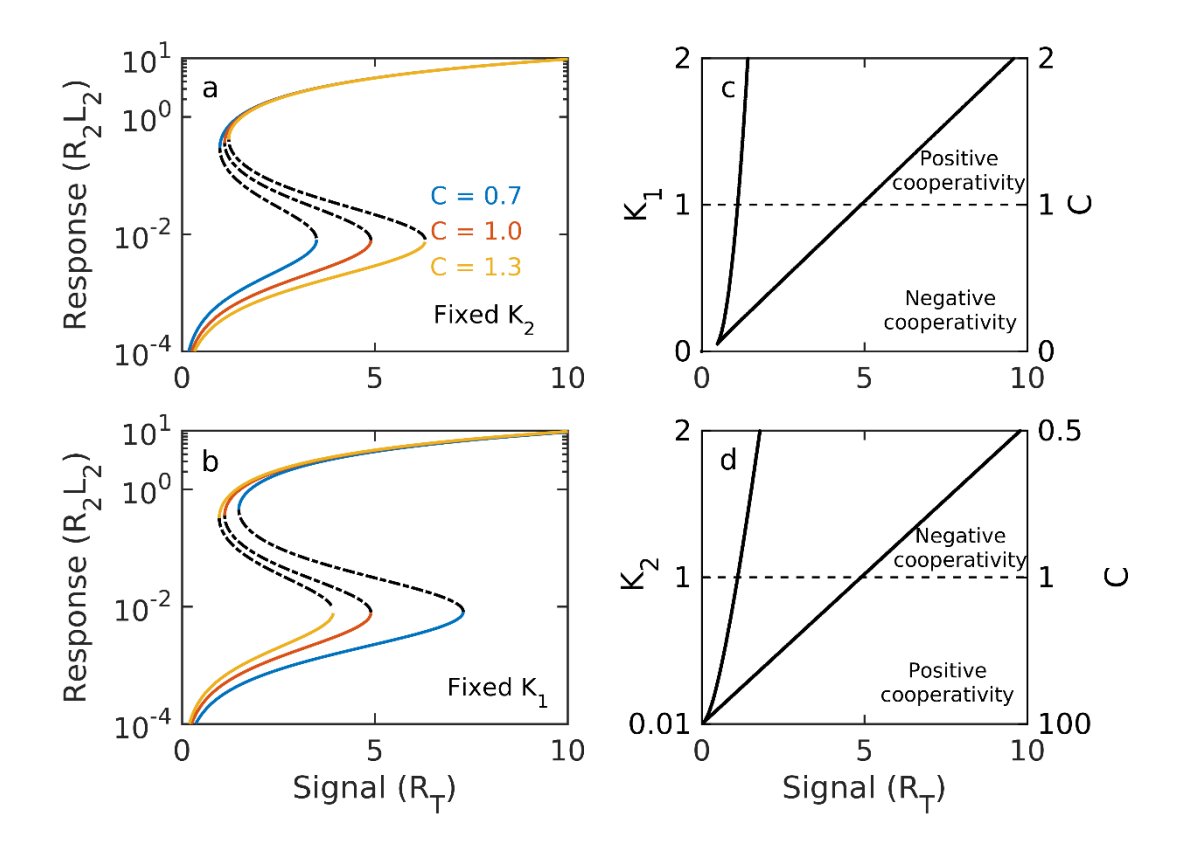


Figure 5.6: Bifurcation analysis for the model with total receptors as the bifurcation parameter: (a,b) One-parameter bifurcation diagrams showing the effect of different cooperativities by varying K_1 (a) and varying K_2 (b). (c,d) Two-parameter bifurcations at different cooperativity regime modified by varying K_1 (c) and varying K_2 (d).

5.3.2. Positive feedback in both ligand and receptor upregulation: Fused PFLs

Our aim here was to explore the bistability in different cooperativities when an additional PFL is introduced. Here too, we carried out 2-parameter bifurcation analysis to investigate the effect of different cooperativities on the bistable region. Note that when the PFL in ligand

upregulation is switched-off, the system did not exhibit any bistability at any parameter values even in presence of a PFL in receptor upregulation (Figure 5.7). This happened due to lack of non-linearity when k_L was made zero.

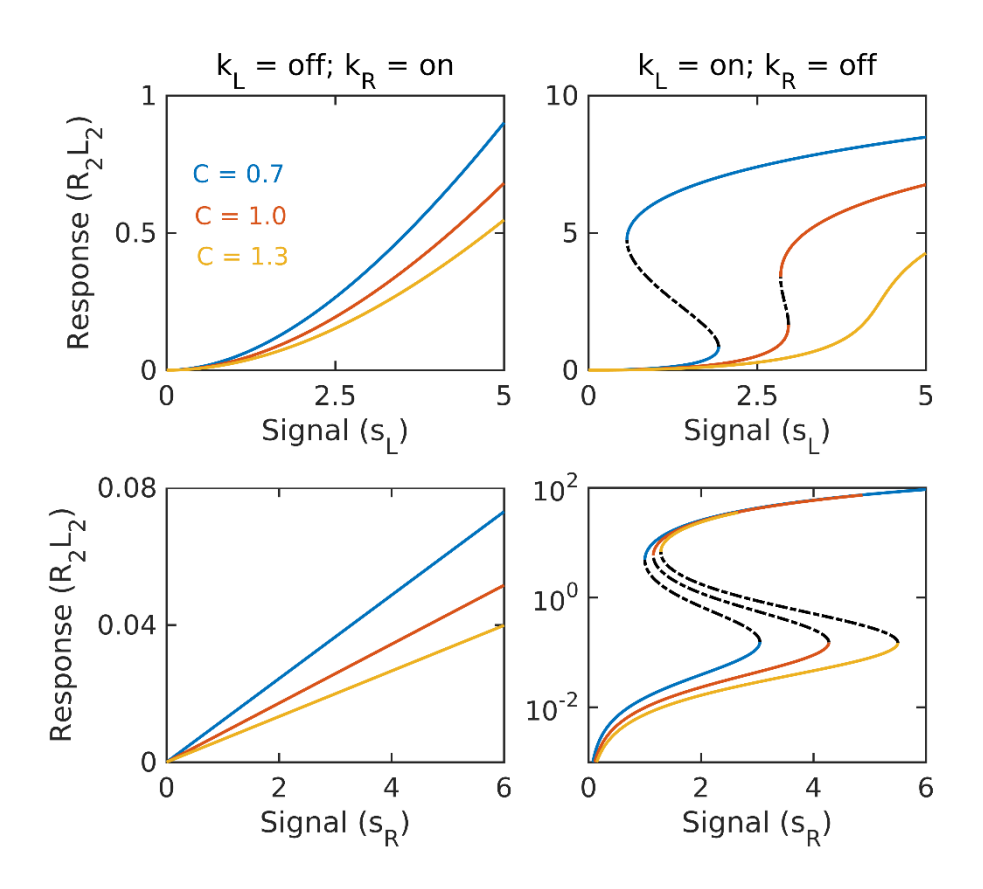


Figure 5.7: One-parameter bifurcation analysis depicting the effect of receptor and ligand upregulation: The model loses bistability when the PFL in ligand upregulation is switched off (left) and bistability is sustained even when the PFL in receptor upregulation is switched off (right).

We used Chemical Reaction Network Theory (CRNT) toolbox 2.35 (http://crnt.osu.edu/CRNTWin) to confirm this. Indeed, CRNT predicted that when both the PFLs are present, the module exhibited multistability. Figure 5.8 present the 2-parameter bifurcation analysis of the model with different cooperativities with different values of receptor upregulation strength (k_R) . The qualitative nature of the bifurcation diagrams are similar to those observed with only one PFL via ligand upregulation. However, here the bifurcations are quite sensitive to k_R . With increased in k_R value, the region of bistability increased significantly. Particularly, the SN_{OFF} bifurcation point is more sensitive to changing

 k_R as compared to ${\sf SN_{ON}}$ points. As k_R was increased, more receptors were synthesized which shifted the equilibrium to the right thus allowing the ON state for increased removal of the ligands. This also shifted the ${\sf SN_{OFF}}$ points to lower values of s_L . Whereas, if the bifurcation parameter is the synthesis rate of receptor (s_R) , the bifurcations are weakly dependent on k_R (Figure 5.8c, d).

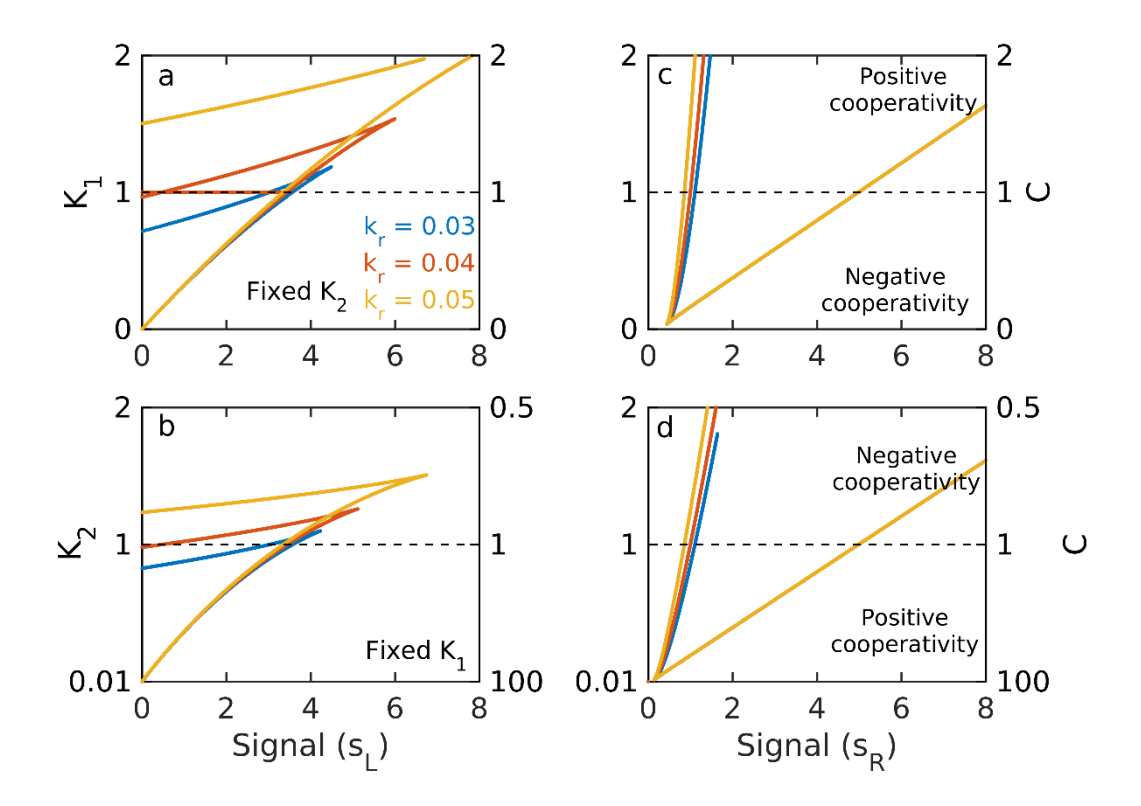


Figure 5.8: Two-parameter bifurcation analysis showing the effect of strength of receptor upregulation (k_R): The different values for the strength of receptor upregulation is indicted in the legend. The parameter values are $k_{1b}=0.2, k_{2b}=0.25, k_{1f}=0.1, k_{2f}=0.5, \gamma_L=0.18, \gamma_R=0.06, k_L=k_R=0.03, s_R=1.0$ when s_L is the bifurcation parameter and $s_L=0.5$ when s_R is the bifurcation parameter.

5.4. Summary and conclusions

Ultrasensitivity in the biochemical reaction network is a prerequisite to generate multistability in a positive feedback regulated network^{199,223}. Mathematical modelling and experiments have recently shown that negative cooperativity in a receptor-ligand binding

dynamics can generate ultrasensitive response when the ligand strongly binds to the receptors²³³. In this work, we have incorporated a PFL in a dimeric receptor-ligand binding system to investigate the effect of different types of cooperative binding on the bistable response. We explored the effect of negative cooperativity on the bistable region by adjusting the dissociation constants K_1 and K_2 . Our results suggest that negative cooperativity can generate robust bistability under certain conditions (Figure 5.4). The bistability in negative cooperativity regime can be observed both in case of amount of ligands (s_L) (Figure 5.3) and amount of receptors (R_T) (Figure 5.6). Negative cooperativity generated robust bistability when K_1 was changed and positive cooperativity generated robust bistability when K_2 was changed with amount of ligands (s_L) as the bifurcation parameter (Figure 5.3). Whereas, if the bifurcation parameter is the amount of receptors (R_T) , negative cooperativity generated robust bistability when K_2 was changed and positive cooperativity generated robust bistability when K_1 was changed (Figure 5.6). The variation of different dissociation constants to achieve different cooperativities resulted in a dichotomous nature of bistability. From our 2-parameter bifurcation analysis, it can be concluded that the relative stability of the singly engaged receptor (R_2L_1) and doubly engaged receptor (R_2L_2) control the bistable region in the models. When the bifurcation parameter is the amount of ligands (s_L) , the stabilization of (R_2L_1) and R_2L_2 generated robust bistability in negative and positive cooperativity, respectively. Alternately, when the bifurcation parameter is the amount of receptors (R_T) , stabilization of R_2L_1 and R_2L_2 favoured robust bistability in positive and negative cooperativities, respectively. Our calculations also suggest that negative cooperativity can generate bigger bistable region with low positive feedback strength and low receptor concentrations (Figure 5.5). Altogether, our modelling and calculations explored the conditions under which negative cooperativity can generate robust bistability in receptorligand dynamics system.

Our results highlights that the nature of bistability defined by the bistable region under different cooperative binding depends on the bifurcation parameter and the tuning of the dissociation constants to change the cooperativity. When the synthesis rate of ligand is the bifurcation parameter, adjusting cooperativity with the first dissociation constant gives robust bistability in negative cooperativity and when the second dissociation constant is

changed, positive cooperativity generate robust bistability. This behaviour is however, quite opposite, when the bifurcation parameter is changed to amount of receptors (R_T) . Thus our model shows a contrasting and dichotomous nature of the bistability that depends on the choice of parameters used to modify cooperativity and the choice of bifurcation parameter.

While traditionally, ultrasensitivity has been achieved using Hill functions for positive cooperativity, the zero-order ultrasensitive Goldbeter-Koshland switch in enzyme kinetics²⁴⁰, multisite phosphorylation^{241–244} and molecular titration^{245,246}, it is indeed important to note that negative cooperativity also has potential to generate ultrasensitive response. Particularly in the case of synthetic biology approaches, negative cooperativity can be explored further to explore its potential to develop new devices.

Chapter 6

Summary, Conclusions and Future Scopes

Cell-fate decisions are crucial for a cell's survival and growth as well as the survival and growth of the multicellular organism of which the cell is a part of. During the development of the embryo, the embryonic stem cells differentiate into organ specific cells that form the different organs in the organism. The cell-fate decisions are tightly coordinated by the interactions between proteins, genes, RNAs and other biomolecules, thus forming a complex network of signalling pathways. Smaller subunits called regulatory motifs form the basic functional unit of the complex network. Positive (activation) and negative (inhibition) regulations are the two different types of regulations found in these regulatory motifs. Feedforward and feedback loops are the two types of regulatory motifs, where the signal is transmitted uni-directionally in the FFLs whereas in feedback loops the signal is transmitted bi-directionally. PFLs are often found to regulate many cell-fate decisions such as the preadipocyte to adipocyte differentiation^{36,61}, differentiation of T helper cells^{76–78}, EMTs^{37,143}. A single PFL can consist of either mutual activation (MA), or mutual inhibition (MI), or self-activation (SA) whereas coupled PFLs are formed by the fusion between two or more PFLs of the similar or different

regulations, thus giving rise to different topologies of the PFLs. PFLs are known to generate multistable switches also known as biological switches in response to signal doses. A biological switch has the potential to convert a graded response to a digital 'all-or-none' response at the population level. A multistable biological switch has stable SSs separated by unstable SSs and the different stable SSs correspond to different expression levels of the genes which are associated with different phenotypic states of the cells.

Stochasticity or chemical noise are often found to interfere with the cell-fate decision making processes which can alter the dynamics and outcome of the decision making. Stochasticity can give rise to population heterogeneity or cellular variabilities in an isogenic population of cells. A cell has to function and produce responses with high degree of accuracy and robustness even under the unavoidable threat from chemical noise. What role the regulatory motifs play in regulating or limiting the effects of chemical noise? Do the topologies of the regulatory motifs contribute to limit the cellular variabilities? This thesis tries to address these questions by mathematically modelling the regulatory motifs involving PFLs and understanding the role of different topologies of the PFLs in generating robust biological switches relevant to cell-fate decisions.

The tristable switch could justify the presence of mixed phenotypic states in many cell-fate decisions such as in EMT, differentiation of naïve CD4+ cells, differentiation of T helper cells. Therefore, we investigated the robustness of different topologies of tristable networks involving two PFLs in generating tristable responses under random variation of parameter space. We generated three sets of 500,000 random parameter combinations where the parameters were sampled from independent distributions. We developed a new automation method of bifurcation analysis using potential energy landscapes which allowed us to generate 1.5 million 1-parameter bifurcation diagrams for each different tristable networks. We then estimated the number of tristable responses each network generated to analyse the robustness score. We found that the networks having mutual inhibition self-activation (MISA) motif are the most robust in producing tristable switches as compared to the networks having mutual activation self-activation (MASA) motif. In the context of cellular differentiation, many natural systems have MISA as the core regulatory network motifs such as differentiation of trophectoderm-inner cell mass¹⁶⁵, primitive endoderm-epiblast¹⁴⁶, myeloid-erythroid

differentiation of T helper cells 139,247, EMT 143,166. The choice of MISA motifs over other motifs in these cell-fate decisions might be the system's evolutionary strategy to adapt to robust networks in the face of chemical noise. The potential energy based method also allowed us to automatically segregate the four different types of tristable responses defined based on the number of ON and OFF thresholds and on the relative ordering of the SN bifurcation points. We observed that Type-IV tristable response with one ON and one OFF signalling threshold is the most robust while Type-I with two ON-OFF signalling thresholds is the least robust. Our investigations on the EMT network suggest that introducing an additional PFL with MI to the core regulatory network of EMT made the pEMT state more accessible as compared to introducing a PFL with MA. It is indeed seen that addition of the TF GRHL2 to ZEB as a mutual inhibition loop in the EMT network 'stabilizes' the pEMT state^{38,159,160}. Furthermore, systematic analysis of the bi- and tri-stable switches for the perturbed and unperturbed networks revealed that introduction of a SA to the MI loop generated and stabilized the intermediate stable SS as compared to the same when the SA was introduced to a MA loop.

The potential energy based method of automated bifurcation analysis has an advantage over the existing numerical continuation method of bifurcation analysis such as XPPAUT and Oscil8. The potential energy based method can identify bifurcations with broken branches such as isola whereas it is difficult to identify one using the numerical continuation method. Thus, the potential method can analyse both the typical multistable switches as well as the atypical isola and mushroom bifurcations. The isola and mushroom bifurcations are known to regulate neural stem cell differentiation, heat shock protein dynamics under different stress levels. What are the minimal networks that generate the atypical bifurcations? What is the origin of the isola and mushroom bifurcations? How the robustness of the atypical bifurcations depend on the networks modelled with different input gate configurations? To address these issues, we investigated the robustness of networks with a PFL fused to a FFL that have the potential to generate typical and atypical bistable bifurcations. Based on the regulations in the FFL, we classified the networks into incoherent and coherent where in the incoherent networks the regulation on the two arms of the FFL are different whereas in coherent networks the regulations are same. We then generated 500,000 random parameter

sets to analyse the robustness of the networks in generating bistable bifurcations. We found that the incoherent networks generated both typical as well as atypical bistable bifurcations whereas the coherent networks produced only typical bistable responses. To understand why the coherent networks are not potent in producing atypical isola and mushrooms, we looked into the origin of the atypical bifurcations. We perturbed the incoherent networks by deleting the different regulations from the input signal to the self-activating node. We found that the atypical isola and mushroom bifurcations are formed due to the congregation of two qualitatively opposite bistable bifurcations. The qualitatively opposite bifurcations are generated by incoherent networks due to the presence of opposite regulations in the FFL whereas coherent networks produced similar bistable bifurcations due to the presence of similar regulations in the FFL. Furthermore, we found that if the regulations in the incoherent networks are modelled using OR gate configurations, the inverted isola (II) and inverted mushrooms (IMs) are more robust than the normal isola (NI) and normal mushrooms (NMs) whereas the results are opposite for AND and MIXED gate configurations. We showed that the NI and NMs are formed if the positive and negative regulations in the FFL is initiated at lower and higher signals, respectively whereas if the opposite occurred, II and IMs are formed. In differentiation programmes, chemical noise can give rise to mixed population or cellular variability which can affect the rate of differentiation. Therefore, we investigated how different arrangements of multiple PFLs regulate chemical noise or cellular variability in differentiation programmes. We explored parallel and serial arrangements of PFLs where in parallel arrangements the PFLs independently regulate the master regulator and in serial arrangements the PFLs are in end-to-end chain like fashion. In presence of extrinsic and intrinsic noise, we found that the parallel PFLs have better efficacy in reducing cell-to-cell variability as compared to serial PFLs. To understand the reasons behind these observations, we performed susceptibility analysis of the SN points and SSs in presence of extrinsic and intrinsic noises, respectively. We found that the SN points in serial arrangements are more sensitive to extrinsic noise as compared to the same in parallel PFLs. Using mean residence time calculations, we found that the stable SSs in serial PFLs are more susceptible to intrinsic noise as compared to that of in parallel PFLs. We found similar results using different input configurations such as AND and OR gates and also using different modelling methodologies such as Goldbeter-Koshland (GK) switch and Hill functions. The parallel arrangements of PFLs being robust in reducing cellular variability is indeed found in many cellular systems such as in preadipocyte to adipocyte differentiation³⁶, in the cell cycle network of budding yeast¹²³ and fission yeast²⁰⁴.

A PFL and ultrasensitivity is required to generate a bistable switch. Although positive cooperativity is a source of ultrasensitivity. Recently it was shown that negative cooperativity can generate ultrasensitive response in receptor-ligand (RL) binding dynamics. Therefore, we investigated the role of negative cooperativity in generating bistable switches in the RL binding systems. We incorporated a PFL in the system by upregulating the ligand synthesis by the active receptors. We found that the conditions where positive cooperativity generated robust bistability, negative cooperativity showed poor bistability and vice-versa, thus exhibiting the dichotomous nature of the bistability under different types of cooperativities. Furthermore, we showed that the dichotomous nature of the bistability depends on the control parameters, the bifurcation parameters and the stability of the RL complex. In our RL system, we have modified the dissociation rate constants to adjust the cooperativities. In vitro experimental modifications of the dissociation constants are difficult to achieve, nevertheless, this feat has been achieved by introducing mutations in the proteins²⁴⁸.

Future scope

A single PFL can generate a bistable response whereas an additional PFL can generate a tristable response. In general, addition of an extra PFL to an existing PFL(s) has the potential to generate a new pair of stable-unstable SSs. Multistable switches with more than three stable SSs are found to regulate many cell-fate determination systems 145,249,250. However, the dynamics of these multistable switches are not explored much. In multistable switches such as quadrastability, the intermediate stable SSs can reveal the functional and dynamical features of the hybrid phenotypic states of the cells. In a quadrastable switch, there are six SN bifurcation points and based on the relative ordering of these points and the number of ON and OFF signalling thresholds, the quadrastable switch can be categorised into different types. The minimal networks that can generate a quadrastable response consists of three

fused PFLs. Therefore, it would be interesting to investigate the robustness of different topologies of the minimal 2- and 3-C networks with three fused PFLs in generating quadrastable responses under random variation of parameter space. The potential energy based method of bifurcation analysis can be a useful tool in understanding the robustness networks via large number of bifurcation analysis.

Another area which can be of prime focus is understanding the dynamical aspects of the different types of atypical switches with three stable SSs. Typical bistable switch is known to regulate many cell-fate decisions whereas, the atypical switches are not well explored. The new approach of bifurcation analysis using the potential energy method can have great applications in exploring different atypical bifurcations with broken branches.

Understanding the dynamical features of different phenotypic states of the cell is crucial in understanding the physiology of the cell. Mathematical models of biological systems is an important tool in mimicking the functions of the underlying biological systems. The topology of the regulatory motifs that govern the cell-fate decisions play a crucial role in providing robustness to the system to accurately and efficiently function in the presence of chemical noise. Therefore, it is important to investigate and understand the role of regulatory motifs to gain insights into the mechanism of the biological systems such as cancer progression and human disease thereby identifying novel therapeutic targets

References

- 1. Ehebauer, M., Hayward, P. & Arias, A. M. Notch, a universal arbiter of cell fate decisions. Science 314, 1414–1415 (2006).
- 2. Zhang, J., Nie, Q. & Zhou, T. Revealing Dynamic Mechanisms of Cell Fate Decisions From Single-Cell Transcriptomic Data. Front. Genet. 10, 1280 (2019).
- 3. Tatapudy, S., Aloisio, F., Barber, D. & Nystul, T. Cell fate decisions: emerging roles for metabolic signals and cell morphology. EMBO Rep. 18, 2105–2118 (2017).
- 4. Garcia-Ojalvo, J. & Martinez Arias, A. Towards a statistical mechanics of cell fate decisions. Curr. Opin. Genet. Dev. 22, 619-626 (2012).
- 5. Osakada, F., Ikeda, H., Sasai, Y. & Takahashi, M. Stepwise differentiation of pluripotent stem cells into retinal cells. Nat. Protoc. 4, 811–824 (2009).
- 6. Boheler, K. R. et al. Differentiation of Pluripotent Embryonic Stem Cells Into Cardiomyocytes. Circ. Res. 91, 189–201 (2002).
- 7. Yoder, M. C. Differentiation of pluripotent stem cells into endothelial cells. Curr. Opin. Hematol. 22, 252-257 (2015).
- 8. Rajala, K., Pekkanen-Mattila, M. & Aalto-Setälä, K. Cardiac Differentiation of Pluripotent Stem Cells. Stem Cells Int. 2011, 1–12 (2011).
- 9. Dalton, S. Linking the Cell Cycle to Cell Fate Decisions. Trends Cell Biol. 25, 592-600 (2015).
- 10. Ohnuma, S., Philpott, A. & Harris, W. A. Cell cycle and cell fate in the nervous system. Curr. Opin. Neurobiol. 11, 66-73 (2001).
- 11. Pauklin, S. & Vallier, L. The Cell-Cycle State of Stem Cells Determines Cell Fate Propensity. Cell 155, 135-147 (2013).
- 12. Ogawa, M. Differentiation and proliferation of hematopoietic stem cells. Blood 81, 2844-2853 (1993).
- 13. Dharampuriya, P. R. et al. Tracking the origin, development, and differentiation of hematopoietic stem cells. Curr. Opin. Cell Biol. 49, 108-115 (2017).
- 14. Lai, A. Y. & Kondo, M. T and B lymphocyte differentiation from hematopoietic stem cell. Semin. Immunol. 20, 207-212 (2008).
- 15. D, B. Protein molecules as computational elements in living cells. Nature 376, 307-312 (1995).
- 16. Milo, R. et al. Network motifs: simple building blocks of complex networks. Science **298**, 824–827 (2002).
- 17. Shen-Orr, S. S., Milo, R., Mangan, S. & Alon, U. Network motifs in the transcriptional

- regulation network of Escherichia coli. Nat. Genet. 31, 64–68 (2002).
- 18. Alon, U. An Introduction to Systems Biology: Design Principles of Biological Circuits. (Chapman & Hall/CRC, 2007).
- 19. Yeger-Lotem, E. et al. Network motifs in integrated cellular networks of transcriptionregulation and protein-protein interaction. Proc. Natl. Acad. Sci. U. S. A. 101, 5934-9 (2004).
- 20. Wolf, D. M. & Arkin, A. P. Motifs, modules and games in bacteria. Curr. Opin. Microbiol. 6, 125-134 (2003).
- 21. Paranipe, D. A. & Sharma, V. K. Evolution of temporal order in living organisms. J. Circadian Rhythms 3, 7 (2005).
- 22. Spiller, M. P. et al. The Myostatin Gene Is a Downstream Target Gene of Basic Helix-Loop-Helix Transcription Factor MyoD. Mol. Cell. Biol. 22, 7066-7082 (2002).
- 23. Harris, S. L. & Levine, A. J. The p53 pathway: positive and negative feedback loops. Oncogene 24, 2899–2908 (2005).
- 24. Mangan, S. & Alon, U. Structure and function of the feed-forward loop network motif. Proc. Natl. Acad. Sci. U. S. A. 100, 11980-11985 (2003).
- 25. Brandman, O. & Meyer, T. Feedback loops shape cellular signals in space and time. Science **322**, 390–395 (2008).
- 26. Kim, J.-R., Yoon, Y. & Cho, K.-H. Coupled Feedback Loops Form Dynamic Motifs of Cellular Networks. Biophys. J. 94, 359-365 (2008).
- 27. Angeli, D., Ferrell, J. E. & Sontag, E. D. Detection of multistability, bifurcations, and hysteresis in a large class of biological positive-feedback systems. Proc. Natl. Acad. Sci. U. S. A. 101, 1822–1827 (2004).
- 28. Ferrell, J. E. & Xiong, W. Bistability in cell signaling: How to make continuous processes discontinuous, and reversible processes irreversible. Chaos An Interdiscip. J. Nonlinear Sci. 11, 227–235 (2001).
- 29. Leite, M. C. A. & Wang, Y. Multistability, oscillations and bifurcations in feedback loops. Math. Biosci. Eng. 7, 83-97 (2010).
- 30. Siegal-Gaskins, D., Grotewold, E. & Smith, G. D. The capacity for multistability in small gene regulatory networks. BMC Syst. Biol. 3, 96 (2009).
- 31. Ptashne M. A genetic switch: phage lambda revisited. (Cold Spring Harbour Lab, 2004).
- 32. Novick, A. & Weiner, M. Enzyme induction is an all-or-none phenomenon. Proc. Natl. Acad. Sci. U. S. A. 43, 553-566 (1957).
- 33. Acar, M., Becskei, A. & van Oudenaarden, A. Enhancement of cellular memory by reducing stochastic transitions. Nature 435, 228–232 (2005).

- 34. E. M. Ozbudak, M. Thattai, H. N. Lim, B. I. Shraiman & Oudenaarden, A. Van. Multistability in the lactose utilization network of Escherichia coli. Nature 427, 737-740 (2004).
- 35. Gardner, T. S., Cantor, C. R. & Collins, J. J. Construction of a genetic toggle switch in Escherichia coli. Nature 403, 339-342 (2000).
- 36. Park, B. O., Ahrends, R. & Teruel, M. N. Consecutive positive feedback loops create a bistable switch that controls preadipocyte-to-adipocyte conversion. Cell Rep. 2, 976-990 (2012).
- 37. Zhang, J. et al. TGF-β-induced epithelial-to-mesenchymal transition proceeds through stepwise activation of multiple feedback loops. Sci. Signal. 7, ra91 (2014).
- 38. Hong, T. et al. An Ovol2-Zeb1 Mutual Inhibitory Circuit Governs Bidirectional and Multi-step Transition between Epithelial and Mesenchymal States. PLOS Comput. Biol. **11**, e1004569 (2015).
- 39. Chang, D.-E. et al. Building biological memory by linking positive feedback loops. Proc. Natl. Acad. Sci. U. S. A. 107, 175–180 (2010).
- 40. Xiong, W. & Ferrell, J. E. A positive-feedback-based bistable 'memory module' that governs a cell fate decision. Nature 426, 460–465 (2003).
- 41. Sha, W. et al. Hysteresis drives cell-cycle transitions in Xenopus laevis egg extracts. Proc. Natl. Acad. Sci. U. S. A. 100, 975-80 (2003).
- 42. Pomerening, J. R., Sontag, E. D. & Ferrell, J. E. Building a cell cycle oscillator: hysteresis and bistability in the activation of Cdc2. Nat. Cell Biol. 5, 346–351 (2003).
- 43. Yao, G., Tan, C., West, M., Nevins, J. R. & You, L. Origin of bistability underlying mammalian cell cycle entry. Mol. Syst. Biol. 7, 485 (2011).
- 44. Skotheim, J. M., Di Talia, S., Siggia, E. D. & Cross, F. R. Positive feedback of G1 cyclins ensures coherent cell cycle entry. Nature 454, 291–296 (2008).
- 45. Yang, X., Lau, K.-Y., Sevim, V. & Tang, C. Design Principles of the Yeast G1/S Switch. PLoS Biol. 11, e1001673 (2013).
- 46. Ferrell, J. E. Tripping the switch fantastic: how a protein kinase cascade can convert graded inputs into switch-like outputs. Trends Biochem. Sci. 21, 460–466 (1996).
- 47. Wang, L. et al. Bistable switches control memory and plasticity in cellular differentiation. Proc. Natl. Acad. Sci. U. S. A. 106, 6638–6643 (2009).
- 48. Pigolotti, S., Krishna, S. & Jensen, M. H. Oscillation patterns in negative feedback loops. Proc. Natl. Acad. Sci. U. S. A. 104, 6533–6537 (2007).
- 49. Snoussi, E. H. Necessary Conditions for Multistationarity and Stable Periodicity. J. Biol. Syst. **06**, 3–9 (1998).
- 50. Gouzé, J.-L. Positive and Negative Circuits in Dynamical Systems. J. Biol. Syst. 06, 11-15 (1998).

- 51. Hoffmann, A., Levchenko, A., Scott, M. L. & Baltimore, D. The IkappaB-NF-kappaB signaling module: temporal control and selective gene activation. Science 298, 1241-1245 (2002).
- Duong, H. A., Robles, M. S., Knutti, D. & Weitz, C. J. A molecular mechanism for 52. circadian clock negative feedback. Science 332, 1436–1439 (2011).
- 53. Aronson, B. D., Johnson, K. A., Loros, J. J. & Dunlap, J. C. Negative feedback defining a circadian clock: autoregulation of the clock gene frequency. Science 263, 1578-1584 (1994).
- 54. Mika, D., Richter, W. & Conti, M. A CaMKII/PDE4D negative feedback regulates cAMP signaling. Proc. Natl. Acad. Sci. U. S. A. 112, 2023–2028 (2015).
- 55. Liu, Y. et al. Long noncoding RNA LINCO0518 induces radioresistance by regulating glycolysis through an miR-33a-3p/HIF-1 α negative feedback loop in melanoma. *Cell* Death Dis. 12, 245 (2021).
- 56. Aulehla, A. et al. Wnt3a Plays a Major Role in the Segmentation Clock Controlling Somitogenesis. Dev. Cell 4, 395-406 (2003).
- 57. Kageyama, R., Niwa, Y., Isomura, A., González, A. & Harima, Y. Oscillatory gene expression and somitogenesis. Wiley Interdiscip. Rev. Dev. Biol. 1, 629–641 (2012).
- 58. Pfeuty, B. & Kaneko, K. The combination of positive and negative feedback loops confers exquisite flexibility to biochemical switches. Phys. Biol. 6, 046013 (2009).
- 59. Avendaño, M. S., Leidy, C. & Pedraza, J. M. Tuning the range and stability of multiple phenotypic states with coupled positive-negative feedback loops. Nat. Commun. 4, 2605 (2013).
- 60. Hill, A. . The possible effects of the aggregation of the molecules of haemoglobin on its dissociation curves. J. Physiol. 40, i-vii (1910).
- 61. Ahrends, R. et al. Controlling low rates of cell differentiation through noise and ultrahigh feedback. *Science* **344**, 1384–1389 (2014).
- 62. Yildirim, N. & Mackey, M. C. Feedback regulation in the lactose operon: A mathematical modeling study and comparison with experimental data. Biophys. J. 84, 2841–2851 (2003).
- 63. Novak, B. & Tyson, J. J. Numerical analysis of a comprehensive model of M-phase control in Xenopus oocyte extracts and intact embryos. J. Cell Sci. 106, 1153-1168 (1993).
- 64. Tyson, J. J., Chen, K. & Novak, B. Network dynamics and cell physiology. Nat. Rev. *Mol. Cell Biol.* **2**, 908–916 (2001).
- 65. Pomerening, J. R., Kim, S. Y. & Ferrell, J. E. Systems-Level Dissection of the Cell-Cycle Oscillator: Bypassing Positive Feedback Produces Damped Oscillations. Cell 122, 565-578 (2005).

- 66. Ferrell, J. E. & Machleder, E. M. The biochemical basis of an all-or-none cell fate switch in Xenopus oocytes. Science 280, 895-898 (1998).
- 67. Ingolia, N. T. Topology and Robustness in the Drosophila Segment Polarity Network. PLoS Biol. 2, e123 (2004).
- 68. Laslo, P. et al. Multilineage Transcriptional Priming and Determination of Alternate Hematopoietic Cell Fates. Cell 126, 755-766 (2006).
- 69. Shvartsman, S. Y., Muratov, C. B. & Lauffenburger, D. A. Modeling and computational analysis of EGF receptor-mediated cell communication in Drosophila oogenesis. Development 129, 2577–2589 (2002).
- 70. Ferrell, J. E. Self-perpetuating states in signal transduction: positive feedback, doublenegative feedback and bistability. Curr. Opin. Cell Biol. 14, 140-148 (2002).
- 71. Smits, W. K., Kuipers, O. P. & Veening, J.-W. Phenotypic variation in bacteria: the role of feedback regulation. Nat. Rev. Microbiol. 4, 259–271 (2006).
- 72. Guidi, G. M. & Goldbeter, A. Bistability without Hysteresis in Chemical Reaction Systems: A Theoretical Analysis of Irreversible Transitions between Multiple Steady States. J. Phys. Chem. A 101, 9367–9376 (1997).
- 73. Silveira, D. A. & Mombach, J. C. M. Dynamics of the feedback loops required for the phenotypic stabilization in the epithelial-mesenchymal transition. FEBS J. 287, 578-588 (2020).
- 74. Voo, K. S. et al. Identification of IL-17-producing FOXP3+ regulatory T cells in humans. Proc. Natl. Acad. Sci. U. S. A. 106, 4793-4798 (2009).
- 75. Lochner, M. et al. In vivo equilibrium of proinflammatory IL-17+ and regulatory IL-10+ Foxp3+ RORyt+ T cells. J. Exp. Med. 205, 1381-1393 (2008).
- 76. Fang, M., Xie, H., Dougan, S. K., Ploegh, H. & van Oudenaarden, A. Stochastic cytokine expression induces mixed T helper cell States. PLoS Biol. 11, e1001618 (2013).
- 77. Antebi, Y. E. et al. Mapping differentiation under mixed culture conditions reveals a tunable continuum of T cell fates. PLoS Biol. 11, e1001616 (2013).
- 78. Peine, M. et al. Stable T-bet+GATA-3+ Th1/Th2 Hybrid Cells Arise In Vivo, Can Develop Directly from Naive Precursors, and Limit Immunopathologic Inflammation. PLoS Biol. **11**, e1001633 (2013).
- 79. Olsson, A. et al. Single-cell analysis of mixed-lineage states leading to a binary cell fate choice. Nature 537, 698-702 (2016).
- 80. Sarrió, D. et al. Epithelial-Mesenchymal Transition in Breast Cancer Relates to the Basal-like Phenotype. Cancer Res. 68, 989–997 (2008).
- 81. Dey, A. & Barik, D. Parallel arrangements of positive feedback loops limit cell-to-cell variability in differentiation. *PLoS One* **12**, e0188623 (2017).
- 82. Brandman, O., Ferrell, J. E., Li, R. & Meyer, T. Interlinked fast and slow positive

- feedback loops drive reliable cell decisions. Science **310**, 496–498 (2005).
- 83. Raser, J. M. & O'Shea, E. K. Control of stochasticity in eukaryotic gene expression. Science **304**, 1811–1814 (2004).
- 84. Elowitz, M. B., Levine, A. J., Siggia, E. D. & Swain, P. S. Stochastic gene expression in a single cell. Science 297, 1183–1186 (2002).
- 85. Chabot, J. R., Pedraza, J. M., Luitel, P. & van Oudenaarden, A. Stochastic gene expression out-of-steady-state in the cyanobacterial circadian clock. Nature 450, 1249-1252 (2007).
- 86. Newman, J. R. S. et al. Single-cell proteomic analysis of S. cerevisiae reveals the architecture of biological noise. Nature 441, 840-846 (2006).
- 87. Ozbudak, E. M., Thattai, M., Kurtser, I., Grossman, A. D. & van Oudenaarden, A. Regulation of noise in the expression of a single gene. *Nat. Genet.* **31**, 69–73 (2002).
- 88. Raj, A., Peskin, C. S., Tranchina, D., Vargas, D. Y. & Tyagi, S. Stochastic mRNA Synthesis in Mammalian Cells. PLoS Biol. 4, e309 (2006).
- 89. Stewart-Ornstein, J., Weissman, J. S. & El-Samad, H. Cellular Noise Regulons Underlie Fluctuations in Saccharomyces cerevisiae. Mol. Cell 45, 483–493 (2012).
- 90. Becskei, A., Kaufmann, B. B. & van Oudenaarden, A. Contributions of low molecule number and chromosomal positioning to stochastic gene expression. Nat. Genet. 37, 937-944 (2005).
- 91. Blake, W. J., Kærn, M., Cantor, C. R. & Collins, J. J. Noise in eukaryotic gene expression. Nature 422, 633-637 (2003).
- 92. Golding, I., Paulsson, J., Zawilski, S. M. & Cox, E. C. Real-Time Kinetics of Gene Activity in Individual Bacteria. *Cell* **123**, 1025–1036 (2005).
- 93. Dar, R. D. et al. Transcriptional burst frequency and burst size are equally modulated across the human genome. Proc. Natl. Acad. Sci. U. S. A. 109, 17454-17459 (2012).
- 94. Rai, A. & van Oudenaarden, A. Single-Molecule Approaches to Stochastic Gene Expression. Annu. Rev. Biophys. 38, 255–270 (2009).
- 95. Peccoud, J. & Ycart, B. Markovian Modeling of Gene-Product Synthesis. Theor. Popul. Biol. 48, 222-234 (1995).
- 96. Suter, D. M., Molina, N., Naef, F. & Schibler, U. Origins and consequences of transcriptional discontinuity. Curr. Opin. Cell Biol. 23, 657–662 (2011).
- 97. Coulon, A., Chow, C. C., Singer, R. H. & Larson, D. R. Eukaryotic transcriptional dynamics: from single molecules to cell populations. Nat. Rev. Genet. 14, 572-584 (2013).
- 98. Chubb, J. R., Trcek, T., Shenoy, S. M. & Singer, R. H. Transcriptional Pulsing of a Developmental Gene. Curr. Biol. 16, 1018–1025 (2006).

- 99. Chong, S., Chen, C., Ge, H. & Xie, X. S. Mechanism of Transcriptional Bursting in Bacteria. Cell 158, 314–326 (2014).
- 100. Levens, D. & Larson, D. R. A New Twist on Transcriptional Bursting. Cell 158, 241–242 (2014).
- 101. Jones, D. L., Brewster, R. C. & Phillips, R. Promoter architecture dictates cell-to-cell variability in gene expression. Science 346, 1533–1536 (2014).
- 102. Kærn, M., Elston, T. C., Blake, W. J. & Collins, J. J. Stochasticity in gene expression: from theories to phenotypes. Nat. Rev. Genet. 6, 451–464 (2005).
- 103. Cai, L., Friedman, N. & Xie, X. S. Stochastic protein expression in individual cells at the single molecule level. Nature 440, 358-362 (2006).
- 104. Hinczewski, M. & Thirumalai, D. Cellular signaling networks function as generalized Wiener-Kolmogorov filters to suppress noise. *Phys. Rev. X* **4**, 1–15 (2014).
- 105. Balázsi, G., van Oudenaarden, A. & Collins, J. J. Cellular Decision Making and Biological Noise: From Microbes to Mammals. Cell 144, 910–925 (2011).
- 106. D. T, G. The chemical Langevin equation. J. Chem. Phys. **113**, 297–306 (2000).
- 107. Lei, J. Stochastic Modeling in Systems Biology. J. Adv. Math. Appl. 1, 76–88 (2013).
- 108. Gillespie, D. T. A general method for numerically simulating the stochastic time evolution of coupled chemical reactions. J. Comput. Phys. 22, 403–434 (1976).
- 109. Tian, T. & Burrage, K. Stochastic models for regulatory networks of the genetic toggle switch. Proc. Natl. Acad. Sci. U. S. A. 103, 8372-8377 (2006).
- 110. Kobayashi, H. et al. Programmable cells: interfacing natural and engineered gene networks. Proc. Natl. Acad. Sci. U. S. A. 101, 8414-8419 (2004).
- 111. Jolly, M. K., Kulkarni, P., Weninger, K., Orban, J. & Levine, H. Phenotypic Plasticity, Bet-Hedging, and Androgen Independence in Prostate Cancer: Role of Non-Genetic Heterogeneity. Front. Oncol. 8, 50 (2018).
- 112. Zhang, X.-P., Liu, F., Cheng, Z. & Wang, W. Cell fate decision mediated by p53 pulses. Proc. Natl. Acad. Sci. U. S. A. 106, 12245-12250 (2009).
- 113. Purvis, J. E. et al. p53 dynamics control cell fate. Science **336**, 1440–1444 (2012).
- 114. Hafner, A., Bulyk, M. L., Jambhekar, A. & Lahav, G. The multiple mechanisms that regulate p53 activity and cell fate. Nat. Rev. Mol. Cell Biol. 20, 199–210 (2019).
- 115. Luo, Q., Beaver, J., Liu, Y. & Zhang, Z. Dynamics of p53: A Master Decider of Cell Fate. Genes (Basel). 8, 66 (2017).
- 116. Lestas, I., Vinnicombe, G. & Paulsson, J. Fundamental limits on the suppression of molecular fluctuations. Nature 467, 174-178 (2010).
- 117. Wang, D.-G., Wang, S., Huang, B. & Liu, F. Roles of cellular heterogeneity, intrinsic and extrinsic noise in variability of p53 oscillation. Sci. Rep. 9, 5883 (2019).

- 118. Reyes, J. et al. Fluctuations in p53 Signaling Allow Escape from Cell-Cycle Arrest. Mol. Cell 71, 581-591.e5 (2018).
- 119. Freeman, M. Intercellular signalling in development. *Nature* 408, 313–319 (2000).
- 120. Tyson, J. J. Modeling the cell division cycle: cdc2 and cyclin interactions. *Proc. Natl.* Acad. Sci. U. S. A. 88, 7328-7332 (1991).
- 121. Crosby, M. E. Cell Cycle: Principles of Control. *Yale J. Biol. Med.* **80**, 141–142 (2007).
- 122. Hoffmann, I., Clarke, P. R., Marcote, M. J., Karsenti, E. & Draetta, G. Phosphorylation and activation of human cdc25-C by cdc2--cyclin B and its involvement in the selfamplification of MPF at mitosis. EMBO J. 12, 53-63 (1993).
- 123. Barik, D., Ball, D. A., Peccoud, J. & Tyson, J. J. A Stochastic Model of the Yeast Cell Cycle Reveals Roles for Feedback Regulation in Limiting Cellular Variability. PLOS Comput. Biol. 12, e1005230 (2016).
- 124. Olsson, A. et al. Single-cell analysis of mixed-lineage states leading to a binary cell fate choice. Nature **537**, 698–702 (2016).
- 125. Jia, D. et al. Operating principles of tristable circuits regulating cellular differentiation. Phys. Biol. 14, (2017).
- 126. Rosenfeld, N., Elowitz, M. B. & Alon, U. Negative Autoregulation Speeds the Response Times of Transcription Networks. J. Mol. Biol. 323, 785-793 (2002).
- 127. Becskei, A. & Serrano, L. Engineering stability in gene networks by autoregulation. *Nature* **405**, 590–593 (2000).
- Hornung, G. & Barkai, N. Noise propagation and signaling sensitivity in biological networks: a role for positive feedback. PLoS Comput. Biol. 4, e8 (2008).
- 129. Bruggeman, F. J., Blüthgen, N. & Westerhoff, H. V. Noise Management by Molecular Networks. PLOS Comput. Biol. 5, e1000506 (2009).
- 130. Tsai, T. Y.-C. et al. Robust, tunable biological oscillations from interlinked positive and negative feedback loops. *Science* **321**, 126–139 (2008).
- 131. Tian, X. J., Zhang, X. P., Liu, F. & Wang, W. Interlinking positive and negative feedback loops creates a tunable motif in gene regulatory networks. Phys. Rev. E - Stat. Nonlinear, Soft Matter Phys. **80**, 11926 (2009).
- 132. Garcia-Bernardo, J. & Dunlop, M. J. Tunable Stochastic Pulsing in the Escherichia coli Multiple Antibiotic Resistance Network from Interlinked Positive and Negative Feedback Loops. PLOS Comput. Biol. 9, e1003229 (2013).
- 133. Krumsiek, J., Marr, C., Schroeder, T. & Theis, F. J. Hierarchical Differentiation of Myeloid Progenitors Is Encoded in the Transcription Factor Network. PLoS One 6, e22649 (2011).
- 134. Boller, S. & Grosschedl, R. The regulatory network of B-cell differentiation: a focused view of early B-cell factor 1 function. Immunol. Rev. 261, 102–115 (2014).

- 135. Jia, D. et al. Distinguishing Mechanisms Underlying EMT Tristability. Cancer Converg. **1**, 2 (2017).
- 136. Silveira, D. A. & Mombach, J. C. M. Dynamics of the feedback loops required for the phenotypic stabilization in the epithelial-mesenchymal transition. FEBS J. 287, 578-588 (2020).
- 137. Preca, B.-T. et al. A novel ZEB1/HAS2 positive feedback loop promotes EMT in breast cancer. Oncotarget 8, 11530–11543 (2017).
- 138. Antebi, Y. E. et al. Mapping Differentiation under Mixed Culture Conditions Reveals a Tunable Continuum of T Cell Fates. PLoS Biol. 11, e1001616 (2013).
- 139. Peine, M. et al. Stable T-bet+GATA-3+ Th1/Th2 Hybrid Cells Arise In Vivo, Can Develop Directly from Naive Precursors, and Limit Immunopathologic Inflammation. PLoS Biol. **11**, e1001633 (2013).
- 140. Fang, M., Xie, H., Dougan, S. K., Ploegh, H. & van Oudenaarden, A. Stochastic Cytokine Expression Induces Mixed T Helper Cell States. PLoS Biol. 11, e1001618 (2013).
- 141. Leroy, P. & Mostov, K. E. Slug is required for cell survival during partial epithelialmesenchymal transition of HGF-induced tubulogenesis. Mol. Biol. Cell 18, 1943–1952 (2007).
- 142. Williams, E. D., Gao, D., Redfern, A. & Thompson, E. W. Controversies around epithelial-mesenchymal plasticity in cancer metastasis. Nat. Rev. Cancer 19, 716-732 (2019).
- 143. Lu, M., Jolly, M. K., Levine, H., Onuchic, J. N. & Ben-Jacob, E. MicroRNA-based regulation of epithelial-hybrid-mesenchymal fate determination. Proc. Natl. Acad. Sci. U. S. A. 110, 18144–18149 (2013).
- 144. Tian, X. J., Zhang, H. & Xing, J. Coupled reversible and irreversible bistable switches underlying TGFβ-induced epithelial to mesenchymal transition. *Biophys. J.* **105**, 1079– 1089 (2013).
- 145. Guantes, R. & Poyatos, J. F. Multistable Decision Switches for Flexible Control of Epigenetic Differentiation. PLoS Comput. Biol. 4, e1000235 (2008).
- 146. Bessonnard, S. et al. Gata6, Nanog and Erk signaling control cell fate in the inner cell mass through a tristable regulatory network. *Development* **141**, 3637–3648 (2014).
- 147. De Mot, L. et al. Cell Fate Specification Based on Tristability in the Inner Cell Mass of Mouse Blastocysts. *Biophys. J.* **110**, 710–722 (2016).
- 148. Tosenberger, A. et al. A multiscale model of early cell lineage specification including cell division. npj Syst. Biol. Appl. 3, 16 (2017).
- 149. Huang, S., Guo, Y. P., May, G. & Enver, T. Bifurcation dynamics in lineage-commitment in bipotent progenitor cells. Dev. Biol. 305, 695–713 (2007).
- 150. Macía, J., Widder, S. & Solé, R. Why are cellular switches Boolean? General conditions

- for multistable genetic circuits. J. Theor. Biol. 261, 126–135 (2009).
- 151. Lu, M. et al. Tristability in Cancer-Associated MicroRNA-TF Chimera Toggle Switch. J. Phys. Chem. B 117, 13164-13174 (2013).
- 152. Strogatz, S. . Nonlinear Dynamics and Chaos: With Applications to Physics, Biology, Chemistry, And Enginnering. (Westview Press, 2001).
- 153. Kuznetsov, Y. Elements of Applied Bifurcation Theory. (Springer-Verlag, 2004).
- 154. Waddington, C. H. *The Strategy of the Genes*. (George Allen and Unwin, 1957).
- 155. Wang, J., Zhang, K., Xu, L. & Wang, E. Quantifying the Waddington landscape and biological paths for development and differentiation. Proc. Natl. Acad. Sci. U. S. A. **108**, 8257–8262 (2011).
- 156. Ermentrout GB. Simulating, Analyzing, and Animating Dynamical systems: A Guide to XPPAUT for Researchers and Students. (2002).
- 157. Huang, B., Xia, Y., Liu, F. & Wang, W. Realization of tristability in a multiplicatively coupled dual-loop genetic network. Sci. Rep. 6, 28096 (2016).
- 158. Huang, B. et al. Interrogating the topological robustness of gene regulatory circuits by randomization. PLoS Comput. Biol. 13, e1005456 (2017).
- 159. Jolly, M. K. et al. Stability of the hybrid epithelial/mesenchymal phenotype. Oncotarget 7, 27067-27084 (2016).
- 160. Jia, D. et al. OVOL guides the epithelial-hybrid-mesenchymal transition. Oncotarget 6, 15436–15448 (2015).
- 161. Graf, T. & Enver, T. Forcing cells to change lineages. *Nature* **462**, 587–594 (2009).
- 162. Moris, N., Pina, C. & Arias, A. M. Transition states and cell fate decisions in epigenetic landscapes. Nat. Rev. Genet. 17, 693-703 (2016).
- 163. Ye, Z. & Sarkar, C. A. Towards a Quantitative Understanding of Cell Identity. Trends Cell Biol. 28, 1030–1048 (2018).
- 164. Huang, S. Hybrid T-helper cells: stabilizing the moderate center in a polarized system. PLoS Biol. 11, e1001632 (2013).
- 165. Niwa, H. et al. Interaction between Oct3/4 and Cdx2 determines trophectoderm differentiation. *Cell* **123**, 917–929 (2005).
- 166. Burk, U. et al. A reciprocal repression between ZEB1 and members of the miR-200 family promotes EMT and invasion in cancer cells. EMBO Rep. 9, 582–589 (2008).
- 167. Siemens, H. et al. miR-34 and SNAIL form a double-negative feedback loop to regulate epithelial-mesenchymal transitions. *Cell Cycle* **10**, 4256–4271 (2011).
- 168. Ye, Y., Kang, X., Bailey, J., Li, C. & Hong, T. An enriched network motif family regulates multistep cell fate transitions with restricted reversibility. PLOS Comput. Biol. 15, e1006855 (2019).

- 169. Song, H., Smolen, P., Av-Ron, E., Baxter, D. A. & Byrne, J. H. Bifurcation and Singularity Analysis of a Molecular Network for the Induction of Long-Term Memory. Biophys. J. **90**, 2309–2325 (2006).
- 170. Sengupta, D. & Kar, S. Deciphering the Dynamical Origin of Mixed Population during Neural Stem Cell Development. *Biophys. J.* **114**, 992–1004 (2018).
- 171. Wang, J., Li, C. & Wang, E. Potential and flux landscapes quantify the stability and robustness of budding yeast cell cycle network. Proc. Natl. Acad. Sci. U. S. A. 107, 8195–8200 (2010).
- 172. Zhang, B. & Wolynes, P. G. Stem cell differentiation as a many-body problem. *Proc.* Natl. Acad. Sci. U. S. A. 111, 10185-10190 (2014).
- 173. Li, C. & Balazsi, G. A landscape view on the interplay between EMT and cancer metastasis. npj Syst. Biol. Appl. 4, 34 (2018).
- 174. Sriram, K., Rodriguez-Fernandez, M. & Doyle, F. J. A Detailed Modular Analysis of Heat-Shock Protein Dynamics under Acute and Chronic Stress and Its Implication in Anxiety Disorders. PLoS One 7, e42958 (2012).
- 175. Raj, A. & van Oudenaarden, A. Nature, Nurture, or Chance: Stochastic Gene Expression and Its Consequences. Cell 135, 216–226 (2008).
- 176. Thattai, M. & van Oudenaarden, A. Intrinsic noise in gene regulatory networks. *Proc.* Natl. Acad. Sci. U. S. A. 98, 8614–8619 (2001).
- 177. Das, D., Dey, S., Brewster, R. C. & Choubey, S. Effect of transcription factor resource sharing on gene expression noise. PLoS Comput. Biol. 13, e1005491 (2017).
- 178. Huh, D. & Paulsson, J. Non-genetic heterogeneity from stochastic partitioning at cell division. Nat. Genet. 43, 95-100 (2011).
- 179. Sherman, M. S., Lorenz, K., Lanier, M. H. & Cohen, B. A. Cell-to-Cell Variability in the Propensity to Transcribe Explains Correlated Fluctuations in Gene Expression. Cell *Syst.* **1**, 315–325 (2015).
- 180. Volfson, D. et al. Origins of extrinsic variability in eukaryotic gene expression. Nature **439**, 861–864 (2006).
- 181. Talia, S. Di, Skotheim, J. M., Bean, J. M., Siggia, E. D. & Cross, F. R. The effects of molecular noise and size control on variability in the budding yeast cell cycle. Nature **448**, 947–951 (2007).
- 182. Geva-Zatorsky, N. et al. Oscillations and variability in the p53 system. Mol. Syst. Biol. **2**, 2006.0033 (2006).
- 183. Spencer, S. L., Gaudet, S., Albeck, J. G., Burke, J. M. & Sorger, P. K. Non-genetic origins of cell-to-cell variability in TRAIL-induced apoptosis. *Nature* **459**, 428–432 (2009).
- 184. Burnett, J. C., Miller-Jensen, K., Shah, P. S., Arkin, A. P. & Schaffer, D. V. Control of Stochastic Gene Expression by Host Factors at the HIV Promoter. PLoS Pathog. 5,

- e1000260 (2009).
- 185. Weinberger, L. S., Burnett, J. C., Toettcher, J. E., Arkin, A. P. & Schaffer, D. V. Stochastic Gene Expression in a Lentiviral Positive-Feedback Loop: HIV-1 Tat Fluctuations Drive Phenotypic Diversity. Cell 122, 169–182 (2005).
- 186. Beach, R. R. et al. Aneuploidy Causes Non-genetic Individuality. Cell 169, 229-242.e21 (2017).
- 187. Acar, M., Mettetal, J. T. & Van Oudenaarden, A. Stochastic switching as a survival strategy in fluctuating environments. Nat. Genet. 40, 471–475 (2008).
- 188. Çağatay, T., Turcotte, M., Elowitz, M. B., Garcia-Ojalvo, J. & Süel, G. M. Architecture-Dependent Noise Discriminates Functionally Analogous Differentiation Circuits. Cell **139**, 512–522 (2009).
- 189. Ghusinga, K. R., Dennehy, J. J. & Singh, A. First-passage time approach to controlling noise in the timing of intracellular events. Proc. Natl. Acad. Sci. U. S. A. 114, 693-698 (2017).
- 190. Simpson, M. L., Cox, C. D. & Sayler, G. S. Frequency domain analysis of noise in autoregulated gene circuits. Proc. Natl. Acad. Sci. U. S. A. 100, 4551–4556 (2003).
- 191. Lestas, I., Vinnicombe, G. & Paulsson, J. Fundamental limits on the suppression of molecular fluctuations. *Nature* **467**, 174–178 (2010).
- 192. Tomioka, R., Kimura, H., J. Kobayashi, T. & Aihara, K. Multivariate analysis of noise in genetic regulatory networks. J. Theor. Biol. 229, 501–521 (2004).
- 193. Swain, P. S. Efficient Attenuation of Stochasticity in Gene Expression Through Posttranscriptional Control. J. Mol. Biol. **344**, 965–976 (2004).
- 194. Maithreye, R. & Sinha, S. Propagation of extrinsic perturbation in a negatively autoregulated pathway. Phys. Biol. 4, 48-59 (2007).
- 195. Dublanche, Y., Michalodimitrakis, K., Kümmerer, N., Foglierini, M. & Serrano, L. Noise in transcription negative feedback loops: simulation and experimental analysis. Mol. Syst. Biol. 2, 41 (2006).
- 196. Niwa, H., Miyazaki, J. & Smith, A. G. Quantitative expression of Oct-3/4 defines differentiation, dedifferentiation or self-renewal of ES cells. Nat. Genet. 24, 372-376 (2000).
- 197. Hooshangi, S., Thiberge, S. & Weiss, R. Ultrasensitivity and noise propagation in a synthetic transcriptional cascade. Proc. Natl. Acad. Sci. U. S. A. 102, 3581-3586 (2005).
- 198. Wang, L., Xin, J. & Nie, Q. A Critical Quantity for Noise Attenuation in Feedback Systems. PLOS Comput. Biol. 6, e1000764 (2010).
- 199. Tyson, J. J., Chen, K. C. & Novak, B. Sniffers, buzzers, toggles and blinkers: Dynamics of regulatory and signaling pathways in the cell. Curr. Opin. Cell Biol. 15, 221–231 (2003).

- 200. Goldbeter, A. & Koshland, D. E. An amplified sensitivity arising from covalent modification in biological systems. Proc. Natl. Acad. Sci. U. S. A. 78, 6840-6844 (1981).
- 201. W, H. & Lefever, R. *Noise Induced Transitions*. (Springer-Verlag, 1984).
- 202. Feinerman, O., Veiga, J., Dorfman, J. R., Germain, R. N. & Altan-Bonnet, G. Variability and robustness in T cell activation from regulated heterogeneity in protein levels. *Science* **321**, 1081–1084 (2008).
- 203. Tyson, J. J. & Novák, B. Functional Motifs in Biochemical Reaction Networks. Annu. Rev. Phys. Chem. 61, 219-240 (2010).
- 204. Sveiczer, A. Modelling the fission yeast cell cycle. Briefings Funct. Genomics Proteomics 2, 298-307 (2004).
- 205. Heldin, C.-H. & Moustakas, A. Signaling Receptors for TGF-β Family Members. Cold Spring Harb. Perspect. Biol. 8, a022053 (2016).
- 206. Renauld, J.-C. Class II cytokine receptors and their ligands: Key antiviral and inflammatory modulators. Nat. Rev. Immunol. 3, 667–676 (2003).
- 207. Wang, X., Lupardus, P., LaPorte, S. L. & Garcia, K. C. Structural Biology of Shared Cytokine Receptors. Annu. Rev. Immunol. 27, 29-60 (2009).
- 208. Broughton, S. E., Hercus, T. R., Lopez, A. F. & Parker, M. W. Cytokine receptor activation at the cell surface. Curr. Opin. Struct. Biol. 22, 350–359 (2012).
- 209. Platanias, L. C. Mechanisms of type-I- and type-II-interferon-mediated signalling. *Nat.* Rev. Immunol. 5, 375-386 (2005).
- 210. Gschwind, A., Fischer, O. M. & Ullrich, A. The discovery of receptor tyrosine kinases: targets for cancer therapy. Nat. Rev. Cancer 4, 361–370 (2004).
- 211. Furnari, F. B., Cloughesy, T. F., Cavenee, W. K. & Mischel, P. S. Heterogeneity of epidermal growth factor receptor signalling networks in glioblastoma. Nat. Rev. Cancer 15, 302-310 (2015).
- 212. Dorsam, R. T. & Gutkind, J. S. G-protein-coupled receptors and cancer. Nat. Rev. Cancer 7, 79–94 (2007).
- 213. Rosenbaum, D. M., Rasmussen, S. G. F. & Kobilka, B. K. The structure and function of G-protein-coupled receptors. Nature 459, 356–363 (2009).
- 214. Whitty, A. Cooperativity and biological complexity. *Nat. Chem. Biol.* **4**, 435–439 (2008).
- 215. Cornish-Bowden, A. Understanding allosteric and cooperative interactions in enzymes. FEBS J. 281, 621–632 (2014).
- 216. Koshland, D. E. J. & Hamadani, K. Proteomics and models for enzyme cooperativity. J. Biol. Chem. 277, 46841-46844 (2002).

- 217. Cornish-Bowden, A. The physiological significance of negative cooperativity revisited. Journal of theoretical biology vol. 319 144–147 (2013).
- 218. von Krbek, L. K. S., Schalley, C. A. & Thordarson, P. Assessing cooperativity in supramolecular systems. Chem. Soc. Rev. 46, 2622–2637 (2017).
- 219. Weiss, J. N. The Hill equation revisited: uses and misuses. FASEB J. 11, 835–841 (1997).
- 220. Prinz, H. Hill coefficients, dose–response curves and allosteric mechanisms. J. Chem. Biol. 3, 37-44 (2010).
- 221. Ferrell, J. E., Jr & Ha, S. H. Ultrasensitivity part II: multisite phosphorylation, stoichiometric inhibitors, and positive feedback. Trends Biochem. Sci. 39, 556-569 (2014).
- 222. Straube, R. Analysis of network motifs in cellular regulation: Structural similarities, input-output relations and signal integration. Biosystems 162, 215-232 (2017).
- 223. Ferrell, J. E. & Ha, S. H. Ultrasensitivity part III: cascades, bistable switches, and oscillators. Trends Biochem. Sci. 39, 612-618 (2014).
- 224. Bush, E. C. et al. Modeling the Role of Negative Cooperativity in Metabolic Regulation and Homeostasis. PLoS One 7, e48920 (2012).
- 225. Macdonald, J. L. & Pike, L. J. Heterogeneity in EGF-binding affinities arises from negative cooperativity in an aggregating system. Proc. Natl. Acad. Sci. U. S. A. 105, 112-117 (2008).
- 226. Alvarado, D., Klein, D. E. & Lemmon, M. A. Structural Basis for Negative Cooperativity in Growth Factor Binding to an EGF Receptor. Cell 142, 568–579 (2010).
- 227. Arkhipov, A., Shan, Y., Kim, E. T. & Shaw, D. E. Membrane Interaction of Bound Ligands Contributes to the Negative Binding Cooperativity of the EGF Receptor. PLoS Comput. Biol. 10, e1003742 (2014).
- 228. Levitzki, A. Negative cooperativity at the insulin receptor. *Nature* **289**, 442–443 (1981).
- 229. De Meyts, P. The insulin receptor: a prototype for dimeric, allosteric membrane receptors? Trends Biochem. Sci. 33, 376-384 (2008).
- 230. Surinya, K. H. et al. An Investigation of the Ligand Binding Properties and Negative Cooperativity of Soluble Insulin-like Growth Factor Receptors. J. Biol. Chem. 283, 5355-5363 (2008).
- 231. Urizar, E. et al. Glycoprotein hormone receptors: link between receptor homodimerization and negative cooperativity. EMBO J. 24, 1954–1964 (2005).
- 232. Kiselyov, V. V., Versteyhe, S., Gauguin, L. & De Meyts, P. Harmonic oscillator model of the insulin and IGF1 receptors' allosteric binding and activation. Mol. Syst. Biol. 5, 243 (2009).

- 233. Ha, S. H. & Ferrell, J. E. Thresholds and ultrasensitivity from negative cooperativity. Science 352, 990-993 (2016).
- 234. Shvartsman, S. Y. et al. Autocrine loops with positive feedback enable contextdependent cell signaling. Am. J. Physiol. Physiol. 282, C545–C559 (2002).
- 235. Afkarian, M. et al. T-bet is a STAT1-induced regulator of IL-12R expression in naïve CD4+ T cells. Nat. Immunol. 3, 549-557 (2002).
- 236. Busse, D. et al. Competing feedback loops shape IL-2 signaling between helper and regulatory T lymphocytes in cellular microenvironments. Proc. Natl. Acad. Sci. U. S. A. **107**, 3058–3063 (2010).
- 237. Becskei, A. & Grusby, M. J. Contribution of IL-12R mediated feedback loop to Th1 cell differentiation. FEBS Lett. 581, 5199-5206 (2007).
- 238. Waysbort, N., Russ, D., Chain, B. M. & Friedman, N. Coupled IL-2-Dependent Extracellular Feedbacks Govern Two Distinct Consecutive Phases of CD4 T Cell Activation. J. Immunol. 191, 5822-5830 (2013).
- 239. Tkach, K. E. et al. T cells translate individual, quantal activation into collective, analog cytokine responses via time-integrated feedbacks. Elife 3, e01944 (2014).
- 240. Goldbeter, A. & Koshland, D. E. An amplified sensitivity arising from covalent modification in biological systems. Proc. Natl. Acad. Sci. U. S. A. 78, 6840–6844 (1981).
- 241. Gunawardena, J. Multisite protein phosphorylation makes a good threshold but can be a poor switch. *Proc. Natl. Acad. Sci. U. S. A.* **102**, 14617–14622 (2005).
- 242. Huang, C. Y. & Ferrell, J. E. Ultrasensitivity in the mitogen-activated protein kinase cascade. Proc. Natl. Acad. Sci. U. S. A. 93, 10078-10083 (1996).
- 243. Kapuy, O., Barik, D., Domingo Sananes, M. R., Tyson, J. J. & Novák, B. Bistability by multiple phosphorylation of regulatory proteins. Proq. Biophys. Mol. Biol. 100, 47-56 (2009).
- 244. Markevich, N. I., Hoek, J. B. & Kholodenko, B. N. Signaling switches and bistability arising from multisite phosphorylation in protein kinase cascades. J. Cell Biol. 164, 353-359 (2004).
- 245. Buchler, N. E. & Cross, F. R. Protein sequestration generates a flexible ultrasensitive response in a genetic network. Mol. Syst. Biol. 5, 272 (2009).
- 246. Cuba Samaniego, C., Giordano, G., Kim, J., Blanchini, F. & Franco, E. Molecular Titration Promotes Oscillations and Bistability in Minimal Network Models with Monomeric Regulators. ACS Synth. Biol. 5, 321–333 (2016).
- 247. Fang, M., Xie, H., Dougan, S. K., Ploegh, H. & van Oudenaarden, A. Stochastic Cytokine Expression Induces Mixed T Helper Cell States. PLOS Biol. 11, e1001618 (2013).
- 248. Seo, M.-H., Park, J., Kim, E., Hohng, S. & Kim, H.-S. Protein conformational dynamics

- dictate the binding affinity for a ligand. Nat. Commun. 5, 3724 (2014).
- 249. Wu, F., Su, R.-Q., Lai, Y.-C. & Wang, X. Engineering of a synthetic quadrastable gene network to approach Waddington landscape and cell fate determination. Elife 6, e23702 (2017).
- 250. Ye, Y., Kang, X., Bailey, J., Li, C. & Hong, T. An enriched network motif family regulates multistep cell fate transitions with restricted reversibility. PLOS Comput. Biol. 15, e1006855 (2019).

Understanding the Robustness of Regulatory Motifs in Generating Biological Switches Relevant to Cell-fate Decisions

by Anupam Dey

Submission date: 08-Jun-2021 02:42AM (UTC+0530)

Submission ID: 1602411603

File name: 15CHPH34 AnupamDey PlagiarismCheck.pdf (6.05M)

Word count: 33938

Character count: 178530

Understanding the Robustness of Regulatory Motifs in Generating Biological Switches Relevant to Cell-fate Decisions

ORIGINALITY REPORT

23_%

4%

20%

3%

SIMILARITY INDEX

INTERNET SOURCES

PUBLICATIONS

STUDENT PAPERS

PRIMARY SOURCES

Anupam Dey, Debashis Barik. "Potential Landscapes, Bifurcations, and Robustness of Tristable Networks", ACS Synthetic Biology, 2021

Publication

Certified that the primary sources No. L, 213 are Assortion from the publications of the studentino

Anupam Dey, Debashis Barik. "Parallel Hyderaba arrangements of positive feedback loops limit cell-to-cell variability in differentiation", PLOS ONE, 2017

Publication

Dr. Debashos Barik
Associate Professor
School of Chemistry
University of Hyderabad
Hyderabad-500 046, India.

Anupam Dey, Debashis Barik. "Dichotomous Nature of Bistability Generated by Negative Cooperativity in Receptor–Ligand Binding", ACS Synthetic Biology, 2019

Publication

Dr. Debashis Barik
Associate Professor
School of Chemistry
University of Hogerabad

Submitted to Imperial College of Science, Hyderabad-500 of Technology and Medicine

Student Paper

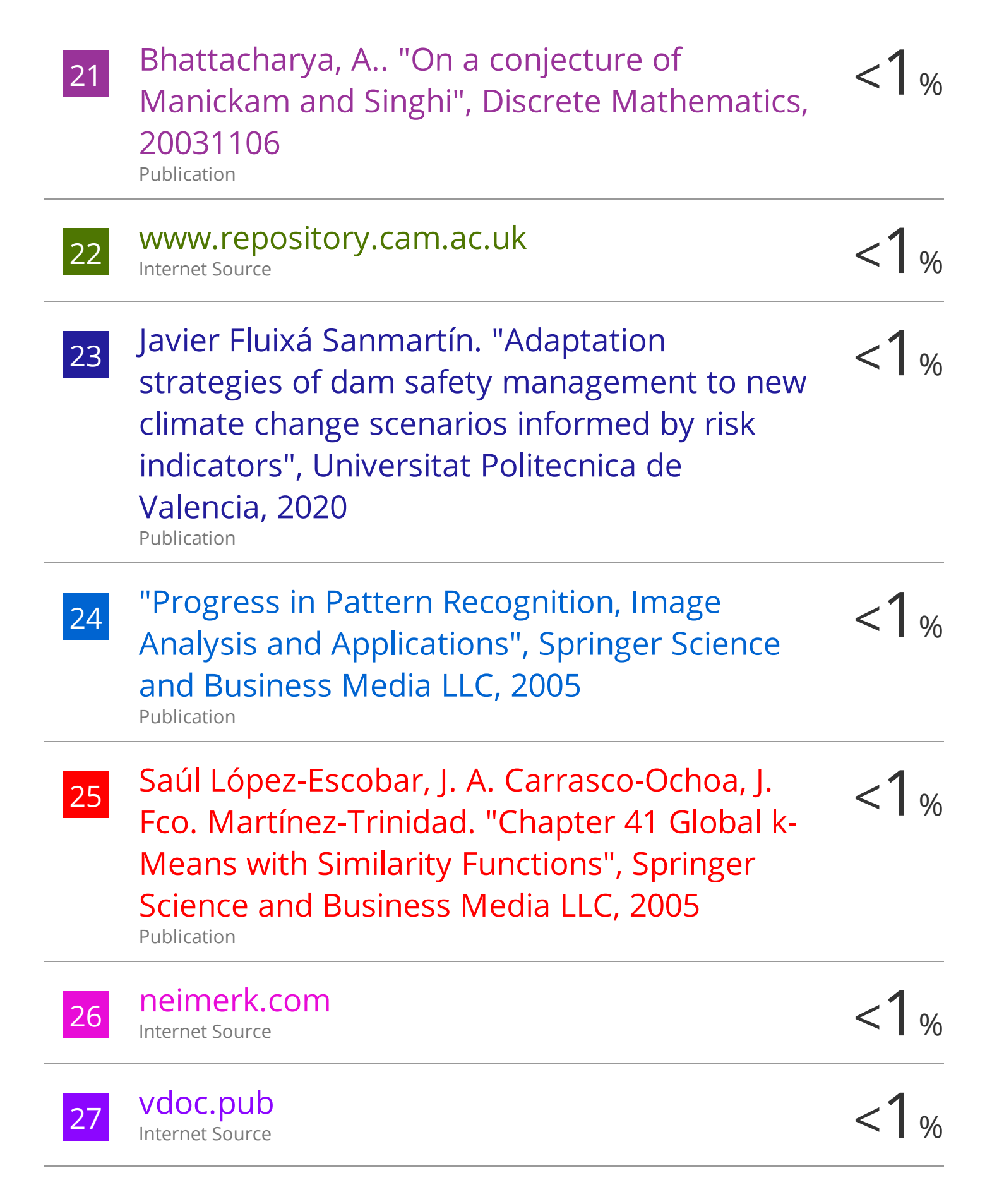
Submitted to Tezpur University
Student Paper

1 %

olndia.

6	www.ncbi.nlm.nih.gov Internet Source	<1%
7	cdn.vizio.com Internet Source	<1%
8	"Formal Methods for Computational Systems Biology", Springer Science and Business Media LLC, 2008 Publication	<1%
9	Alexander Y. Mitrophanov. "Positive feedback in cellular control systems", BioEssays, 06/2008 Publication	<1%
10	ale.physics.sunysb.edu Internet Source	<1%
11	jov.arvojournals.org Internet Source	<1%
12	Kerner, Boris S "Complex Dynamics of Traffic Management, Introduction to", Encyclopedia of Complexity and Systems Science, 2009. Publication	<1%
13	Rotem Golan, Christian Jacob, Savraj Grewal, Jörg Denzinger. "Predicting patterns of gene expression during drosophila embryogenesis", Proceedings of the 2014 conference on Genetic and evolutionary computation - GECCO '14, 2014 Publication	<1%

14	John J. Tyson. "Design principles of biochemical oscillators", Nature Reviews Molecular Cell Biology, 10/30/2008 Publication	<1%
15	oa.upm.es Internet Source	<1%
16	epub.uni-regensburg.de Internet Source	<1%
17	Konstantinos P. Koutsoumanis, Zafiro Aspridou. "Individual cell heterogeneity in Predictive Food Microbiology: Challenges in predicting a "noisy" world", International Journal of Food Microbiology, 2017	<1%
18	open.library.ubc.ca Internet Source	<1%
19	Ali H. Nayfeh, Balakumar Balachandran. "Applied Nonlinear Dynamics", Wiley, 1995	<1%
20	Anissa Guillemin, Elisabeth Roesch, Michael P.H. Stumpf. "Uncertainty in cell fate decision making: Lessons from potential landscapes of bifurcation systems", Cold Spring Harbor Laboratory, 2021 Publication	<1%



Exclude quotes On Exclude matches < 14 words

Exclude bibliography On